Draft version June 16, 2020
Typeset using LaTeX **twocolumn** style in AASTeX62

The *R*-process Alliance : First Magellan/MIKE Release from the Southern Search for *R*-Process-enhanced Stars*

Rana Ezzeddine,[1,2,3] Kaitlin Rasmussen,[4,2] Anna Frebel,[3,2] Anirudh Chiti,[3,2] Karina Hinojisa,[3] Vinicius M. Placco,[4,2] Ian U. Roederer,[5,2] Alexander P. Ji,[6,7,2] Timothy C. Beers,[4,2] Terese T. Hansen,[8] Charli M. Sakari,[9] and Jorge Melendez[10]

[1] *Department of Astronomy, University of Florida, Bryant Space Science Center, Gainesville, FL 32611, USA*
[2] *Joint Institute for Nuclear Astrophysics - Center for Evolution of the Elements, USA*
[3] *Department of Physics & Kavli Institute for Astrophysics and Space Research, Massachusetts Institute of Technology, Cambridge, MA 02139, USA*
[4] *Department of Physics, University of Notre Dame, Notre Dame, IN 46556, USA*
[5] *Department of Astronomy, University of Michigan, Ann Arbor, MI 48109, USA*
[6] *The Observatories of the Carnegie Institution for Science, 813 Santa Barbara St., Pasadena, CA 91101, USA*
[7] *Hubble Fellow*
[8] *Mitchell Institute for Fundamental Physics and Astronomy and Department of Physics and Astronomy, Texas A&M University, College Station, TX 77843, USA*
[9] *Department of Astronomy, University of Washington, Seattle, WA 98195-1580, USA*
[10] *Instituto de Astronomia, Geofísica e Ciências Atmosféricas, Universidade de São Paulo, SP 05508-900, Brazil*

ABSTRACT

Extensive progress has been recently made into our understanding of heavy element production via the *r*-process in the Universe, specifically with the first observed neutron star binary merger (NSBM) event associated with the gravitational wave signal detected by LIGO, GW170817. The chemical abundance patterns of metal-poor *r*-process-enhanced stars provides key evidence into the dominant site(s) of the *r*-process, and whether NSBMs are sufficiently frequent or prolific *r*-process sources to be responsible for the majority of r-process material in the Universe. We present atmospheric stellar parameters (using a Non-Local Thermodynamic Equilibrium analysis) and abundances from a detailed analysis of 141 metal-poor stars, carried out as part of the *R*-Process Alliance (RPA) effort. We obtained high-resolution "snapshot" spectroscopy of the stars using the MIKE spectrograph on the 6.5 m Magellan Clay telescope at Las Campanas Observatory in Chile. We find 10 new highly enhanced *r*-II (with [Eu/Fe] $> +1.0$), 62 new moderately enhanced *r*-I ($+0.3 <$ [Eu/Fe] $\leq +1.0$) and 17 new limited-*r* ([Eu/Fe] $< +0.3$) stars. Among those, we find 17 new carbon-enhanced metal-poor (CEMP) stars, of which five are CEMP-no. We also identify one new *s*-process-enhanced ([Ba/Eu]$> +0.5$), and five new *r*/*s* ($0.0 <$ [Ba/Eu] $< +0.5$) stars. In the process, we discover a new ultra metal-poor (UMP) star at [Fe/H]$= -4.02$. One of the *r*-II stars shows a deficit in α and Fe-peak elements, typical of dwarf galaxy stars. Our search for *r*-process-enhanced stars by RPA efforts, has already roughly doubled the known *r*-process sample.

Keywords: nucleosynthesis — stars: abundances — stars: Population II — stars: atmospheres — stars: fundamental parameters

1. INTRODUCTION

The production of elements with $Z \geq 38$ occurs via the rapid (*r*-) and slow (*s*-) neutron-capture processes. While the site of the *s*-process is well-understood (Gallino et al. 2005; Karakas & Lugaro 2010; Frebel 2018), a number of sites for the *r*-process have been proposed over the last few decades. A key requirement is the ability to provide the strong neutron flux needed for rapid neutron capture to occur. This has been predicted to happen in extreme sites like neutron star binary mergers (NSBM) (e.g., Lattimer & Schramm 1974),

Corresponding author: Rana Ezzeddine
ranae@mit.edu

* This paper includes data gathered with the 6.5 meter Magellan Telescopes located at Las Campanas Observatory, Chile.

magneto-rotationally driven jets (e.g., Winteler et al. 2012), or collapsar disk winds (e.g., Siegel et al. 2019).

Metal-poor stars enhanced in r-process elements have been found in both the Milky Way halo (e.g., Hansen et al. 2018, Sakari et al. 2018 and Roederer et al. 2018b) as well as dwarf galaxies, most notably the r-process ultra-faint dwarf galaxy Reticulum II (Ret II) (Ji et al. 2016a; Roederer et al. 2016). These stars formed from gas that was previously enriched by a nucleosynthesis event during which heavy r-process elements were made. Altogether, they thus provide the best accessible evidence for the early operation of the r-process, as many r-process elements can be detected in their spectra, and the corresponding chemical abundances be measured.

In 2017, the LIGO/Virgo gravitational wave observatory discovered the first NSBM event GW170817 (Abbott et al. 2017), after which a kilonova, likely powered by the decay of newly synthesized of r-process elements, was observed (e.g., Pian et al. 2017). Together with chemical-evolution models of the Galaxy that implement NS-NS mergers (Cescutti et al. 2015; Wehmeyer et al. 2015; Côté et al. 2017) and the existence of Reticulum II, these lines of evidence support the hypothesis that NS mergers are likely a dominant site of r-process nucleosynthesis. However, improved chemical-evolution models by Côté et al. (2018), more recently suggested that NSBM may not in fact be the only sources of r-process elements in the Galaxy. Additional sources, such as magneto-rotational ("jet") supernovae (Nishimura et al. 2017) could be needed to reproduce the observed r-process patterns in, for e.g., moderately enhanced r-process (r-I: $+0.3 <$ [Eu/Fe] $\leq +1.0$) metal-poor stars. Alternative sites for highly r-process-enhanced (r-II: [Eu/Fe] $> +1.0$) stars have also been suggested, such as collapsars (Siegel et al. 2019). This conundrum underscores the need for studying large numbers of r-process-enhanced stars, to better interpret and place constraints on heavy-element formation through the r-process, and all of its associated astrophysical site(s) throughout cosmic history.

Motivated by the importance of r-process-enhanced halo stars, the R-Process Alliance (RPA) collaboration aims at significantly increasing the numbers of such stars, as, until recently, only a relatively small number of them were known. Moreover, a major goal is to combine r-process observations, r-process theory efforts, and results from chemical-evolution simulations to eventually produce a more complete understanding of the origin of the r-process-enhanced star population in the Galactic halo. To this end, two extensive "data release" papers have already been published by Hansen et al. (2018) (hereafter RPA-1) and Sakari et al. (2018) (hereafter RPA-2) which report on many newly discovered r-process-enhanced stars. This paper (hereafter RPA-3) describes the third data release, based on spectra collected with the 6.5 m Magellan Clay telescope.

With the emergence of a large r-process-enhanced star sample, and thus statistically meaningful measures of chemical abundances, kinematics, frequencies, etc. of these stars, questions about their formation and any prior enrichment of their birth gas clouds can soon be addressed more rigorously. This is also of interest with respect to establishing possible connections between the r-process signature observed in the Ret II stars and that of r-process stars found in the Galactic halo. Given their nearly identical abundance patterns, the halo stars likely originated in ancient dwarf galaxy analogs similar to Ret II (Roederer et al. 2018a). Establishing the origin story of halo r-process-enhanced stars will provide important insides into the environment in which the earliest r-process events took place.

From a cosmological perspective, the r-process-enhanced stars also offer another advantage, since they can be dated from their abundance ratios of long-lived isotopes of Th and U relative to abundances of stable r-process elements such as Eu (e.g., Cayrel et al. 2001; Frebel et al. 2007; Placco et al. 2017; Holmbeck et al. 2018). With half-lives of 4.5 Gyrs and 14.05 Gyrs, respectively, ^{238}U and ^{232}Th decay over cosmologically relevant timescales. Such ages could be used, for example, to place lower limits on the time of their associated r-process production event(s). We note, however, that such ratios can not be reliably used for actinide-boost r-process stars (Schatz et al. 2002), which are known to exhibit unusually high Th and U abundances as compared to stable elements, such as Eu. Interestingly, the actinide elements ratio, Th/U (if measured simultaneously in a star), seems to remain a robust tool to determine the ages of actinide-boost r-process stars (Holmbeck et al. 2019).

This paper is outlined as follows. In Section 2, we describe the observations, data reduction, and radial-velocity measurements. In Section 3, we present the stellar parameter determinations of the sample using both 1D (1-Dimensional), LTE (Local Thermodynamic Equilibrium) and 1D, NLTE (Non-Local Thermodynamic Equilibrium) methods. Section 4 presents the chemical abundances of the light elements and the α-elements, as well as the Fe-peak and neutron-capture elements determined for the stars. We then discuss the results and conclude in Sections 5 and 6, respectively.

2. OBSERVATIONS

2.1. *Target Selection and Observations*

Metal-poor, candidate r-process-enhanced target stars were selected from various metal-poor surveys, including the RAdial Velocity Experiment (RAVE; Steinmetz et al. 2006), Large Sky Area Multi-Object Fibre Spectroscopic Telescope (LAMOST) (C. Liu, private communication), Best & Brightest (B&B; Schlaufman & Casey 2014; Placco et al. 2019), SkyMapper[1] (Wolf et al. 2018), Melendez & Placco (M&P; Meléndez et al. 2016), and the Hamburg/ESO Survey (HES; Christlieb et al. 2008). Most of our targets were selected from the RAVE fourth and fifth data releases (DR4 and DR5; Kordopatis et al. 2013; Kunder et al. 2017). For those latter stars, their metal-poor nature was vetted by Placco et al. (2018), who derived estimates of their stellar parameters based on medium-resolution spectroscopy acquired on a number of different telescopes. Additional details on the selection criteria for these stars is presented in Hansen et al. (2018) and Placco et al. (2018, 2019).

All targets were observed at high spectral resolution using the Magellan Inamori Kryogenic Echelle (MIKE) spectrograph (Bernstein et al. 2003) on the Clay (Magellan II) telescope at Las Campanas Observatory, Chile. Overall, a total of 148 stars with visual magnitudes (V) between 10.0 and 14.5 were observed. The spectra were collected over the course of three years, from January 2015 through December 2018. Either the $0\farcs7$ or $1\farcs0$ slit with 2×2 binning was used, yielding nominal resolving powers of $R \sim$28,000 or $R \sim$22,000 in the red, and $R \sim 35,000$ or $R \sim 28,000$ in the blue, respectively. All spectra cover the wavelength range from $\sim$ 3860 Å to $\sim$ 9000 Å.

Exposure times depended on magnitude and weather conditions, but were typically between 900 s for brighter stars to 1800 s for fainter ones, aiming for Signal-to-Noise (S/N) values of 25 pixel^{-1} at 4000 Å. When needed, more than one exposure was taken to increase the S/N to the desired level. The quality of these spectra enables the detection or a meaningful upper limit on the Eu II line at 4129 Å, which serves as the major r-process diagnostic. Many other elements can also be detected, including C, Sr, and Ba. The Two Micron All Sky Survey (2MASS) IDs, right ascension (R.A.) and declination (Decl.), visual magnitudes (V), exposure times, Modified Julian Dates (MJD), slit widths, S/N ratios at 4000 Å and survey sources are listed in Table 1.

[1] The SkyMapper stars are taken from the extremely metal poor (EMP; [Fe/H]< -3) sample discussed in Da Costa et al. (2019); specifically it includes all stars that satisfy $g_{\rm SkyMapper} \leq 14.1$ and $-3.0 \leq$ [Fe/H]$_{\rm fitter} \leq -2.0$, where [Fe/H]$_{\rm fitter}$ is the abundance estimated from the low-resolution spectra (see Da Costa et al. 2019 for details).

2.2. *Data Reduction and Radial-Velocity Measurements*

Data were reduced using the latest versions of the `Carnegie Python Distribution`[2] (Kelson 2003). Each order of each spectrum was then normalized and merged into a final spectrum, which was also radial-velocity shifted by cross-correlation with the Ca II line near 8542 Å of the spectrum of HD 140283, using the `Spectroscopy Made Hard` (`SMH`) analysis software (first described in Casey 2014). Heliocentric velocity (RV$_{\rm helio}$) corrections were then determined with the `rvcorrect` package in `IRAF`. We compare our RV$_{\rm helio}$ values to those from the *Gaia* second data release (DR2; Gaia Collaboration et al. 2018), whenever available (110 stars). We present the comparisons in Figure 1. The radial velocities for eleven of the stars differ significantly from the *Gaia* velocities, up to 60 km s^{-1}. Excluding these outliers, our velocities agree with those from *Gaia* within a mean difference of 1.93 km s^{-1}, with a standard deviation of $\sigma = 3.10$ km s^{-1}. We also compute the biweight-scale standard deviation[3] of the full sample (including outliers). We find that $\sigma_{\rm biweight} = 3.73$ agrees well with our reported σ. Seven of those are found to be double-lined spectroscopic binaries (SB2), as their spectra exhibit clear contamination from a companion; these are labeled as such in Table 1. No spectral disentanglement of the two components was attempted for these stars, and thus they were not further analyzed with the rest of the sample. We note that it is highly unlikely that the source of the r-process enhancement is due to binarity, as it is unable to produce the neutron flux density ($n_n > 10^{22}$ cm^{-3}) needed to induce the r-process (Thielemann et al. 2017).

3. STELLAR ATMOSPHERIC PARAMETERS

We determined stellar atmospheric parameters for the sample stars, namely the effective temperature ($T_{\rm eff}$), surface gravity ($\log g$), metallicity ([Fe/H]), and microturbulent velocity (ξ_t), from the abundances of Fe I and Fe II lines as determined from equivalent width (EW) measurements. The EWs of the lines were obtained by fitting Gaussian line profiles to the spectral absorption features using `SMH`. The Fe I and Fe II abundances were derived with 1D stellar atmospheric models, using three different spectroscopic methods: (i) assuming LTE, (ii) assuming LTE with $T_{\rm eff}$ corrected to a photometric scale, following Frebel et al. (2013), as well as (iii) assuming NLTE. The atomic line-by-line properties for the Fe I

[2] https://code.obs.carnegiescience.edu/mike

[3] https://docs.astropy.org/en/stable/api/astropy.stats.biweight.biweight_scale.html

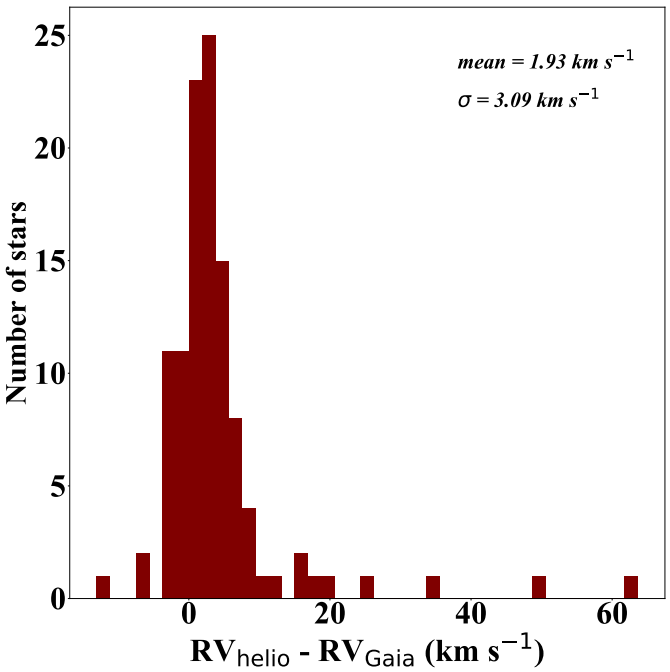

Figure 1. Histogram showing radial-velocity differences of our targets, as measured in this study and by Gaia DR2. Eleven stars display significant differences $> 1\sigma = 3.09\,\mathrm{km\,s^{-1}}$ (value determined excluding outliers). Seven of those stars were found to be SB2 binaries, and are labeled as such in Table 1.

and Fe II lines, including their EW and abundance measurements, are shown in Table 2. The linelist is compiled from several data sources, and the log gf values for our lines are adopted from the up-to-date list compiled by Roederer et al. (2018b) (see their Table 2 and the references therein).

3.1. *LTE Stellar Parameters*

The LTE stellar atmospheric parameters were estimated from the abundances of Fe I and Fe II lines using the 2017 version of the LTE radiative transfer code MOOG (Sneden 1973), including Rayleigh scattering treatment following Sobeck et al. (2011)[4]. Stellar 1D, LTE atmospheric models from Castelli & Kurucz (2004), with standard α-element enhancement of $[\alpha/\mathrm{Fe}] = +0.4$ were used. $T_{\rm eff}$ values were determined by enforcing excitation equilibrium of the abundance of Fe I lines as a function of excitation potential, χ. The $\log g$ values were determined by enforcing ionization equilibrium between the abundances inferred from the Fe I and Fe II lines.

[4] https://github.com/alexji/moog17scat

The ξ_t parameter was determined by ensuring no Fe I abundance trends with reduced equivalent widths existed (REW; $\log(\mathrm{EW}/\lambda)$). The [Fe/H] abundances were determined from the average abundances of the Fe I and Fe II lines. The number of Fe I and Fe II lines used, as well as the LTE stellar parameters derived for each star, are listed in Table 3. Stellar parameter uncertainties are determined assuming systematic uncertainties following the analysis in Ji et al. (2016b), and they are estimated to be up to 150 K, 0.3 dex, and $0.2\,\mathrm{km\,s^{-1}}$ for $T_{\rm eff}$, $\log g$, and ξ_t, respectively. The [Fe/H] uncertainties are determined from the standard deviations of the Fe I and Fe II abundances.

3.2. *Corrected LTE Stellar Parameter Estimates*

Spectroscopic stellar parameters derived using the assumption of LTE have long been known to suffer from systematic uncertainties, especially for cooler metal-poor stars where atomic collisions are not sufficiently frequent to ensure that actual excitation and ionization equilibrium of the atomic populations is achieved. Determinations of $T_{\rm eff}$ via photometric methods have been shown to be less prone to uncertainties compared to the LTE spectroscopic approach (Casagrande et al. 2010). However, these require known absolute magnitudes and reddening toward the stars. As a middle ground, we thus also determined the $T_{\rm eff}$ of our target stars by "correcting" the LTE spectroscopic temperatures to a photometric scale, following the empirical calibration introduced in Frebel et al. (2013), hereafter denoted as $T_{\rm eff}$(FR13 corr.):

$$T_{\rm eff}(\mathrm{FR13\ corr.}) = 0.9\times T_{\rm eff}(\mathrm{LTE}) + 670$$

For comparison to the "strict" LTE $T_{\rm eff}$ results, we divide the stars into three categories covering different $T_{\rm eff}$ ranges: $T_{\rm eff} \leq 4500$ K, $4500 < T_{\rm eff} < 5000$ K and $T_{\rm eff} \geq 5000$ K. We show the differences obtained relative to the strict LTE results in Figure 2, for each $T_{\rm eff}$ range. By design, the differences in the temperatures are more pronounced for cooler stars ($T_{\rm eff} < 4500$ K), by up to 250 K, while smaller shifts were obtained for the hotter stars ($T_{\rm eff} > 5000$ K), up to 150 K.

After fixing $T_{\rm eff}$ to the FR13 corrected scale, we then also derived $\log g$, ξ_t, and [Fe/H] as explained in Section 3.1, by forcing both ionization equilibrium and no abundance trends with line strengths. We compare the "corrected" $\log g$, ξ_t, and [Fe/H] to those determined strictly in LTE, as again shown in the boxplots in Figure 2. For $\log g$, the differences are presented for three surface gravity sub-categories: $\log g \leq 1.5$, $1.5 < \log g < 3.0$ and $\log g \geq 3.0$. The shifts from LTE are largest for the giant stars with $\log g \leq 1.5$, up to $\sim +1.0$ dex,

while slightly smaller differences, up to +0.7 dex, were obtained for the giants and sub-giants with $1.5 < \log g < 3.0$. For stars with $\log g \geq 3.0$, the resulting differences were smaller still, up to +0.2 dex, and lie within the LTE $\log g$ uncertainties.

We also note that the differences obtained for [Fe/H] increase with decreasing metallicities, and are the largest for the extremely metal-poor stars (EMP) with [Fe/H] ≤ -3.0 (Figure 2), reaching up to +0.5 dex. On average, the corrections are $\sim +0.2$ dex. The corrections for ξ_t are negative relative to the uncorrected LTE case, and are decreasing with increasing ξ_t, reaching $-0.5\,\mathrm{km\,s^{-1}}$ for $\xi_t \geq 3.0\,\mathrm{km\,s^{-1}}$.

3.3. *NLTE Stellar Parameter Estimates*

Atmospheric stellar parameter determinations for metal-poor stars from LTE spectroscopic methods are affected by unaccounted-for departures from statistical equilibrium that can introduce significant systematic uncertainties, since line formation and populations of non-dominant species (in this case Fe I) can potentially deviate from the Saha–Boltzmann equilibrium assumed in LTE (Lind et al. 2012; Amarsi et al. 2016; Ezzeddine et al. 2017). To account for such departures, especially in giant and warm stars, it is necessary to investigate the formation of iron lines in NLTE. Therefore, we also determine stellar parameters for our target stars using 1D, NLTE radiative transfer models.

3.3.1. *NLTE Methods*

NLTE abundances were computed for Fe I and Fe II lines from their EWs using the radiative transfer code `MULTI` in its 2.3 version (Carlsson 1986, 1992), and employing 1D `MARCS` model atmospheres (Gustafsson et al. 1975, 2008) interpolated to the corresponding parameters. Blanketing from background opacities, excluding Fe lines, were employed from the `MARCS` opacity package (B. Plez, private communication).

The Fe I/Fe II atomic model used in the NLTE calculations is described in more detail in Ezzeddine et al. (2017). This model was built adopting up-to-date atomic data. Quantum computations of inelastic collision rates of Fe I with neutral hydrogen atoms were implemented from Barklem (2018). These collisions play an important dominant role (over electrons) in NLTE calculations of cool stars.

The NLTE stellar parameters were derived following the procedure in Ezzeddine et al. (2017), where first approximations of the parameters were derived simultaneously by multi-dimensional fitting of the observed Fe I and Fe II EW of the target stars to theoretical NLTE EW in a pre-computed dense grid of $T_{\rm eff}$, $\log g$, ξ_t, and [Fe/H] parameter space, using the Levenberg-Marquardt algorithm. The excitation and ionization equilibrium, as well as the trends with reduced EW, were then checked for each star, ensuring no trends.

3.3.2. *NLTE Results*

The derived NLTE stellar parameters are shown in Table 3. For $T_{\rm eff}$, $\log g$, and ξ_t, we adopt typical total uncertainties arising from the uncertainties in the atomic data and abundance slopes versus χ and REW, of 100 K in $T_{\rm eff}$, 0.3 dex in $\log g$, and $0.2\,\mathrm{km\,s^{-1}}$ in ξ_t. [Fe/H] uncertainties were adopted from the standard deviations of the line-by-line abundances and are shown in Table 3, which vary from 0.08 to 0.18 dex. The NLTE gravities, as a function of $T_{\rm eff}$ and [Fe/H], are shown on the left panel of Figure 3, over-plotted on four 12.5 Gyr Dartmouth isochrones (Dotter et al. 2008), with [α/Fe] = +0.4 and [Fe/H] = −1.00, [Fe/H] = −1.50, [Fe/H] =−2.00, and [Fe/H] = −2.50, respectively. The stars mostly occupy the upper portion of the giant branch in the $T_{\rm eff}$-$\log g$ diagram. This likely stems from our target selection bias toward cool bright giants for the search for r-process stars by the RPA (Placco et al. 2018, 2019). We note that, despite this bias, the RPA sample in this work, as well as other RPA data releases, are expected to be fairly representative, as all initial "snapshot" spectra of the target stars were exposed to determine a reliable r-process enhancement measurement, by adjusting exposure times accordingly to obtain S/N ratios > 30 (per pixel) in the blue around the Eu II line at 4129 Å (a representative line of r-process enhancement, see Section 4.1 below). Four of the stars are found to be hot dwarfs ($T_{\rm eff} > 5500$ K, $\log g > 4.0$), while another two stars are field horizontal-branch stars. Additionally, one of the stars, 2MASS J09291557+0838002, is a newly identified ultra-metal-poor (UMP) star at [Fe/H](NLTE)= −4.02. Four r-process-enhanced stars at the r-I, r/s, and limited-r levels are detected at [Fe/H] > −1.5. We also plot, on the right panel of Figure 3, $\log g$ versus ξ_t for our target stars. For comparison, we also show the results from previous studies by Cayrel et al. (2004) and Barklem et al. (2005) for their very metal-poor star samples. We fit the $\log g$-ξ_t dependence for both our target stars, as well as those from previous studies with third degree polynomials[5]. We find that ξ_t increases for giant stars with lower $\log g$ as compared to the dwarfs. A similar trend is obtained from previous studies, as shown by the black star mark-

[5] The fitting coefficients for the third degree polynomial, $y = ax^3 + bx^2 + cx + d$ (where x and y correspond to $\log g$ and ξ_t, respectively), obtained for our target stars are a = −0.02, b = 0.37, c= −1.98, and d = 4.73.

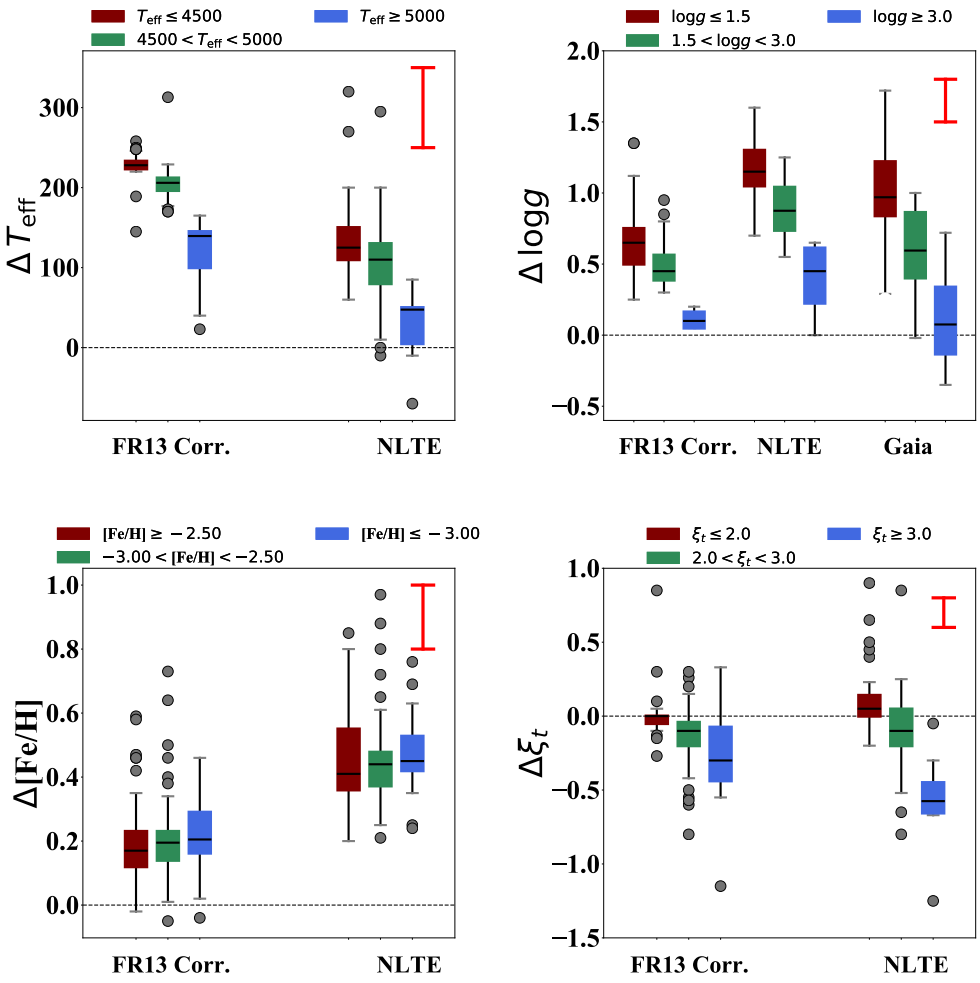

Figure 2. Boxplots showing the stellar parameter changes for $T_{\rm eff}$, $\log g$, [Fe/H], and ξ_t, when comparing LTE results with those from applying the Frebel et al. (2013) correction (labeled as FR13 Corr.), and from using a NLTE approach (labeled NLTE). The boxplots are color-coded for the ranges of stellar parameters (in LTE), as indicated on top of each panel. For $\log g$, we also show the differences arising from using *Gaia* DR2 parallaxes and our uncorrected LTE values. Red uncertainty bars represent typical NLTE parameter uncertainties, corresponding to 100 K for $T_{\rm eff}$, 0.3 dex for $\log g$, 0.2 dex for [Fe/H], and 0.2 km s^{-1} for ξ_t.

ers and their third degree polynomial fit on the same Figure, although the NLTE dependence from our study shows a more severe increase for ξ_t for the giant stars. These positive NLTE ξ_t corrections are nominally driven by the abundance differences obtained between LTE and NLTE from the stronger saturated Fe I lines (with $EW > 50$ mÅ), as explained in the detailed NLTE study by Lind et al. (2012).

We also compare the NLTE stellar parameters from our sample and from the RPA-1 and RPA-2 papers (Hansen et al. 2018; Sakari et al. 2018) to their corresponding LTE values (Figure 2). We find that the NLTE temperatures are higher than those determined in LTE, and the shifts are more pronounced for cooler stars, reaching up to +200 K. On average, the $T_{\rm eff}$ shifts between NLTE and LTE are +150 K for $T_{\rm eff} \leq 4500$ K, +120 K for $4500 < T_{\rm eff} \leq 5000$ K and +50 K for $T_{\rm eff} > 5000$ K. The NLTE corrections ($T_{\rm eff}$(NLTE)$-$ $T_{\rm eff}$(LTE)) are, however, lower than those obtained by using the FR13 corrections, by ~ 100 K, on average.

The NLTE corrections in $\log g$, defined by $\log g$(NLTE) $-$ $\log g$(LTE), are also positive, and found to be in-

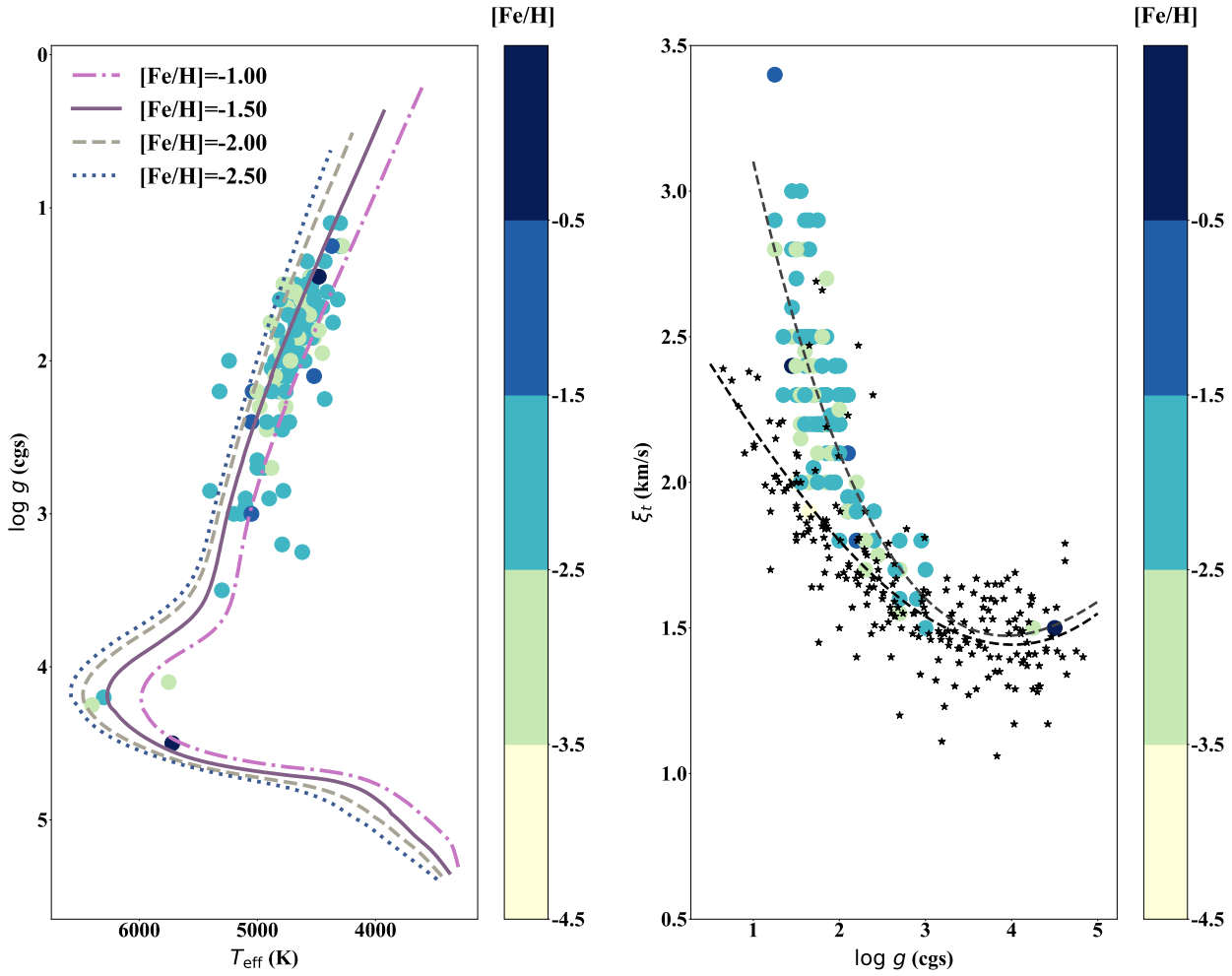

Figure 3. Left panel: NLTE stellar parameters of the target stars ($T_{\rm eff}$ and $\log g$ color-coded as a function of [Fe/H]), overplotted with Dartmouth isochrones at 12.5 Gyrs for four different metallicities, [Fe/H] = −1.00, [Fe/H] = −1.50, [Fe/H] = −2.00, and [Fe/H] = −2.50, respectively (Dotter et al. 2008). Right panel: NLTE $\log g$ versus ξ_t for the target stars, color-coded as a function of [Fe/H]. The polynomial fit to the data is shown by the gray dotted line. Also shown, for comparison, are the stars (show by the small star markers) from Cayrel et al. (2004) and Barklem et al. (2005), as well as the polynomial fit to their $\log g$-ξ_t (black dotted line).

creasing toward lower gravities, up to +1.2 dex. These corrections agree with those derived for the stars in Sakari et al. (2018). On average, the corrections are +1.2 dex for $\log g \leq 1.5$, +1.0 dex for $1.5 < \log g < 3.0$, and +0.5 dex for $\log g \geq 3.0$. The corrections in [Fe/H] are also increasing toward lower metallicities, in line with other NLTE predictions (Mashonkina et al. 2011; Lind et al. 2012; Amarsi et al. 2016), and can reach up to +0.6 for [Fe/H] ≤ −3.0, +0.45 for −3.0 < [Fe/H] < −2.0, and +0.3 for [Fe/H] ≥ −2.0. We note that these metallicity NLTE corrections are expected to be larger, on average, than those nominally obtained by fixing the $T_{\rm eff}$ and $\log g$ values prior to determining the LTE and NLTE [Fe/H] (e.g., Lind et al. 2012; Mashonkina et al. 2011). Therefore, the [Fe/H] corrections obtained in our study also reflect the abundance changes due to the $T_{\rm eff}$ and $\log g$ NLTE corrections obtained for the target stars. Finally, the NLTE ξ_t corrections are negative, and agree on average with those obtained by applying the FR13 corrections. The corrections are, however, slightly lower in NLTE for $\xi_t \geq 3.0\,{\rm km\,s^{-1}}$, and can reach $-0.6\,{\rm km\,s^{-1}}$.

We note that any differences in the atmospheric models used in the NLTE and LTE calculations (`MARCS` vs.

ATLAS) are expected to have negligible effects on the resulting stellar parameters in LTE. Roederer et al. (2014) showed in their analysis of a large number of metal-poor stars, including both giants and subgiants, that differences obtained between both models are less than 8 K for $T_{\rm eff}$, 0.005 dex for $\log g$, 0.002 km s^{-1} for ξ_t, and 0.006 dex for [Fe/H]. These values are negligible as compared to the differences obtained for the stellar parameters between NLTE and LTE.

3.4. *Estimates of log g from Gaia DR2 Parallaxes*

For $\log g$, we also derive surface gravities from *Gaia* DR2 parallax-based distances (Bailer-Jones et al. 2018). To calculate distance-based surface gravities, we adopt a relation between $\log g$, stellar mass, $V_{\rm mag}$, and bolometric corrections. For the dwarfs and giants in our sample, a mass of 0.7 and 0.8 solar masses was adopted, respectively. The RAVE $V_{\rm mag}$ were used, and the bolometric corrections were adopted from Casagrande & VandenBerg (2014).

The derived $\log g^{Gaia}$ values are shown in the last column of Table 3. For comparison, we also show the differences between $\log g^{Gaia}$ and those derived in LTE in Figure 2. The gravity corrections are more pronounced for the giant stars with $\log g \leq 1.5$, with an average shift of $\sim +1.2$ dex. Slightly lower shifts are obtained for stars with $1.5 < \log g < 3.0$, of up to +0.6 dex, and for stars with $\log g \geq 3.0$, up to +0.1 dex. The *Gaia* gravities agree with those obtained in NLTE within uncertainties of $\sim$0.3 dex, on average.

We note that 26 of our sample stars have *Gaia* DR2 parallax-based distances larger than 6 kpc (Bailer-Jones et al. 2018). Those stars are likely to lead to larger uncertainties in the derived $\log g^{Gaia}$ (> 0.2 dex), due to the larger systematic shifts of their *Gaia* DR2 parallaxes (Arenou et al. 2018). We flag these stars as such in Table 3, and warn against the use of their *Gaia* $\log g$.

Given that the NLTE $\log g$ values agree overall with those from non-spectroscopic ones (*Gaia*), and that the NLTE stellar parameters are considered to be better representatives of the stellar atmospheres of metal-poor stars than LTE (e.g., see review by Asplund 2005), we decided to adopt the NLTE stellar parameters for our target stars, and use them to determine the chemical abundances of our stars. Nevertheless, our analysis clearly shows that in the absence of a full NLTE approach, the FRE13 values (calibrated to photometric $T_{\rm eff}$) provide reasonable stellar parameters, lying within the uncertainty levels of the corresponding NLTE values, where typical values of 100 K for $T_{\rm eff}$, 0.3 dex for $\log g$, 0.2 dex for [Fe/H], and 0.2 km s^{-1} for ξ_t are shown by the red error bars on Figure 2.

4. CHEMICAL ABUNDANCES

We derive abundances for the light elements, α elements, and Fe-peak elements for the target stars, including C, O, Na, Mg, Al, Si, K, Ca, Sc, Ti I, Ti II, V, Cr, Mn, Co, Ni, and Zn using MOOG. Additionally, we derive the abundances for the neutron-capture elements Eu, Ba, and Sr, in order to sort our target stars into the sub-classifications suggested by the reviews of Beers & Christlieb (2005) and Frebel (2018). The abundance ratios [X/H] are calculated relative to the solar abundances presented by Asplund et al. (2009). The abundances (except for C, O, Al, and the neutron-capture elements) were derived from a line-by-line analysis using EWs of the lines and a curve-of-growth (COG) method. Sufficiently weak lines lying on the linear part of the COG were chosen with REW ≤ -4.5. The remaining abundances were derived using spectrum synthesis of their corresponding lines, taking into account isotopic ratios. Linelists for each region of interest are generated with linemake[6] (Sneden et al. 2008). The Hyperfine structure (HFS) was considered for the Fe-peak elements, including Sc, V, Mn, and Co, when necessary. For carbon, an average isotopic shift ratio of ^{12}C/^{13}C = 4/1 was used. This was determined for each star individually, by fitting the lines around the 4313 Å CH feature, specifically, those at 4217 Å, 4225 Å, as well as 4302 Å. Upper limits were determined by matching the noise levels in the observed spectral lines with the corresponding synthetic spectral lines. Our line-by-line atomic data, EW and abundances are listed in Table 2. The average abundances are also shown in Table 6.

4.1. *Neutron-Capture Element Abundances*

Strontium abundances were derived from the Sr II lines at 4077 Å, 4161 Å, and 4215 Å. With the line at 4077 Å being saturated in most of the stars, and the line 4161 Å being very weak, especially in EMP stars, the Sr abundances were primarily derived from the line at 4215 Å. We note that the strong 4077 and 4215 Å Sr II lines may be affected by NLTE effects, however, Short & Hauschildt (2006) reported an offset of < 0.1 dex for these lines for stellar parameters similar to those of our sample of stars. Barium abundances were derived mainly from the two Ba II lines at 5853 Å and 6141 Å, which are not saturated, unlike the line at 4554 Å. For Eu, the abundances were derived from several Eu II lines at 3907 Å, 4129 Å, 4205 Å, 4435 Å, 6437 Å, and 6645 Å, following Hansen et al. (2018). The bluer line at 3907 Å was used when the blue S/N of the spectra was high

[6] https://github.com/vmplacco/linemake

enough (≥ 80). However, the strongest Eu line, located at 4129 Å, was was the primary line used for most stars. Examples of observed Sr, Ba, and Eu lines at 4215 Å, 5853 Å, and 4129 Å, respectively, for representative r-II, r-I, and limited-r stars, as well as their abundance syntheses, are shown in Figure 4.

The abundance ratios [Sr/Fe], [Ba/Fe] and [Eu/Fe], calculated with NLTE [Fe/H] values, are listed in Table 4. They were also used to classify our stars into their sub-classes following Frebel (2018):

- r-II: [Eu/Fe] $> +1.0$ and [Ba/Eu] < 0.0
- r-I: $+0.3 \leq$ [Eu/Fe] $\leq +1.0$ and [Ba/Eu] < 0.0
- limited-r: [Eu/Fe] $< +0.3$, [Sr/Ba] $> +0.5$, and [Sr/Eu] > 0.0
- s-process: [Ba/Fe] $> +1.0$ and [Ba/Eu] $> +0.5$
- r/s: $0.0 <$ [Ba/Eu] $< +0.5$
- CEMP-r: [C/Fe] $> +0.7$, [Eu/Fe] $> +0.3$, and [Ba/Eu]< 0.0
- CEMP-no: [C/Fe] $> +0.7$ and [Ba/Fe] < 0.0
- Non-r-process enhanced (non-RPE): [Eu/Fe] $< +0.3$, [Sr/Ba] ≤ 0.5, and [Sr/Eu] < 0.0

4.2. *CO and the Light-Element Abundances*

We derive the C abundances via spectrum synthesis of the molecular CH G-band at 4313 Å (Masseron et al. 2014). As most of our stars lie on the red giant branch (see Figure 3), the carbon abundances are assumed to be depleted by the CN cycle having operated during the stars' evolution. Relative [C/Fe] ratios of the target stars were therefore corrected for evolutionary status following Placco et al. (2014). We show both uncorrected and corrected values in Table 4. Additionally, we derive abundances of the light elements O and Na, using the forbidden O I lines at 6300 and 6363 Å for O (whenever detectable), and the Na I doublet at 5889 and 5895 Å for Na, if the lines are sufficiently weak. We note that Lind et al. (2011) reported non-significant NLTE abundance corrections of < 0.1 dex for the Na I doublet at our metallicity range. The [O/H] and [Na/H] abundances are listed in Table 5.

4.3. *The α-element, K, and Al abundances*

We derive α-element abundances for Mg I, Ca I, Ti I, and Ti II from the EWs of their corresponding lines. Potassium abundances were determined when the K I lines at 7664 and 7698 Å were found to be unpolluted by telluric lines. For Al, we determine the abundances by synthesizing the blue resonance Al I line at 3961 Å, taking into account the C abundance. We caution that this line can be prone to significant 3D and NLTE corrections, up to 0.6 dex for our range of metallicities, as reported by Nordlander & Lind (2017).

4.4. *Iron-Peak Element Abundances*

We also derive the Fe-peak abundances for our target stars using Sc II, V II, Cr II, Mn I, Co I, Ni I and Zn I from their EWs using a multitude of lines, whenever available. We did not derive abundances from V I and Cr I lines, as they are prone to larger NLTE effects than their corresponding ionized species, V II and Cr II (Bergemann & Cescutti 2010). We note that recent results by Bergemann et al. (2019) showed that Mn I lines can be prone to large NLTE and 3D effects, which they found to be increasingly larger for lower metallicities. For our sample of stars in this work, with [Fe/H] ranging typically between $-3.0 <$ [Fe/H] < -2.0, the authors report 3D, NLTE corrections between 0.3 and 0.6 dex for Mn I lines. We do not include these corrections in this paper, but anticipate to include them in future papers once the correction grids have been made publicly available.

5. DISCUSSION

5.1. *R-Process-Enhanced Stars*

Following the neutron-capture sub-classifications defined in Beers & Christlieb (2005) and Frebel (2018), we identify in this work 10 new r-II, 62 new r-I, and 17 new limited-r stars. Additionally, we find one s-process-enhanced and five r/s stars. Overall, 46 stars from our target sample of 141 stars are non-r-process-enhanced (hereafter non-RPE, following the definition in Sakari et al. 2018). This shows that our overall selection procedure works well. One of our non-RPE stars, 2MASS J00452379−2112161, is a rediscovery of the ultra metal-poor star CD−38 °245 (Bessell & Norris 1984). Seventeen of the 141 stars were found to be Carbon-enhanced metal-poor (CEMP) stars, one enhanced at the r-II level, four at the r-I level, and three are limited-r stars. Additionally, three out of five of the r/s-enhanced stars are CEMP stars, as well as the s-process-enhanced star. Five stars were also found to be CEMP-no stars.

This brings up the total number of r-process-enhanced stars (at the r-II, r-I, limited-r, and r/s levels) identified by the RPA efforts from this work, Hansen et al. (2018), Sakari et al. (2018), Roederer et al. (2018b), Holmbeck et al. (2018), Cain et al. (2018), Gull et al. (2018), and Placco et al. (2017) to 253 out of a total of 381 stars. Of those, a total of 28 stars are enhanced at the r-II level (7.4%), 163 stars at the r-I level (42.7%),

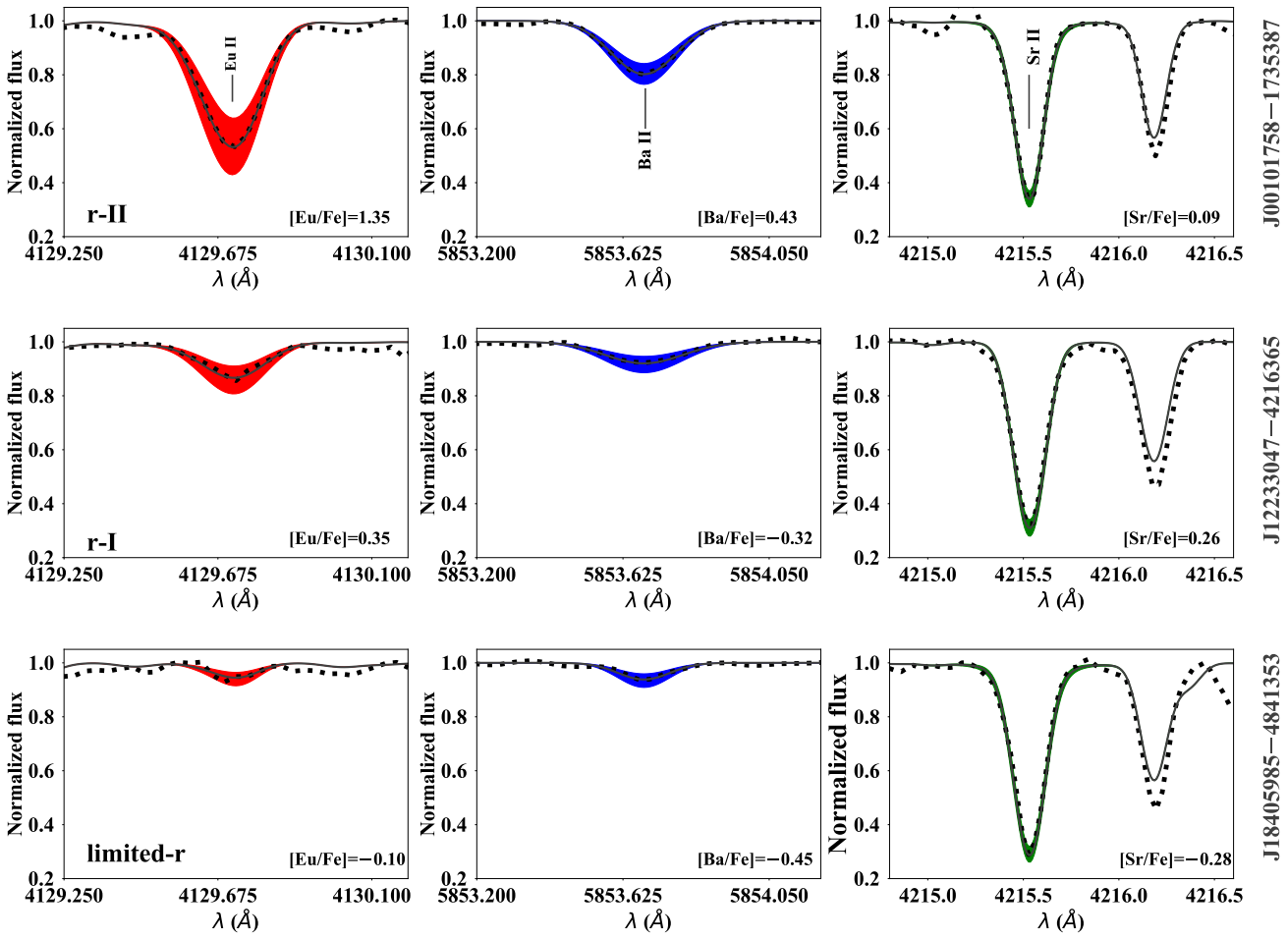

Figure 4. Observed spectral lines (dotted lines) and their abundance syntheses (gray lines) of Sr II at 4215 Å, Ba II at 5853 Å, and Eu II at 4129 Å for r-II (J00101758−1735387, top panel), r-I (J12233047−4216365, middle panel), and limited-r (J18405985−4841353, bottom panel) stars discovered in our sample. Representative uncertainties of ±0.2 dex are shown for each lines by the filled syntheses colors.

56 stars at the limited-r level (14.7%), and 6 stars are enhanced at the r/s level (1.6%). We caution that these values should not be used as physically interpretable estimates of the percentage of r-process enhanced stars. They likely represent upper bounds as some stars were selected for publication on account of their high level of r-process enhancement (Placco et al. 2017; Cain et al. 2018; Gull et al. 2018; Holmbeck et al. 2018), and other sample selection biases have not yet been fully quantified. The RPA intends to report more definitive estimates of the percentage of r-process enhanced stars in future work.

Figure 5 shows the cumulative histograms of newly identified r-I, r-II, and limited-r stars in this work, as a function of metallicity (upper panels) and V magnitudes (lower panels). None of those were previously identified in the RPA-1 and RPA-2 samples (open histograms; Hansen et al. 2018; Sakari et al. 2018). Similar to the results found in the RPA-1 and RPA-2 samples (also shown on the plots), we find r-I and r-II stars over a wide metallicity range, from [Fe/H] = −3.5 to [Fe/H] = −1.2. The limited-r stars are found primarily between [Fe/H] = −2.8 and [Fe/H]=−1.5. Our r-I stars cover a wider range of metallicities than those of the RPA-

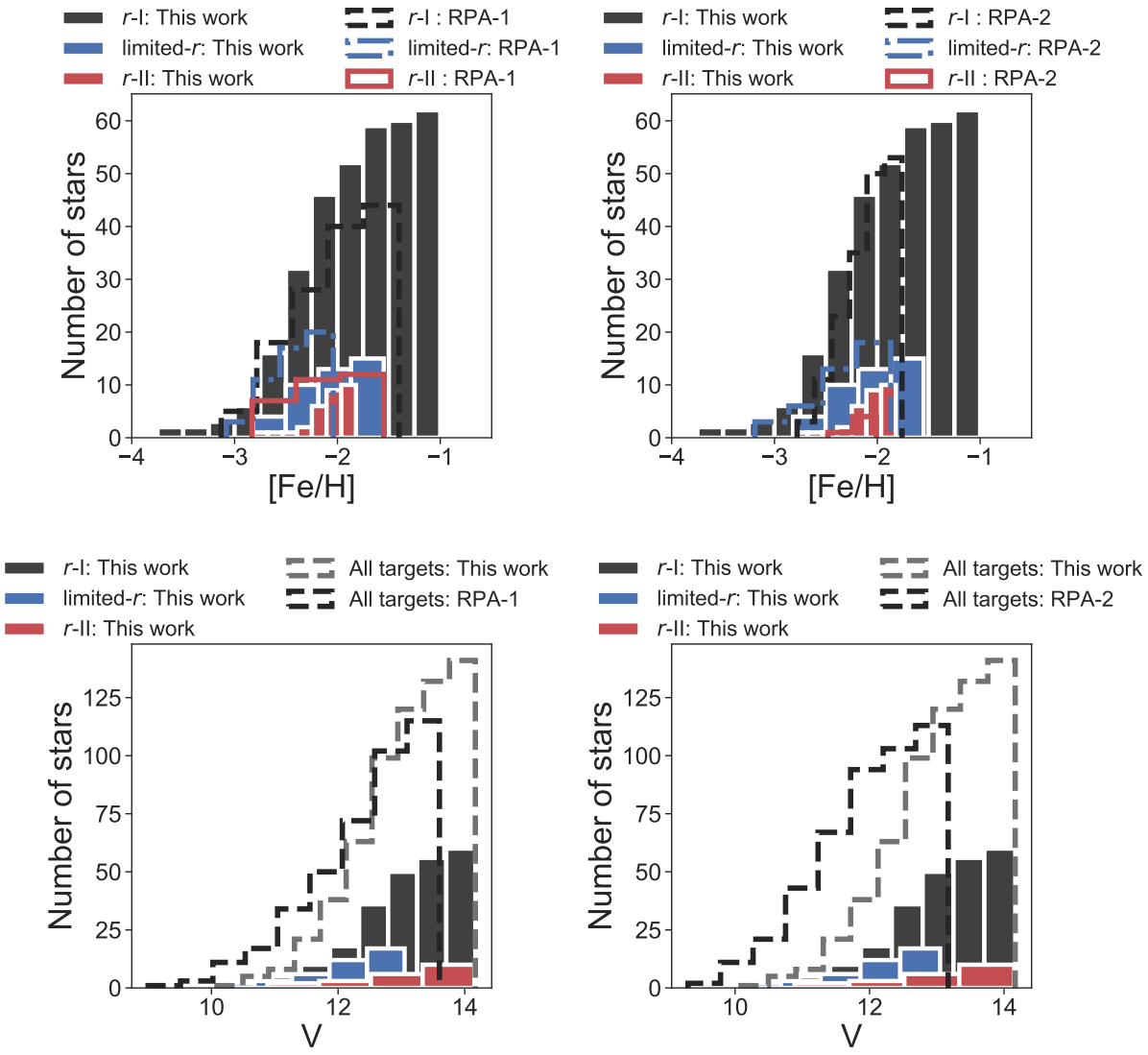

Figure 5. Cumulative histograms showing the number of *r*-I (filled gray), *r*-II (filled red), and limited-*r* (filled blue) stars discovered in this work, as a function of NLTE [Fe/H](upper panels) and V magnitudes (lower panels). Also shown, for comparison, are all the stars discovered and analyzed in the RPA-1 (Hansen et al. 2018) and RPA-2 (Sakari et al. 2018) samples, as well as the total targets (dashed gray histogram) analyzed in this work (including non-RPE).

1 and RPA-2 samples, with one *r*-I star identified at [Fe/H] = −3.4, and another at [Fe/H]= −1.2. A similar cutoff in the *r*-I stars distribution is found around [Fe/H]= −3.0. The mean metallicity of our newly identified *r*-II stars is [Fe/H] ∼ −2.3, which agrees with the RPA-2 results. The [Fe/H] distribution from the RPA-1 sample is slightly shifted toward more metal-poor values, which can be explained by their implementation of an LTE analysis as compared to the 1D, NLTE and <3D>, NLTE analyses implemented in this work and RPA-2 papers respectively. Our sample of stars also shift toward higher V magnitudes than those analyzed by the RPA-1 and RPA-2 efforts (Figure 5, lower panels). This shift correlates with the sizes of the telescopes used in this work and those by RPA-1 and RPA-2 efforts. Our *r*-II stars are particularly extended up to $V = 14.2$ dex.

We also show the [Eu/Fe] abundance distribution, as a function of metallicity, in Figure 6. For comparison, we also show the stars from the RPA-1 and RPA-2 samples, as well as those from literature studies by Westin et al. (2000), Johnson (2002), Cayrel et al. (2004), Honda et al. (2004), Barklem et al. (2005), Ivans et al. (2006),

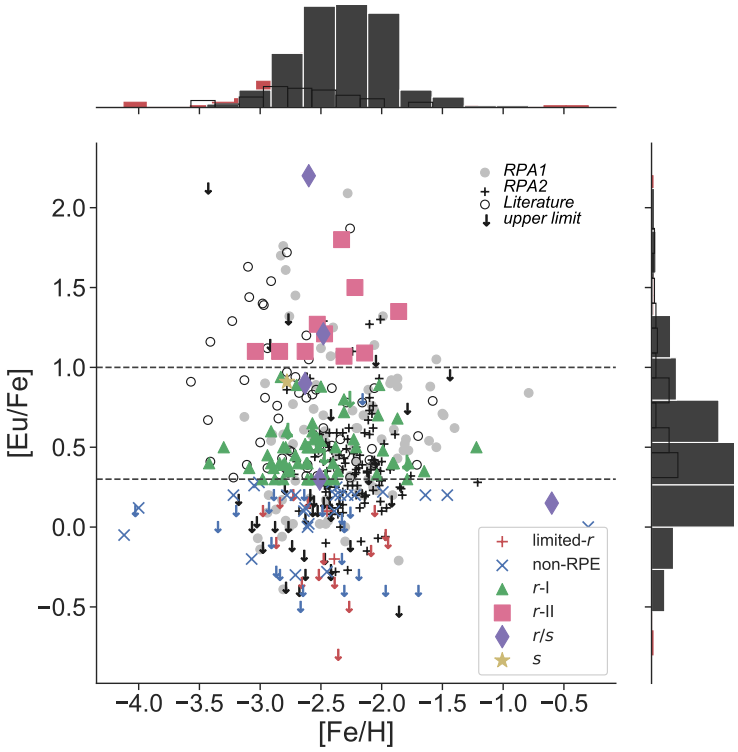

Figure 6. Derived [Eu/Fe] abundances, as a function of [Fe/H], for the r-I, r-II, limited-r, r/s, as well as non-RPE stars. Also shown are the stars from the RPA-1 (Hansen et al. 2018) and RPA-2 (Sakari et al. 2018) samples, as well as r-I and r-II stars from the literature (extracted from JINAbase Abohalima & Frebel 2018). The arrows display upper limit measurements. Statistics of the RPA-3 stars are shown by marginal red histograms for both the [Eu/Fe] and [Fe/H] ranges, and those of RPA-1 and RPA-2 stars are shown by marginal gray histograms. r-I and r-II stars from the literature are shown by open black histograms. Literature values are taken from Westin et al. (2000), Johnson (2002), Cayrel et al. (2004), Honda et al. (2004), Barklem et al. (2005), Ivans et al. (2006), Mashonkina et al. (2010), Siqueira Mello et al. (2014), and Roederer et al. (2014). Upper limits from the literature data have been suppressed for clarity.

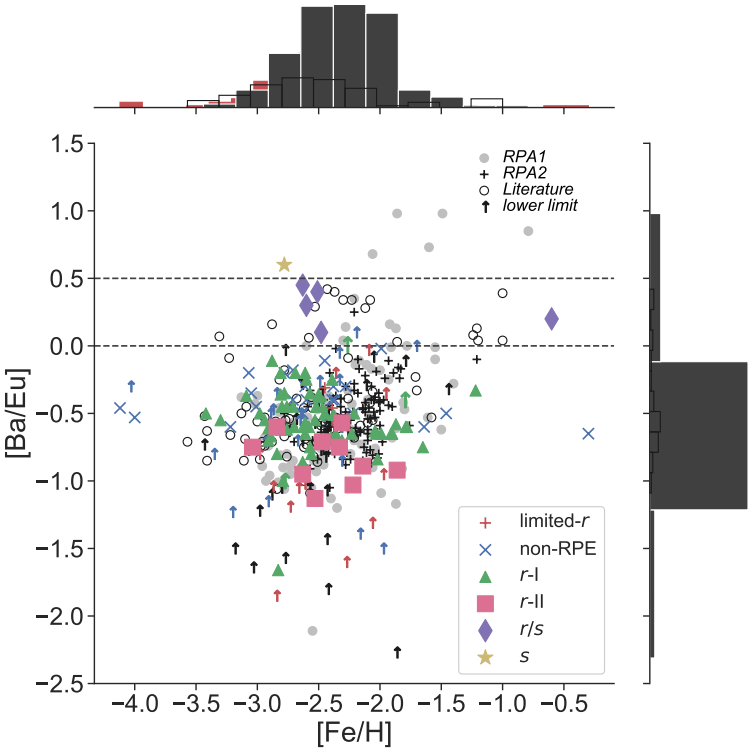

Figure 7. Same as in Figure 6, but for [Ba/Eu] abundance ratios. Dividing dotted lines indicating differences between the s-process-enhanced stars ([Ba/Eu] $> +0.5$), r/s-enhanced stars ($0.0 <$ [Ba/Eu] $< +0.5$), and r-process-enhanced stars ([Ba/Eu] < 0.0) abundance ratios are also shown.

Mashonkina et al. (2010), Siqueira Mello et al. (2014), and Roederer et al. (2014). The histograms on the top and right axes represent the number of stars covering each abundance range. Our results broadly overlap with the literature values, where the [Eu/Fe] ratios also cover a wide range of metallicities. This reiterates the interpretation by Sneden et al. (2000), who suggested multiple formation sites for r-process-enhanced stars and a need for investigating r-process production and its site(s). We also plot the absolute Eu abundances derived for our target stars, as a function of [Fe/H] in Figure 8. A clear increase of Eu with Fe is seen for the r-II, r-I, limited-r, and non-RPE stars. A similar trend was found by the RPA-1 survey (Hansen et al. 2018).

We additionally show the [Ba/Eu] ratios, as a function of [Fe/H], in Figure 7. This can be used as a diagnostic for the level of r- versus s-process origin of the neutron-capture elements measured in stars (Frebel 2018). We also plot the RPA-1 and RPA-2 stars on the same plot for comparison. Just as in previous work, the majority of newly identified r-II stars strictly have [Ba/Eu] < -0.5, indicating a pure r-process origin, while the r-I and limited-r stars show larger variations in [Ba/Eu].

5.2. *Other Elemental Abundances*

The abundance ratios of the light elements, α-elements, and Fe-peak elements relative to Fe are shown in Figure 9, compared with literature values from Cayrel et al. (2004), Barklem et al. (2005), and Cohen et al. (2013). Classes of r-II, r-I, limited-r, and non-RPE star are distinguished to investigate possible systematic differences.

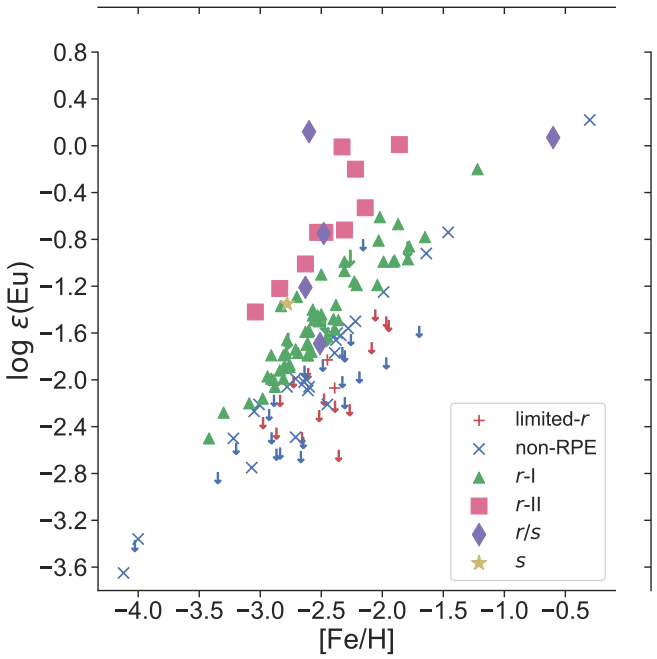

Figure 8. Absolute Eu abundances, as a function of [Fe/H], for the *r*-II, *r*-I, limited-*r*, *r*/*s*, and *s*-process-enhanced stars identified in this work.

[C/Fe] and [O/Fe] ratios exhibit increasing trends toward lower metallicities. [Mg/Fe], [Si/Fe], and [Ca/Fe] ratios show typical [α/Fe] enhancements, of $\sim +0.4$, on average, while the [Al/Fe] ratios exhibit sub-solar values, except for one limited-*r* and four *r*-I stars. We note that [Ti/Fe] ratios derived from the Ti II lines are shown, as they are less prone to NLTE effects than Ti I lines (Sitnova et al. 2016).

Fe-peak element abundance ratios mostly agree with those from the literature. [Co/Fe] and [Zn/Fe] abundances exhibit increasing trends toward lower metallicities, in agreement with literature results (e.g., Ezzeddine et al. 2019), whereas [Mn/Fe] abundances show decreasing trends toward lower metallicities.

The abundances of the majority of our stars agree with typical Galactic field metal-poor star abundances, with the exception of the *r*-II star 2MASS J00101758−1735387 (shown by black star symbol in Figure 9), which exhibits sub-solar and lower abundance ratios than the rest of the sample stars for C, Na, Mg, Al, K, Ca, Sc, Ti, V, Cr, Mn, Co, Ni, and Zn. This star exhibits similar abundance patterns to other halo *r*-I and *r*-II stars identified in Sakari et al. (2019) and Xing et al. (2019). These stars exhibit similar abundance patters to those identified in Milky Way (MW) dwarf galaxies (McWilliam et al. 2018). The former studies suggested that such halo stars have an accretion origin from a dwarf galaxy previously enriched by a NS merger event, which enriched the gas from which 2MASS J00101758−1735387 was formed. Additional investigation of its full *r*-process abundance pattern is underway, and will be presented in a future paper.

Another *r*-II star, 2MASS J05241392−0336543 exhibits a substantially enhanced [Na/Fe] ratio (+1.46). As shown in Figure 9 by the yellow circle marker, the [Mg/Fe] ratio in this star ([Mg/Fe] = +0.09) is slightly lower than most other stars in the sample, but all other light-element abundance ratios in 2MASS J05241392−0336543 are typical for its metallicity ([Fe/H]= −2.50).

The atypical [Na/Fe] and [Mg/Fe] abundance ratios appear unrelated to the light-element abundance variations typically observed in globular cluster stars, and discussion of its abundance anomalies and their origin is deferred to a future paper.

6. SUMMARY AND CONCLUSIONS

In this paper we have presented high-resolution spectroscopic observations for 148 newly studied metal-poor stars. We identify 32 new stars with $-2.0 \leq$ [Fe/H] < -1.0, 103 stars with $-3.0 \leq$ [Fe/H] < -2.0, 5 stars with $-4.0 \leq$ [Fe/H] < -3.0, as well as one new ultra metal-poor star at [Fe/H] < -4.0. One of the stars is a rediscovery of the previously observed ultra metal-poor star, CD−38 °245. This is part of the ongoing RPA effort to identify new *r*-process-enhanced stars in the Galaxy. Seven stars were found to be double-lined spectroscopic binaries, and were thus excluded from further study, leaving the sample to contain 141 newly studied stars.

We determine 1D, NLTE atmospheric stellar parameters for all stars, and derive abundances for the light elements, including C and O, the α-elements, the Fe-peak elements, and the neutron-capture elements, whenever suitable spectral lines are available. Among the 141 stars, we find 10 new *r*-II, 62 new *r*-I, and 17 new limited-*r* stars, based on their Eu, Ba, and Sr abundances. Additionally, we identified one new *s*-process-enhanced star and five new *r*/*s* stars.

Of the ten *r*-II stars, one is a CEMP star, another is found to exhibit sub-solar elemental abundance ratios relative to Fe for many of the light, α, and Fe-peak elements, consistent with accretion from a dwarf galaxy. All of the *r*-II stars exhibit consistently low ratios of [Ba/Eu] (< -0.5), which is a signature of pure

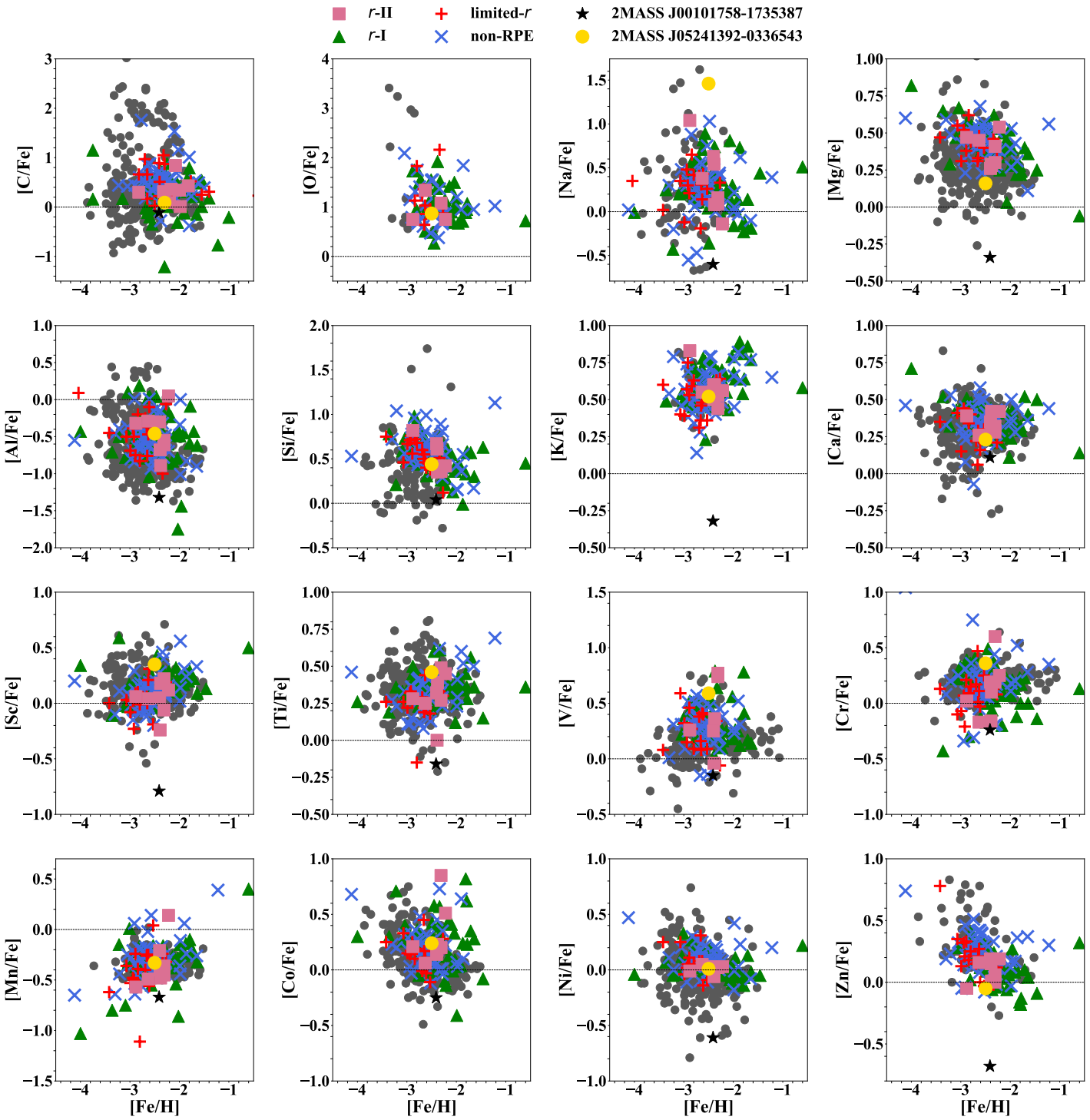

Figure 9. Light, α and fe-peak abundance ratios (relative to Fe) of the target stars, as a function of [Fe/H], for the different r-process sub-classifications. Literature studies (shown as gray points) by Cayrel et al. (2004), Barklem et al. (2005), and Cohen et al. (2013), and Roederer et al. (2014) are also shown for comparison. Stars with distinguished abundance patterns (see discussion in Section 5.2), 2MASS J00101758−1735387 and 2MASS J05241392−0336543, are also shown by the black star and yellow circle, respectively.

r-process enhancement. The r-II and r-I stars span a range of metallicities, from -3.0 to -1.5 in [Fe/H], with one r-I star detected at [Fe/H] $= -3.4$ and another at [Fe/H] $= -1.2$.

The neutron-capture and other elemental abundance ratios were compared to literature values, including the results from the RPA-1 and RPA-2 pilot samples of Hansen et al. (2018) and Sakari et al. (2018), respectively. The metallicity distribution of our stars derived using 1D, NLTE agrees with those derived for the RPA-2 sample (Sakari et al. 2018) using <3D>, NLTE. The RPA-1 [Fe/H] distribution, determined using 1D, LTE, is slightly shifted to the metal-poor end as compared to our sample, due to NLTE effects. Our sample is also shifted toward less bright stars as compared to the RPA-1 and RPA-2 sample. Our r-II stars cover a range of magnitudes, centered roughly around $V = 13$. The results from the three RPA releases from the Southern Hemisphere (this work, and Hansen et al. 2018) and the Northern Hemisphere (Sakari et al. 2018) have significantly increased the numbers of known r-II, r-I, and limited-r stars, roughly doubling the previously known samples to a total of 28 r-II stars, 163 r-I stars, and 56 limited-r stars, as well as 6 stars enhanced at the r/s level. The RPA has already obtained snapshot spectroscopy for $\sim$ 1500 bright metal-poor stars, and new snapshot spectra for $\sim$ 1000 additional candidate stars are presently being obtained with a variety of telescopes in the Northern and Southern Hemispheres. These observations are planned to be publicly released, as the data are reduced and analyzed, over the course of the next several years.

The full sample obtained by the RPA will be used to establish what fraction of accreted dwarf galaxies may have contributed metal-poor stars to the halo of the Milky Way; some partial information is already feasible to obtain (Roederer et al. 2018a). In addition, detailed information on the nature of the environment in which the r-process events associated with individual stars occurred is being explored by consideration of the association of r-process-enhanced stars with the so-called "Dynamically Tagged Groups" (DTGs) of very metal-poor stars (Yuan et al., submitted; Gudin et al., in preparation), following the pioneering work of Roederer et al. (2018a). When ultimately combined with new accelerator results on the fundamental nuclear properties for isotopes specific to the r-process (using, e.g., the Facility for Rare Isotope Beams; FRIB, expected 2022 Horowitz et al. 2019), stellar abundances will provide key missing information required to answer many of the outstanding questions regarding the nature and astrophysical sites of the r-process.

We thank Gary Da Costa for providing the SkyMapper targets. R.E., A.F., V.M.P, T.C.B., and I.U.R. acknowledge support from JINA-CEE (Joint Institute for Nuclear Astrophysics - Center for the Evolution of the Elements), funded by the NSF under Grant No. PHY-1430152. I.U.R. acknowledges partial support from NSF grants AST-1613536 and AST-1815403. A.F. is partially supported by NSF-CAREER grant AST-1255160 and NSF grant 1716251. JM thanks FAPESP (2014/18100-4). This work made use of NASA's Astrophysics Data System Bibliographic Services, and the SIMBAD database, operated at CDS, Strasbourg, France (Wenger et al. 2000). This work has made use of data from the European Space Agency (ESA) mission *Gaia* (https://www.cosmos.esa.int/gaia), processed by the *Gaia* Data Processing and Analysis Consortium (DPAC, https://www.cosmos.esa.int/web/gaia/dpac/consortium). Funding for the DPAC has been provided by national institutions, in particular the institutions participating in the *Gaia* Multilateral Agreement.

Facilities: Magellan-Clay (MIKE, Bernstein et al. 2003)

Software: IRAF (Tody 1993), matplotlib (Hunter 2007), MOOG (Sneden 1973; Sobeck et al. 2011), MULTI (Carlsson 1986, 1992), MARCS (Gustafsson et al. 1975, 2008)

REFERENCES

Abbott, B. P., Abbott, R., Abbott, T. D., et al. 2017, Physical Review Letters, 119, 161101

Abohalima, A., & Frebel, A. 2018, ApJS, 238, 36

Amarsi, A. M., Lind, K., Asplund, M., Barklem, P. S., & Collet, R. 2016, MNRAS, 463, 1518

Arenou, F., Luri, X., Babusiaux, C., et al. 2018, A&A, 616, A17

Asplund, M. 2005, ARA&A, 43, 481

Asplund, M., Grevesse, N., Sauval, A. J., & Scott, P. 2009, ARA&A, 47, 481

Bailer-Jones, C. A. L., Rybizki, J., Fouesneau, M., Mantelet, G., & Andrae, R. 2018, The Astronomical Journal, 156, 58

Barklem, P. S. 2018, A&A, 612, A90

Barklem, P. S., Christlieb, N., Beers, T. C., et al. 2005, A&A, 439, 129

Beers, T. C., & Christlieb, N. 2005, ARA&A, 43, 531

Bergemann, M., & Cescutti, G. 2010, A&A, 522, A9

Bergemann, M., Gallagher, A. J., Eitner, P., et al. 2019, A&A, 631, A80

Bernstein, R., Shectman, S. A., Gunnels, S. M., Mochnacki, S., & Athey, A. E. 2003, in Proc. SPIE, Vol. 4841, Instrument Design and Performance for Optical/Infrared Ground-based Telescopes, ed. M. Iye & A. F. M. Moorwood, 1694–1704

Bessell, M. S., & Norris, J. 1984, ApJ, 285, 622

Cain, M., Frebel, A., Gull, M., et al. 2018, ApJ, 864, 43

Carlsson, M. 1986, Uppsala Astronomical Observatory Reports, 33

Carlsson, M. 1992, in Astronomical Society of the Pacific Conference Series, Vol. 26, Cool Stars, Stellar Systems, and the Sun, ed. M. S. Giampapa & J. A. Bookbinder, 499

Casagrande, L., Ramírez, I., Meléndez, J., Bessell, M., & Asplund, M. 2010, A&A, 512, A54

Casagrande, L., & VandenBerg, D. A. 2014, MNRAS, 444, 392

Casey, A. R. 2014, PhD thesis, Australian National University, doi:10.5281/zenodo.49493

Castelli, F., & Kurucz, R. L. 2004, astro-ph/0405087

Cayrel, R., Hill, V., Beers, T. C., et al. 2001, Nature, 409, 691

Cayrel, R., Depagne, E., Spite, M., et al. 2004, A&A, 416, 1117

Cescutti, G., Romano, D., Matteucci, F., Chiappini, C., & Hirschi, R. 2015, A&A, 577, A139

Christlieb, N., Schörck, T., Frebel, A., et al. 2008, A&A, 484, 721

Cohen, J. G., Christlieb, N., Thompson, I., et al. 2013, ApJ, 778, 56

Côté, B., Belczynski, K., Fryer, C. L., et al. 2017, The Astrophysical Journal, 836, 230

Côté, B., Fryer, C. L., Belczynski, K., et al. 2018, ApJ, 855, 99

Da Costa, G. S., Bessell, M. S., Mackey, A. D., et al. 2019, MNRAS, 489, 5900

Dotter, A., Chaboyer, B., Jevremović, D., et al. 2008, ApJS, 178, 89

Ezzeddine, R., Frebel, A., & Plez, B. 2017, ApJ, 847, 142

Ezzeddine, R., Frebel, A., Roederer, I. U., et al. 2019, ApJ, 876, 97

Frebel, A. 2018, Annual Review of Nuclear and Particle Science, 68, 237

Frebel, A., Casey, A. R., Jacobson, H. R., & Yu, Q. 2013, ApJ, 769, 57

Frebel, A., Johnson, J. L., & Bromm, V. 2007, MNRAS, 380, L40

Gaia Collaboration, Brown, A. G. A., Vallenari, A., et al. 2018, A&A, 616, A1

Gallino, R., Delaude, D., Husti, L., et al. 2005, NuPhA, 758, 485

Gull, M., Frebel, A., Cain, M. G., et al. 2018, ApJ, 862, 174

Gustafsson, B., Bell, R. A., Eriksson, K., & Nordlund, A. 1975, A&A, 42, 407

Gustafsson, B., Edvardsson, B., Eriksson, K., et al. 2008, A&A, 486, 951

Hansen, T. T., Holmbeck, E. M., Beers, T. C., et al. 2018, ApJ, 858, 92

Holmbeck, E. M., Frebel, A., McLaughlin, G. C., et al. 2019, ApJ, 881, 5

Holmbeck, E. M., Beers, T. C., Roederer, I. U., et al. 2018, ApJL, 859, L24

Honda, S., Aoki, W., Kajino, T., et al. 2004, ApJ, 607, 474

Horowitz, C. J., Arcones, A., Côté, B., et al. 2019, Journal of Physics G Nuclear Physics, 46, 083001

Hunter, J. D. 2007, Computing in Science & Engineering, 9, 90

Ivans, I. I., Simmerer, J., Sneden, C., et al. 2006, ApJ, 645, 613

Ji, A. P., Frebel, A., Chiti, A., & Simon, J. D. 2016a, Nature, 531, 610

Ji, A. P., Frebel, A., Simon, J. D., & Chiti, A. 2016b, The Astrophysical Journal, 830, 93

Johnson, J. A. 2002, ApJS, 139, 219

Karakas, A., & Lugaro, M. 2010, in Nuclei in the Cosmos, 42

Kelson, D. D. 2003, PASP, 115, 688

Kordopatis, G., Gilmore, G., Steinmetz, M., et al. 2013, AJ, 146, 134

Kunder, A., Kordopatis, G., Steinmetz, M., et al. 2017, AJ, 153, 75

Lattimer, J. M., & Schramm, D. N. 1974, ApJL, 192, L145

Lind, K., Asplund, M., Barklem, P. S., & Belyaev, A. K. 2011, A&A, 528, A103

Lind, K., Bergemann, M., & Asplund, M. 2012, MNRAS, 427, 50

Mashonkina, L., Christlieb, N., Barklem, P. S., et al. 2010, A&A, 516, A46

Mashonkina, L., Gehren, T., Shi, J.-R., Korn, A. J., & Grupp, F. 2011, A&A, 528, A87

Masseron, T., Plez, B., Van Eck, S., et al. 2014, A&A, 571, A47

McWilliam, A., Piro, A. L., Badenes, C., & Bravo, E. 2018, ApJ, 857, 97

Meléndez, J., Placco, V. M., Tucci-Maia, M., et al. 2016, A&A, 585, L5

Nishimura, N., Sawai, H., Takiwaki, T., Yamada, S., & Thielemann, F. K. 2017, ApJL, 836, L21

Nordlander, T., & Lind, K. 2017, A&A, 607, A75

Pian, E., D'Avanzo, P., Benetti, S., et al. 2017, Nature, 551, 67
Placco, V. M., Frebel, A., Beers, T. C., & Stancliffe, R. J. 2014, ApJ, 797, 21
Placco, V. M., Holmbeck, E. M., Frebel, A., et al. 2017, ApJ, 844, 18
Placco, V. M., Beers, T. C., Santucci, R. M., et al. 2018, AJ, 155, 256
Placco, V. M., Santucci, R. M., Beers, T. C., et al. 2019, ApJ, 870, 122
Roederer, I. U., Hattori, K., & Valluri, M. 2018a, AJ, 156, 179
Roederer, I. U., Preston, G. W., Thompson, I. B., et al. 2014, AJ, 147, 136
Roederer, I. U., Sakari, C. M., Placco, V. M., et al. 2018b, ApJ, 865, 129
Roederer, I. U., Mateo, M., Bailey, John I., I., et al. 2016, AJ, 151, 82
Sakari, C. M., Placco, V. M., Farrell, E. M., et al. 2018, ApJ, 868, 110
Sakari, C. M., Roederer, I. U., Placco, V. M., et al. 2019, ApJ, 874, 148
Schatz, H., Toenjes, R., Pfeiffer, B., et al. 2002, ApJ, 579, 626
Schlaufman, K. C., & Casey, A. R. 2014, ApJ, 797, 13
Short, C. I., & Hauschildt, P. H. 2006, ApJ, 641, 494
Siegel, D. M., Barnes, J., & Metzger, B. D. 2019, Nature, 569, 241
Siqueira Mello, C., Hill, V., Barbuy, B., et al. 2014, A&A, 565, A93
Sitnova, T. M., Mashonkina, L. I., & Ryabchikova, T. A. 2016, MNRAS, 461, 1000
Sneden, C., Cowan, J. J., & Gallino, R. 2008, ARA&A, 46, 241
Sneden, C., Cowan, J. J., Ivans, I. I., et al. 2000, ApJL, 533, L139
Sneden, C. A. 1973, PhD thesis, University of Texas at Austin
Sobeck, J. S., Kraft, R. P., Sneden, C., et al. 2011, AJ, 141, 175
Steinmetz, M., Zwitter, T., Siebert, A., et al. 2006, AJ, 132, 1645
Thielemann, F. K., Eichler, M., Panov, I. V., & Wehmeyer, B. 2017, Annual Review of Nuclear and Particle Science, 67, 253
Tody, D. 1993, Astronomical Society of the Pacific Conference Series, Vol. 52, IRAF in the Nineties, ed. R. J. Hanisch, R. J. V. Brissenden, & J. Barnes, 173
Wehmeyer, B., Pignatari, M., & Thielemann, F. K. 2015, MNRAS, 452, 1970
Wenger, M., Ochsenbein, F., Egret, D., et al. 2000, A&AS, 143, 9
Westin, J., Sneden, C., Gustafsson, B., & Cowan, J. J. 2000, ApJ, 530, 783
Winteler, C., Käppeli, R., Perego, A., et al. 2012, ApJL, 750, L22
Wolf, C., Onken, C. A., Luvaul, L. C., et al. 2018, PASA, 35, e010
Xing, Q.-F., Zhao, G., Aoki, W., et al. 2019, Nature Astronomy, 3, 631

Table 1. Observational Details of the Target Stars

Star ID	R.A.	Decl.	V mag[a]	Exp. Time	Slit	MJD	S/N	RV_{helio}	RV_{helio}(Gaia)	Source
	(J2000)			(sec)	(arcsec)		(@4000Å)	($km\,s^{-1}$)	($km\,s^{-1}$)	
2MASS J00011195+0321051	00:01:12.000	+03:21:03.600	12.802	1500	1.0	58034.5	60	−211.75	−208.14	RAVE
2MASS J00101758−1735387	00:10:17.520	−17:35:38.400	11.539	1200	0.7	56940.5	100	191.80	191.76	M&P
2MASS J00162809−0505519	00:16:28.100	−05:05:52.100	12.921	1200	0.7	58385.5	65	−168.57	−173.48	SkyMapper
2MASS J00195350−0145445	00:19:53.520	−01:45:43.200	12.838	1800	1.0	58034.5	50	−301.34	−321.93	RAVE
2MASS J00282278−3934598	00:28:22.800	−39:34:59.900	12.547	1200	1.0	58380.5	60	29.20	23.56	SkyMapper
2MASS J00372794−2045307	00:37:27.930	−20:45:30.640	12.642	1200	0.7	58385.5	65	68.11	64.14	RAVE
2MASS J00452379−2112161	00:45:23.800	−21:12:16.100	12.538	1200	0.7	58385.5	75	26.15	21.19	SkyMapper
2MASS J00463619−3739335[b]	00:46:36.190	−37:39:33.550	11.929	1200	1.0	58362.5	60	42.70	48.28	RAVE
2MASS J00512646−1053170	00:51:26.500	−10:53:17.300	10.883	1200	0.7	57675.5	160	58.03	56.51	HES
2MASS J00524174−0902235	00:52:41.760	−09:02:24.000	11.046	600	0.7	57675.5	80	−237.86	−238.08	HES
2MASS J01165010−6307441	01:16:50.160	−63:07:44.410	11.669	1200	1.0	58380.5	60	127.31	122.72	RAVE
2MASS J01374434−4301490	01:37:44.300	−43:01:49.000	12.457	2400	1.0	58380.5	75	55.12	51.40	SkyMapper
2MASS J01473804−1130474	01:47:38.000	−11:30:47.000	12.994	1200	0.7	57675.5	40	30.38	28.31	RAVE
2MASS J01501343+0725010	01:50:13.424	+07:25:00.980	11.468	900	1.0	58362.5	75	−34.11	−40.91	LAMOST
2MASS J01553180−4919420	01:55:31.800	−49:19:41.800	12.750	1200	0.7	58380.5	60	130.80	···	SkyMapper
2MASS J01555066−6400155	01:55:50.700	−64:00:15.700	12.668	1200	1.0	58380.5	50	249.63	239.98	SkyMapper
2MASS J02005020−4657352	02:00:50.200	−46:57:35.000	13.244	2400	0.7	57674.5	50	−6.00	···	B&B
2MASS J02111462−8107085	02:11:14.690	−81:07:08.520	11.505	360	1.0	58362.5	70	251.17	266.57	RAVE
2MASS J02395318−7019014	02:39:53.100	−70:19:01.000	13.098	2764	0.7	57674.5	80	29.44	···	RAVE
2MASS J03073894−0502491	03:07:38.934	−05:02:49.120	12.928	9265	1.0	58380.5	90	−59.92	−61.37	LAMOST
2MASS J03154102−7626329	03:15:41.040	−76:26:32.780	11.411	500	1.0	58362.5	50	255.26	255.70	RAVE
2MASS J03270229+0132322	03:27:02.400	+01:32:31.200	12.135	900	1.0	57675.5	45	186.19	183.07	HES
2MASS J03423645−1335529	03:42:36.550	−13:35:53.480	11.987	600	1.0	58362.5	80	172.63	···	RAVE
2MASS J04245677−6500173	04:24:56.770	−65:00:17.400	11.668	300	1.0	58363.5	45	180.78	183.75	RAVE
2MASS J04304875−4613535	04:30:48.720	−46:13:51.600	13.090	600	1.0	57675.5	20	139.25	137.36	HES
2MASS J05030025−7601462	05:03:00.300	−76:01:46.300	13.682	2700	0.7	58184.5	30	214.13	···	SkyMapper
2MASS J05202930−5825297	05:20:29.300	−58:25:29.000	11.488	900	1.0	57492.5	75	324.41	324.10	RAVE/SkyMapper
2MASS J05241392−0336543	05:24:13.929	−03:36:54.300	13.894	1200	0.7	58185.5	15	110.02	101.06	LAMOST
2MASS J05384334−5147228	05:38:43.400	−51:47:23.000	13.050	1200	0.7	58183.5	50	189.71	···	SkyMapper
2MASS J05432623−8051334	05:43:26.160	−80:51:32.400	13.570	900	0.7	58184.5	25	160.37	150.58	SkyMapper
2MASS J05573684−5127209	05:57:36.800	−51:27:21.000	11.481	900	1.0	57492.5	60	132.09	120.90	RAVE
2MASS J06392518−7414056	06:39:25.200	−74:14:05.600	12.499	1200	0.7	58385.5	50	104.57	106.03	SkyMapper

Table 1 continued

Table 1 *(continued)*

Star ID	R.A.	Decl.	V mag[a]	Exp. Time	Slit	MJD	S/N	RV_{helio}	RV_{helio}(Gaia)	Source
	(J2000)			(sec)	(arcsec)		(@4000Å)	($km\,s^{-1}$)	($km\,s^{-1}$)	
2MASS J07123398−4814049	07:12:33.900	−48:14:04.000	11.566	1200	0.7	57493.5	80	361.65	352.57	RAVE
2MASS J07150266−0154092	07:15:02.677	−01:54:09.060	12.767	1200	0.7	58385.5	40	8.13	8.68	LAMOST
2MASS J07151852−5252051	07:15:18.500	−52:52:05.000	12.093	900	0.7	57493.5	60	229.48	230.25	M&P
2MASS J07250021−7022038	07:25:00.200	−70:22:04.100	13.528	900	0.7	58184.5	30	269.00	···	SkyMapper
2MASS J07443970−4425135	07:44:39.700	−44:25:13.000	12.412	900	0.7	57494.5	45	156.12	155.76	RAVE
2MASS J08025449−5224304	08:02:54.400	−52:24:30.000	12.375	2700	0.7	56763.5	60	142.05	137.08	RAVE
2MASS J08295142−7242542	08:29:51.360	−72:42:53.900	13.600	1500	0.7	58185.5	45	339.11	···	SkyMapper
2MASS J09103481+0518228	09:10:34.815	+05:18:22.900	14.165	1200	0.7	58184.5	25	123.94	···	LAMOST
2MASS J09291557+0838002	09:29:15.600	+08:37:55.000	11.144	1200	0.7	57493.5	140	267.17	···	M&P
2MASS J09531322+0744515	09:53:13.226	+07:44:51.690	13.687	4800	0.7	58184.5	50	319.72	···	LAMOST
2MASS J10063414−7030212	10:06:34.100	−70:30:21.300	13.836	3000	0.7	58184.5	25	135.95	···	SkyMapper
2MASS J10073075+0348357	10:07:30.768	+03:48:35.800	12.375	1200	0.7	58303.5	20	273.74	262.79	LAMOST
2MASS J10524610−0336012	10:52:46.104	−03:36:01.120	14.037	1200	0.7	58184.5	25	−22.54	···	LAMOST
2MASS J10550658+1931580	10:55:06.588	+19:31:57.900	12.196	921	0.7	58302.5	25	52.69	27.67	LAMOST
2MASS J11165400−7250160	11:16:54.000	−72:50:16.000	11.409	1200	0.7	58302.5	30	218.34	209.55	RAVE
2MASS J11191233−1609467	11:19:12.300	−16:09:46.000	12.371	1800	0.7	58303.5	30	100.63	92.37	RAVE
2MASS J11264370−7525473[c]	11:26:43.682	−75:25:48.000	12.667	900	0.7	58185.5	30	12.01	−8.49	B&B
2MASS J11303693+0224037	11:30:36.936	+02:24:03.730	12.425	1200	0.7	58303.5	40	190.02	178.39	LAMOST
2MASS J11410885−4535283[c]	11:41:08.860	−45:35:28.390	11.970	3600	0.7	58302.5	55	95.30	84.61	RAVE
2MASS J11471027+0341265	11:47:10.257	+03:41:26.560	12.642	1200	0.7	58304.5	35	250.98	241.63	LAMOST
2MASS J11510227−6940416	11:51:02.280	−69:40:41.650	11.889	1200	0.7	58302.5	35	227.97	220.35	RAVE
2MASS J11555529−0447460[c]	11:55:55.284	−04:47:46.050	12.920	1500	0.7	58303.5	15	128.63	118.04	LAMOST
2MASS J11565537+0320329	11:56:55.378	+03:20:32.960	14.061	3000	0.7	58184.5	30	−154.65	···	LAMOST
2MASS J12170829+0415146	12:17:08.284	+04:15:14.530	14.153	6773	0.7	58184.5	50	282.41	···	LAMOST
2MASS J12203297+0257138	12:20:32.985	+02:57:13.930	14.167	900	0.7	58184.5	25	136.18	···	LAMOST
2MASS J12233047−4216365	12:23:30.500	−42:16:36.600	12.515	900	0.7	58184.5	60	114.95	114.23	SkyMapper
2MASS J12255123−2351074	12:25:51.200	−23:51:07.600	13.836	900	0.7	58185.5	20	106.27	···	SkyMapper
2MASS J12331670+1622563	12:33:16.701	+16:22:56.360	11.823	900	0.7	58304.5	25	14.31	4.04	LAMOST
2MASS J12351734+0945333	12:35:17.347	+09:45:33.270	13.003	600	0.7	58184.5	20	31.73	−17.89	LAMOST
2MASS J12474968−3442274[c]	12:47:49.700	−34:42:27.500	13.557	1800	0.7	58184.5	60	16.66	···	SkyMapper
2MASS J12591462−7049592	12:59:14.600	−70:49:59.000	12.351	600	0.7	57495.5	15	203.41	202.65	RAVE
2MASS J13052137−1137220	13:05:21.300	−11:37:22.000	13.370	2680	0.7	57495.5	40	0.49	···	RAVE
2MASS J13260199−0322434[c]	13:26:01.900	−03:22:43.000	10.484	600	0.7	57495.5	150	4.63	−59.01	M&P
2MASS J13261792−0945176	13:26:17.920	−09:45:17.670	13.276	900	0.7	58184.5	40	108.94	···	RAVE

Table 1 continued

Table 1 *(continued)*

Star ID	R.A.	Decl.	V mag[a]	Exp. Time	Slit	MJD	S/N	RV_{helio}	RV_{helio}(Gaia)	Source
	(J2000)			(sec)	(arcsec)		(@4000Å)	($km\,s^{-1}$)	($km\,s^{-1}$)	
2MASS J13273676−1710384	13:27:36.760	−17:10:38.500	12.534	600	0.7	58184.5	45	90.66	84.46	B&B
2MASS J13275198+0342396	13:27:51.989	+03:42:39.660	13.415	900	0.7	58185.5	30	−23.66	−29.52	LAMOST
2MASS J13373017−7717500	13:37:30.000	−77:17:49.190	12.668	600	0.7	57494.5	30	301.80	299.86	M&P
2MASS J13494713−7423395	13:49:47.130	−74:23:39.510	12.453	1200	0.7	58304.5	40	207.50	196.26	RAVE
2MASS J13511539−7340363	13:51:15.410	−73:40:36.200	13.159	600	0.7	58184.5	20	376.75	391.54	B&B
2MASS J13524835+1254216	13:52:48.350	+12:54:21.400	12.886	1200	0.7	57909.5	45	−87.85	−85.24	B&B
2MASS J13554406−3750455	13:55:44.000	−37:50:45.500	13.605	600	0.7	58184.5	25	−211.38	···	SkyMapper
2MASS J13592232−6821493	13:59:22.300	−68:21:46.600	12.968	600	0.7	57494.5	30	41.10	···	B&B
2MASS J14075721−1717102[c]	14:07:57.200	−17:17:10.000	13.407	2100	0.7	58184.5	25	22.94	···	RAVE
2MASS J14100568−0701443	14:10:05.696	−07:01:44.360	13.207	900	0.7	58184.5	30	264.20	259.93	LAMOST
2MASS J14112614−1137453	14:11:26.000	−11:37:47.300	12.370	900	0.7	58184.5	30	96.50	91.81	RAVE
2MASS J14234371−4025526	14:23:43.680	−40:25:51.600	11.888	1200	0.7	57493.5	40	−64.64	−72.99	M&P
2MASS J14335592−1240357	14:33:55.920	−12:40:37.200	11.773	2400	0.7	58304.5	50	115.91	104.52	HES
2MASS J14355850−0719265	14:35:58.500	−07:19:26.500	12.877	600	0.7	58304.5	25	−95.96	···	B&B
2MASS J14443014−1320092	14:44:30.140	−13:20:09.230	13.050	600	0.7	58184.5	30	−53.11	−50.15	RAVE
2MASS J14533268−3614555	14:53:32.600	−36:14:55.000	12.187	600	0.7	57545.5	70	170.83	167.50	M&P
2MASS J14534137+0040467	14:53:41.384	+00:40:46.750	13.196	900	0.7	57494.5	30	122.24	122.15	LAMOST
2MASS J14543792+0830379	14:54:37.920	+08:30:37.700	12.783	600	0.7	58184.5	30	14.16	16.26	B&B
2MASS J14564556−1615432	14:56:45.560	−16:15:43.230	11.778	900	0.7	58184.5	70	−76.52	−86.94	RAVE
2MASS J14590234−0916105	14:59:02.400	−09:16:10.500	13.299	900	0.7	58304.5	30	141.67	···	SkyMapper
2MASS J15013452−2443310	15:01:34.500	−24:43:30.900	13.557	900	0.7	58184.5	25	218.63	···	SkyMapper
2MASS J15042611−2231523	15:04:25.900	−22:31:55.100	13.212	900	0.7	58184.5	30	−20.82	···	B&B
2MASS J15133549−1244339	15:13:35.400	−12:44:34.000	12.742	600	0.7	58185.5	45	23.63	25.09	RAVE
2MASS J15204531−1742486	15:20:45.300	−17:42:48.700	13.781	900	0.7	58184.5	30	−148.09	···	SkyMapper
2MASS J15240713−0319509	15:24:07.100	−03:19:50.900	13.424	900	0.7	58184.5	30	−64.23	−72.62	SkyMapper
2MASS J15272126−1445153	15:27:21.300	−14:45:15.400	13.488	600	0.7	58184.5	25	377.72	···	SkyMapper
2MASS J16115667−8034422	16:11:56.680	−80:34:42.250	13.330	2400	1.0	58184.5	18	197.26	195.03	RAVE
2MASS J16163600−5700568	16:16:35.900	−57:00:57.000	10.559	600	0.7	58034.5	120	−126.60	···	M&P
2MASS J16592172−6827199	16:59:21.740	−68:27:19.790	13.084	1800	1.0	57494.5	30	472.76	471.43	RAVE
2MASS J17043634−6219457	17:04:35.700	−62:19:49.900	13.140	1200	1.0	58036.5	30	232.56	···	B&B
2MASS J17060555+0412354	17:06:05.550	+04:12:35.440	12.774	1200	0.7	57674.5	45	−195.43	−210.85	LAMOST
2MASS J17070759−7817561	17:07:07.570	−78:17:56.200	12.777	1200	1.0	58380.5	20	89.67	87.50	B&B
2MASS J17131974−7113010	17:13:19.750	−71:13:01.100	12.605	600	1.0	57675.5	30	36.36	33.09	B&B
2MASS J17163340−7009028	17:16:33.400	−70:09:02.800	13.131	600	1.0	57675.5	15	−21.45	−24.19	B&B

Table 1 continued

Table 1 *(continued)*

Star ID	R.A.	Decl.	V mag[a]	Exp. Time	Slit	MJD	S/N	RV_{helio}	RV_{helio}(Gaia)	Source
	(J2000)			(sec)	(arcsec)		(@4000Å)	($km\,s^{-1}$)	($km\,s^{-1}$)	
2MASS J17360167−5145296	17:36:02.300	−51:45:44.600	12.228	900	1.0	57675.5	45	−112.98	···	RAVE
2MASS J17541561−5148268	17:54:15.600	−51:48:25.200	12.889	3000	1.0	58380.5	60	202.45	202.15	B&B
2MASS J18272432−5655165	18:27:24.242	−56:55:15.600	12.611	1200	0.7	58033.5	45	−34.66	−38.71	B&B
2MASS J18284356−8441346	18:28:43.440	−84:41:34.810	11.527	1200	0.7	58381.5	20	−49.72	−50.34	RAVE
2MASS J18294359−4924253	18:29:43.680	−49:24:25.200	12.762	1200	0.7	58381.5	25	23.10	20.95	RAVE
2MASS J18332056−3802590	18:33:20.900	−38:02:56.700	12.912	1800	1.0	58381.5	50	15.88	···	B&B
2MASS J18333188−4840403	18:33:31.890	−48:40:40.640	12.639	1200	0.7	58036.5	45	127.95	···	RAVE/SkyMapper
2MASS J18361214−7333443	18:36:12.120	−73:33:44.170	11.798	450	1.0	58381.5	50	44.15	41.93	RAVE
2MASS J18405985−4841353	18:40:59.850	−48:41:35.300	13.004	1200	0.7	58381.5	42	76.88	72.35	B&B
2MASS J18560360−6403465	18:56:03.600	−64:03:46.800	12.782	1200	0.7	57675.5	50	248.72	261.76	SkyMapper
2MASS J19092677−5140208	19:09:26.880	−51:40:22.800	12.804	900	1.0	58381.5	30	217.49	211.73	B&B
2MASS J19105886−4059412	19:10:59.100	−40:59:40.800	12.457	500	1.0	58036.5	30	−36.12	···	RAVE
2MASS J19175585−5440147	19:17:55.800	−54:40:14.000	10.778	600	0.7	57493.5	100	34.44	31.21	RAVE
2MASS J19192768−5959140	19:19:27.700	−59:59:13.000	10.497	3353	0.7	57910.5	200	−66.33	−78.50	RAVE
2MASS J19282163−2457545	19:28:21.600	−24:57:54.000	12.600	1200	0.7	58381.5	60	189.59	188.51	RAVE
2MASS J19291910−5528181	19:29:19.000	−55:28:18.000	12.842	3900	0.7	57494.5	60	−95.67	−101.29	RAVE
2MASS J19310426−3707397	19:31:04.270	−37:07:39.830	12.779	900	1.0	58036.5	35	−13.87	−13.40	RAVE
2MASS J19320444−7309178	19:32:04.400	−73:09:17.000	10.088	600	0.7	57493.5	60	53.90	40.65	RAVE
2MASS J19504989−3321107	19:50:49.800	−33:21:10.000	12.291	4300	0.7	57191.5	80	45.06	43.96	M&P
2MASS J19532495−3647303	19:53:25.200	−36:47:35.200	12.250	900	0.7	58381.5	50	−181.59	···	RAVE
2MASS J19552158−4613569	19:55:21.570	−46:13:57.000	11.943	300	1.0	58363.5	40	157.02	155.07	RAVE
2MASS J19563822−4054235	19:56:38.200	−40:54:23.600	11.552	240	1.0	58363.5	60	−316.47	−318.36	RAVE
2MASS J19570893−3317320	19:57:08.880	−33:17:31.200	12.403	5097	0.7	57191.5	80	1.50	−0.90	RAVE
2MASS J20035532−5028100	20:03:55.310	−50:28:10.150	11.927	500	1.0	58363.5	65	−315.74	−316.66	RAVE
2MASS J20192202−6130149	20:19:22.000	−61:30:15.000	11.799	600	0.7	57493.5	60	−14.45	−16.20	RAVE
2MASS J20202917−2707347	20:20:29.100	−27:07:34.000	11.172	2150	1.0	58362.5	60	−24.67	−21.00	RAVE
2MASS J20234398−0815472	20:23:44.000	−08:15:47.700	12.657	3600	0.7	58386.5	80	−140.46	−174.85	SkyMapper
2MASS J20242122−2656435	20:24:21.200	−26:56:43.000	12.867	1200	0.7	58386.5	50	226.80	223.66	RAVE
2MASS J20374042−5520500	20:37:40.410	−55:20:49.980	12.750	4500	1.0	58033.5	60	−6.02	−4.98	RAVE
2MASS J20445065−3714000	20:44:50.600	−37:14:00.000	12.342	600	0.7	57493.5	25	160.54	162.49	RAVE
2MASS J20501790−0549230	20:50:17.900	−05:49:23.600	12.696	1200	0.7	58381.5	50	−163.33	−174.10	SkyMapper
2MASS J20585505−1759007	20:58:55.000	−17:59:00.000	12.375	2900	0.7	57493.5	85	−153.02	−155.09	RAVE
2MASS J21220020−0820333	21:22:00.204	−08:20:33.430	12.752	1200	0.7	58381.5	25	−60.93	−63.92	LAMOST
2MASS J21234588−0839448	21:23:45.800	−08:39:44.000	12.209	3150	1.0	57191.5	70	−169.16	−167.75	RAVE

Table 1 continued

Table 1 *(continued)*

Star ID	R.A.	Decl.	V mag[a]	Exp. Time	Slit	MJD	S/N	RV_{helio}	RV_{helio}(Gaia)	Source
	(J2000)			(sec)	(arcsec)		(@4000Å)	($km\,s^{-1}$)	($km\,s^{-1}$)	
2MASS J21352343−5722598	21:35:23.400	−57:23:00.100	11.836	500	1.0	58363.5	60	86.23	87.33	SkyMapper
2MASS J21372375−5302178[c]	21:37:23.700	−53:02:17.800	11.320	1200	0.7	58381.5	40	−17.50	···	SkyMapper
2MASS J21553580−0905118	21:55:35.800	−09:05:11.800	12.532	1200	0.7	58386.5	60	−89.21	−94.23	SkyMapper
2MASS J22182082−3827554	22:18:20.880	−38:27:54.000	13.462	1800	0.7	57675.5	50	252.26	···	HES
2MASS J22215794−3602090	22:21:58.000	−36:02:09.200	11.926	240	1.0	58363.5	50	73.38	77.23	SkyMapper
2MASS J22220344−8024592	22:22:03.400	−80:24:59.000	11.813	1500	1.0	57674.5	50	252.00	249.99	RAVE
2MASS J22253443−2027171	22:25:34.440	−20:27:17.270	11.821	360	1.0	58363.5	60	−218.25	−214.96	RAVE
2MASS J22300238−6332191	22:30:02.390	−63:32:19.100	13.073	600	1.0	57675.5	40	−24.73	−25.28	B&B
2MASS J22302641−1949527	22:30:26.410	−19:49:52.800	12.831	4597	0.7	58386.5	40	−42.24	−45.33	B&B
2MASS J22344202−0826492	22:34:42.030	−08:26:49.400	12.368	1200	0.7	58386.5	65	−175.28	−180.04	RAVE
2MASS J22345447−6605172	22:34:54.480	−66:05:16.790	11.359	500	1.0	58362.5	60	−57.33	−54.88	RAVE
2MASS J22394827−0803536	22:39:48.260	−08:03:53.610	13.167	3600	1.0	58034.5	30	−274.24	−274.20	RAVE
2MASS J23100319−7702165	23:10:03.230	−77:02:16.640	11.943	300	1.0	58363.5	30	−56.11	−53.87	RAVE
2MASS J23411581−6406440	23:41:15.800	−64:06:44.100	12.783	1200	0.7	58386.5	60	122.33	120.67	SkyMapper

[a] Magnitudes from RAVE DR5 (Kunder et al. 2017).

[b] Re-discovery of the ultra-metal-poor (UMP) star CD-38°245.

[c] Double-lined spectroscopic binaries (SB2).

Table 2. Atomic line properties, equivalent widths and abundances of the target stars. Only one star is shown here. Full table for the rest of sample will be available electronically.

Star ID	λ (Å)	Species	χ (eV)	log gf	EW (mÅ)	$A(X)$ (dex)
2MASS J00011195+0321051	5688.205	Na I	2.10	−0.452	15.09	4.22
2MASS J00011195+0321051	5895.924	Na I	0.00	−0.194	175.60	4.28
2MASS J00011195+0321051	4057.505	Mg I	4.35	−0.890	92.51	6.24
2MASS J00011195+0321051	4167.271	Mg I	4.35	−0.710	88.96	6.00
2MASS J00011195+0321051	4571.096	Mg I	0.00	−5.688	98.88	6.06
2MASS J00011195+0321051	4702.990	Mg I	4.33	−0.380	107.99	5.81
2MASS J00011195+0321051	5528.405	Mg I	4.34	−0.498	113.85	6.00
2MASS J00011195+0321051	5711.090	Mg I	4.34	−1.724	30.35	5.88
2MASS J00011195+0321051	4102.936	Si I	1.91	−3.140	90.72	5.67
2MASS J00011195+0321051	7698.960	K I	0.00	−0.168	84.41	3.70
2MASS J00011195+0321051	4425.440	Ca I	1.88	−0.358	74.48	4.43
2MASS J00011195+0321051	4435.690	Ca I	1.89	−0.519	88.85	4.90
2MASS J00011195+0321051	4455.890	Ca I	1.90	−0.530	76.08	4.65
2MASS J00011195+0321051	5262.244	Ca I	2.52	−0.471	68.06	5.07
2MASS J00011195+0321051	5349.465	Ca I	2.71	−0.310	39.68	4.61
2MASS J00011195+0321051	5581.971	Ca I	2.52	−0.555	37.57	4.60
2MASS J00011195+0321051	5588.760	Ca I	2.52	0.210	84.32	4.69
2MASS J00011195+0321051	5590.120	Ca I	2.52	−0.571	38.64	4.63
2MASS J00011195+0321051	5594.468	Ca I	2.52	0.097	82.24	4.75
2MASS J00011195+0321051	5598.487	Ca I	2.52	−0.087	79.26	4.88
2MASS J00011195+0321051	5601.285	Ca I	2.53	−0.523	38.31	4.58
2MASS J00011195+0321051	5857.450	Ca I	2.93	0.230	59.55	4.66
2MASS J00011195+0321051	6102.720	Ca I	1.88	−0.790	73.46	4.69
2MASS J00011195+0321051	6122.220	Ca I	1.89	−0.315	104.51	4.78
2MASS J00011195+0321051	6162.170	Ca I	1.90	−0.089	114.84	4.75
2MASS J00011195+0321051	6169.055	Ca I	2.52	−0.797	29.29	4.65
2MASS J00011195+0321051	6169.559	Ca I	2.53	−0.478	45.02	4.64
2MASS J00011195+0321051	6439.070	Ca I	2.52	0.470	97.75	4.64
2MASS J00011195+0321051	6449.810	Ca I	2.52	−0.502	46.69	4.67
2MASS J00011195+0321051	6499.649	Ca I	2.52	−0.818	22.82	4.51
2MASS J00011195+0321051	6717.685	Ca I	2.71	−0.524	39.25	4.76
2MASS J00011195+0321051	4246.820	Sc II	0.32	0.240	142.46	1.38
2MASS J00011195+0321051	4400.389	Sc II	0.61	−0.540	88.89	1.10
2MASS J00011195+0321051	4415.544	Sc II	0.59	−0.670	80.84	1.03
2MASS J00011195+0321051	5031.010	Sc II	1.36	−0.400	52.75	1.06
2MASS J00011195+0321051	5239.811	Sc II	1.46	−0.770	33.28	1.19
2MASS J00011195+0321051	5526.785	Sc II	1.77	0.020	50.21	1.04
2MASS J00011195+0321051	5641.000	Sc II	1.50	−1.130	25.07	1.40
2MASS J00011195+0321051	5657.907	Sc II	1.51	−0.600	41.28	1.19
2MASS J00011195+0321051	5667.164	Sc II	1.50	−1.310	13.46	1.25
2MASS J00011195+0321051	5669.055	Sc II	1.50	−1.200	14.52	1.17

Table 2 continued

Table 2 *(continued)*

Star ID	λ (Å)	Species	χ (eV)	log gf	EW (mÅ)	$A(X)$ (dex)
2MASS J00011195+0321051	6604.578	Sc II	1.36	−1.310	17.82	1.18
2MASS J00011195+0321051	3989.760	Ti I	0.02	−0.062	95.71	3.17
2MASS J00011195+0321051	3998.640	Ti I	0.05	0.010	76.04	2.63
2MASS J00011195+0321051	4008.928	Ti I	0.02	−1.016	51.22	3.11
2MASS J00011195+0321051	4512.730	Ti I	0.84	−0.424	28.21	2.96
2MASS J00011195+0321051	4533.249	Ti I	0.85	0.532	72.58	2.85
2MASS J00011195+0321051	4534.780	Ti I	0.84	0.336	66.54	2.91
2MASS J00011195+0321051	4544.687	Ti I	0.82	−0.520	37.42	3.22
2MASS J00011195+0321051	4548.760	Ti I	0.83	−0.298	37.50	3.01
2MASS J00011195+0321051	4555.490	Ti I	0.85	−0.432	28.85	3.00
2MASS J00011195+0321051	4656.470	Ti I	0.00	−1.289	41.73	3.10
2MASS J00011195+0321051	4681.910	Ti I	0.05	−1.015	55.57	3.11
2MASS J00011195+0321051	4840.870	Ti I	0.90	−0.453	29.86	3.07
2MASS J00011195+0321051	4981.730	Ti I	0.84	0.560	85.80	3.02
2MASS J00011195+0321051	4991.070	Ti I	0.84	0.436	93.52	3.29
2MASS J00011195+0321051	4999.500	Ti I	0.83	0.306	77.65	3.08
2MASS J00011195+0321051	5007.206	Ti I	0.82	0.168	86.01	3.37
2MASS J00011195+0321051	5016.160	Ti I	0.85	−0.518	30.48	3.08
2MASS J00011195+0321051	5020.024	Ti I	0.84	−0.358	41.80	3.12
2MASS J00011195+0321051	5035.902	Ti I	1.46	0.260	39.03	3.17
2MASS J00011195+0321051	5036.463	Ti I	1.44	0.186	24.56	2.92
2MASS J00011195+0321051	5038.396	Ti I	1.43	0.069	22.95	2.99
2MASS J00011195+0321051	5039.960	Ti I	0.02	−1.130	49.01	3.04
2MASS J00011195+0321051	5064.650	Ti I	0.05	−0.935	59.82	3.07
2MASS J00011195+0321051	5173.740	Ti I	0.00	−1.062	56.79	3.07
2MASS J00011195+0321051	5192.970	Ti I	0.02	−0.950	73.42	3.27
2MASS J00011195+0321051	5210.390	Ti I	0.05	−0.828	72.35	3.17
2MASS J00011195+0321051	6258.099	Ti I	1.44	−0.299	18.06	3.17
2MASS J00011195+0321051	4025.120	Ti II	0.61	−1.980	82.81	2.92
2MASS J00011195+0321051	4028.338	Ti II	1.89	−0.960	83.05	3.40
2MASS J00011195+0321051	4053.829	Ti II	1.89	−1.210	54.27	3.01
2MASS J00011195+0321051	4161.527	Ti II	1.08	−2.160	69.11	3.31
2MASS J00011195+0321051	4163.634	Ti II	2.59	−0.400	67.78	3.27
2MASS J00011195+0321051	4184.309	Ti II	1.08	−2.510	43.56	3.16
2MASS J00011195+0321051	4330.723	Ti II	1.18	−2.060	53.77	2.99
2MASS J00011195+0321051	4394.059	Ti II	1.22	−1.780	61.91	2.90
2MASS J00011195+0321051	4395.839	Ti II	1.24	−1.930	49.70	2.85
2MASS J00011195+0321051	4399.765	Ti II	1.24	−1.190	99.37	3.16
2MASS J00011195+0321051	4417.714	Ti II	1.17	−1.190	101.12	3.10
2MASS J00011195+0321051	4418.331	Ti II	1.24	−1.970	62.21	3.11
2MASS J00011195+0321051	4441.731	Ti II	1.18	−2.410	53.81	3.33
2MASS J00011195+0321051	4443.801	Ti II	1.08	−0.720	119.70	2.99
2MASS J00011195+0321051	4444.554	Ti II	1.12	−2.240	66.43	3.32
2MASS J00011195+0321051	4450.482	Ti II	1.08	−1.520	93.88	3.15
2MASS J00011195+0321051	4464.448	Ti II	1.16	−1.810	73.78	3.08
2MASS J00011195+0321051	4468.517	Ti II	1.13	−0.600	129.40	3.16

Table 2 continued

Table 2 *(continued)*

Star ID	λ (Å)	Species	χ (eV)	log gf	EW (mÅ)	$A(X)$ (dex)
2MASS J00011195+0321051	4470.853	Ti II	1.17	−2.020	62.19	3.07
2MASS J00011195+0321051	4488.342	Ti II	3.12	−0.820	24.53	3.38
2MASS J00011195+0321051	4493.522	Ti II	1.08	−3.020	27.55	3.33
2MASS J00011195+0321051	4501.270	Ti II	1.12	−0.770	126.14	3.22
2MASS J00011195+0321051	4529.480	Ti II	1.57	−2.030	69.58	3.69
2MASS J00011195+0321051	4563.770	Ti II	1.22	−0.960	117.97	3.31
2MASS J00011195+0321051	4571.971	Ti II	1.57	−0.320	123.90	3.23
2MASS J00011195+0321051	4583.409	Ti II	1.16	−2.920	23.46	3.21
2MASS J00011195+0321051	4589.915	Ti II	1.24	−1.790	86.74	3.40
2MASS J00011195+0321051	4636.320	Ti II	1.16	−3.020	16.12	3.11
2MASS J00011195+0321051	4657.200	Ti II	1.24	−2.240	58.51	3.28
2MASS J00011195+0321051	4708.662	Ti II	1.24	−2.340	47.87	3.19
2MASS J00011195+0321051	4779.979	Ti II	2.05	−1.370	49.30	3.18
2MASS J00011195+0321051	4798.532	Ti II	1.08	−2.680	51.27	3.39
2MASS J00011195+0321051	4805.089	Ti II	2.06	−1.100	69.71	3.29
2MASS J00011195+0321051	4865.610	Ti II	1.12	−2.810	34.10	3.26
2MASS J00011195+0321051	4911.175	Ti II	3.12	−0.340	22.52	2.82
2MASS J00011195+0321051	5129.156	Ti II	1.89	−1.240	71.83	3.24
2MASS J00011195+0321051	5185.902	Ti II	1.89	−1.490	61.55	3.29
2MASS J00011195+0321051	5336.786	Ti II	1.58	−1.590	72.54	3.22
2MASS J00011195+0321051	5381.021	Ti II	1.57	−1.920	51.47	3.16
2MASS J00011195+0321051	3951.960	V II	1.48	−0.784	61.96	2.19
2MASS J00011195+0321051	4005.710	V II	1.82	−0.522	67.16	2.43
2MASS J00011195+0321051	4023.378	V II	1.80	−0.689	39.42	2.01
2MASS J00011195+0321051	4558.594	Cr II	4.07	−0.656	44.49	3.81
2MASS J00011195+0321051	4588.142	Cr II	4.07	−0.826	31.46	3.71
2MASS J00011195+0321051	4591.992	Cr II	4.07	−1.419	12.20	3.76
2MASS J00011195+0321051	4041.357	Mn I	2.11	0.285	72.81	3.18
2MASS J00011195+0321051	4754.048	Mn I	2.28	−0.086	36.13	2.92
2MASS J00011195+0321051	4783.432	Mn I	2.30	0.042	48.15	3.02
2MASS J00011195+0321051	4823.528	Mn I	2.32	0.144	61.32	3.19
2MASS J00011195+0321051	3689.458	Fe I	2.94	−0.168	100.67	5.71
2MASS J00011195+0321051	3753.611	Fe I	2.18	−0.890	105.44	5.67
2MASS J00011195+0321051	3786.677	Fe I	1.01	−2.185	114.74	5.82
2MASS J00011195+0321051	3805.343	Fe I	3.30	0.313	96.74	5.46
2MASS J00011195+0321051	3839.256	Fe I	3.05	−0.330	74.21	5.18
2MASS J00011195+0321051	3845.169	Fe I	2.42	−1.390	81.97	5.72
2MASS J00011195+0321051	3846.800	Fe I	3.25	−0.020	98.44	5.77
2MASS J00011195+0321051	3852.573	Fe I	2.18	−1.180	97.73	5.64
2MASS J00011195+0321051	3863.741	Fe I	2.69	−1.430	69.12	5.74
2MASS J00011195+0321051	3867.216	Fe I	3.02	−0.450	69.65	5.14
2MASS J00011195+0321051	3885.510	Fe I	2.42	−1.090	75.70	5.24
2MASS J00011195+0321051	3917.181	Fe I	0.99	−2.155	109.08	5.46
2MASS J00011195+0321051	3949.953	Fe I	2.18	−1.251	84.59	5.34
2MASS J00011195+0321051	3977.741	Fe I	2.20	−1.120	97.82	5.58
2MASS J00011195+0321051	4001.661	Fe I	2.18	−1.900	62.03	5.42

Table 2 continued

Table 2 *(continued)*

Star ID	λ (Å)	Species	χ (eV)	log gf	EW (mÅ)	$A(X)$ (dex)
2MASS J00011195+0321051	4007.272	Fe I	2.76	−1.280	51.47	5.25
2MASS J00011195+0321051	4014.531	Fe I	3.05	−0.590	83.98	5.65
2MASS J00011195+0321051	4021.866	Fe I	2.76	−0.730	78.54	5.30
2MASS J00011195+0321051	4032.627	Fe I	1.49	−2.380	73.55	5.33
2MASS J00011195+0321051	4044.609	Fe I	2.83	−1.220	59.85	5.43
2MASS J00011195+0321051	4058.217	Fe I	3.21	−1.110	51.18	5.57
2MASS J00011195+0321051	4062.441	Fe I	2.85	−0.860	67.93	5.26
2MASS J00011195+0321051	4067.271	Fe I	2.56	−1.419	71.06	5.57
2MASS J00011195+0321051	4067.978	Fe I	3.21	−0.470	67.82	5.28
2MASS J00011195+0321051	4070.769	Fe I	3.24	−0.790	48.86	5.24
2MASS J00011195+0321051	4073.763	Fe I	3.27	−0.900	54.20	5.49
2MASS J00011195+0321051	4076.629	Fe I	3.21	−0.370	86.90	5.63
2MASS J00011195+0321051	4079.838	Fe I	2.86	−1.360	36.77	5.15
2MASS J00011195+0321051	4095.970	Fe I	2.59	−1.480	67.07	5.56
2MASS J00011195+0321051	4098.176	Fe I	3.24	−0.880	52.83	5.41
2MASS J00011195+0321051	4109.057	Fe I	3.29	−1.560	40.66	5.91
2MASS J00011195+0321051	4109.802	Fe I	2.85	−0.940	69.83	5.38
2MASS J00011195+0321051	4114.445	Fe I	2.83	−1.303	52.44	5.35
2MASS J00011195+0321051	4120.207	Fe I	2.99	−1.270	44.91	5.35
2MASS J00011195+0321051	4121.802	Fe I	2.83	−1.450	50.09	5.45
2MASS J00011195+0321051	4132.899	Fe I	2.85	−1.010	67.16	5.38
2MASS J00011195+0321051	4134.678	Fe I	2.83	−0.649	81.41	5.33
2MASS J00011195+0321051	4136.998	Fe I	3.42	−0.450	56.44	5.25
2MASS J00011195+0321051	4139.927	Fe I	0.99	−3.629	58.40	5.65
2MASS J00011195+0321051	4143.414	Fe I	3.05	−0.200	101.76	5.67
2MASS J00011195+0321051	4147.669	Fe I	1.48	−2.071	85.83	5.27
2MASS J00011195+0321051	4152.169	Fe I	0.96	−3.232	87.36	5.86
2MASS J00011195+0321051	4153.899	Fe I	3.40	−0.320	60.29	5.16
2MASS J00011195+0321051	4154.498	Fe I	2.83	−0.688	81.57	5.38
2MASS J00011195+0321051	4154.805	Fe I	3.37	−0.400	65.58	5.32
2MASS J00011195+0321051	4156.799	Fe I	2.83	−0.808	78.17	5.41
2MASS J00011195+0321051	4157.780	Fe I	3.42	−0.403	63.10	5.33
2MASS J00011195+0321051	4158.793	Fe I	3.43	−0.670	43.23	5.21
2MASS J00011195+0321051	4174.913	Fe I	0.91	−2.938	83.92	5.42
2MASS J00011195+0321051	4175.636	Fe I	2.85	−0.827	71.92	5.30
2MASS J00011195+0321051	4181.755	Fe I	2.83	−0.371	99.73	5.51
2MASS J00011195+0321051	4182.382	Fe I	3.02	−1.180	43.53	5.26
2MASS J00011195+0321051	4184.892	Fe I	2.83	−0.869	72.21	5.33
2MASS J00011195+0321051	4187.039	Fe I	2.45	−0.514	96.76	5.08
2MASS J00011195+0321051	4187.795	Fe I	2.42	−0.510	117.33	5.50
2MASS J00011195+0321051	4191.430	Fe I	2.47	−0.666	98.02	5.29
2MASS J00011195+0321051	4195.329	Fe I	3.33	−0.492	73.34	5.54
2MASS J00011195+0321051	4196.208	Fe I	3.40	−0.700	53.55	5.40
2MASS J00011195+0321051	4199.095	Fe I	3.05	0.156	99.76	5.24
2MASS J00011195+0321051	4216.184	Fe I	0.00	−3.357	115.70	5.55
2MASS J00011195+0321051	4217.545	Fe I	3.43	−0.484	66.54	5.48

Table 2 continued

Table 2 *(continued)*

Star ID	λ (Å)	Species	χ (eV)	log gf	EW (mÅ)	$A(X)$ (dex)
2MASS J00011195+0321051	4222.213	Fe I	2.45	−0.914	89.48	5.30
2MASS J00011195+0321051	4227.427	Fe I	3.33	0.266	109.18	5.68
2MASS J00011195+0321051	4233.603	Fe I	2.48	−0.579	97.90	5.19
2MASS J00011195+0321051	4238.810	Fe I	3.40	−0.233	67.27	5.21
2MASS J00011195+0321051	4250.119	Fe I	2.47	−0.380	111.24	5.28
2MASS J00011195+0321051	4271.154	Fe I	2.45	−0.337	131.47	5.59
2MASS J00011195+0321051	4282.403	Fe I	2.18	−0.779	104.87	5.29
2MASS J00011195+0321051	4337.046	Fe I	1.56	−1.695	115.07	5.65
2MASS J00011195+0321051	4352.735	Fe I	2.22	−1.290	96.79	5.59
2MASS J00011195+0321051	4407.709	Fe I	2.18	−1.970	87.38	5.93
2MASS J00011195+0321051	4422.568	Fe I	2.85	−1.110	75.01	5.60
2MASS J00011195+0321051	4427.310	Fe I	0.05	−2.924	124.54	5.30
2MASS J00011195+0321051	4430.614	Fe I	2.22	−1.659	77.82	5.44
2MASS J00011195+0321051	4442.339	Fe I	2.20	−1.228	104.97	5.59
2MASS J00011195+0321051	4443.194	Fe I	2.86	−1.043	61.67	5.26
2MASS J00011195+0321051	4447.717	Fe I	2.22	−1.339	94.83	5.50
2MASS J00011195+0321051	4454.381	Fe I	2.83	−1.300	57.26	5.39
2MASS J00011195+0321051	4459.118	Fe I	2.18	−1.279	113.69	5.78
2MASS J00011195+0321051	4461.653	Fe I	0.09	−3.194	116.77	5.40
2MASS J00011195+0321051	4466.552	Fe I	2.83	−0.600	92.25	5.47
2MASS J00011195+0321051	4476.019	Fe I	2.85	−0.820	103.98	6.01
2MASS J00011195+0321051	4484.220	Fe I	3.60	−0.860	46.90	5.63
2MASS J00011195+0321051	4489.739	Fe I	0.12	−3.899	94.19	5.58
2MASS J00011195+0321051	4494.563	Fe I	2.20	−1.143	103.05	5.43
2MASS J00011195+0321051	4528.614	Fe I	2.18	−0.822	132.78	5.64
2MASS J00011195+0321051	4531.148	Fe I	1.48	−2.101	98.70	5.50
2MASS J00011195+0321051	4592.651	Fe I	1.56	−2.462	89.63	5.72
2MASS J00011195+0321051	4595.359	Fe I	3.29	−1.758	18.97	5.58
2MASS J00011195+0321051	4602.941	Fe I	1.49	−2.208	90.03	5.41
2MASS J00011195+0321051	4630.120	Fe I	2.28	−2.587	34.30	5.59
2MASS J00011195+0321051	4632.912	Fe I	1.61	−2.913	58.53	5.58
2MASS J00011195+0321051	4643.463	Fe I	3.64	−1.147	17.82	5.32
2MASS J00011195+0321051	4647.434	Fe I	2.95	−1.351	52.00	5.46
2MASS J00011195+0321051	4678.846	Fe I	3.60	−0.830	42.29	5.50
2MASS J00011195+0321051	4691.411	Fe I	2.99	−1.520	52.52	5.68
2MASS J00011195+0321051	4707.274	Fe I	3.24	−1.080	55.33	5.57
2MASS J00011195+0321051	4710.283	Fe I	3.02	−1.610	41.31	5.60
2MASS J00011195+0321051	4736.772	Fe I	3.21	−0.752	71.67	5.52
2MASS J00011195+0321051	4786.806	Fe I	3.00	−1.606	41.77	5.58
2MASS J00011195+0321051	4789.650	Fe I	3.53	−0.957	35.02	5.40
2MASS J00011195+0321051	4859.741	Fe I	2.88	−0.760	87.28	5.46
2MASS J00011195+0321051	4871.318	Fe I	2.87	−0.362	106.70	5.45
2MASS J00011195+0321051	4872.137	Fe I	2.88	−0.567	95.60	5.44
2MASS J00011195+0321051	4890.755	Fe I	2.88	−0.394	103.10	5.42
2MASS J00011195+0321051	4891.492	Fe I	2.85	−0.111	114.99	5.34
2MASS J00011195+0321051	4903.310	Fe I	2.88	−0.926	80.56	5.48

Table 2 continued

Table 2 *(continued)*

Star ID	λ (Å)	Species	χ (eV)	log gf	EW (mÅ)	$A(X)$ (dex)
2MASS J00011195+0321051	4918.994	Fe I	2.85	−0.342	108.20	5.42
2MASS J00011195+0321051	4920.503	Fe I	2.83	0.068	128.01	5.36
2MASS J00011195+0321051	4924.770	Fe I	2.28	−2.114	59.77	5.55
2MASS J00011195+0321051	4938.814	Fe I	2.88	−1.077	70.68	5.42
2MASS J00011195+0321051	4939.687	Fe I	0.86	−3.252	89.37	5.60
2MASS J00011195+0321051	4946.388	Fe I	3.37	−1.170	41.06	5.53
2MASS J00011195+0321051	4966.089	Fe I	3.33	−0.871	57.63	5.49
2MASS J00011195+0321051	4973.102	Fe I	3.96	−0.950	26.98	5.70
2MASS J00011195+0321051	4994.130	Fe I	0.92	−2.969	97.83	5.57
2MASS J00011195+0321051	5001.870	Fe I	3.88	0.050	60.19	5.25
2MASS J00011195+0321051	5006.119	Fe I	2.83	−0.615	93.99	5.37
2MASS J00011195+0321051	5012.068	Fe I	0.86	−2.642	110.36	5.45
2MASS J00011195+0321051	5014.942	Fe I	3.94	−0.300	46.68	5.42
2MASS J00011195+0321051	5022.236	Fe I	3.98	−0.530	35.29	5.47
2MASS J00011195+0321051	5028.127	Fe I	3.56	−1.122	23.07	5.32
2MASS J00011195+0321051	5041.072	Fe I	0.96	−3.090	98.62	5.76
2MASS J00011195+0321051	5041.756	Fe I	1.49	−2.200	107.73	5.71
2MASS J00011195+0321051	5044.212	Fe I	2.85	−2.017	22.96	5.40
2MASS J00011195+0321051	5049.820	Fe I	2.28	−1.355	92.88	5.44
2MASS J00011195+0321051	5051.634	Fe I	0.92	−2.764	105.95	5.53
2MASS J00011195+0321051	5060.080	Fe I	0.00	−5.460	27.83	5.61
2MASS J00011195+0321051	5068.766	Fe I	2.94	−1.041	69.94	5.42
2MASS J00011195+0321051	5074.749	Fe I	4.22	−0.200	50.68	5.71
2MASS J00011195+0321051	5079.224	Fe I	2.20	−2.105	74.97	5.72
2MASS J00011195+0321051	5079.740	Fe I	0.99	−3.245	93.58	5.83
2MASS J00011195+0321051	5083.339	Fe I	0.96	−2.842	105.47	5.64
2MASS J00011195+0321051	5090.770	Fe I	4.26	−0.360	24.27	5.38
2MASS J00011195+0321051	5098.697	Fe I	2.18	−2.030	80.25	5.74
2MASS J00011195+0321051	5110.413	Fe I	0.00	−3.760	119.56	5.69
2MASS J00011195+0321051	5123.720	Fe I	1.01	−3.058	99.09	5.77
2MASS J00011195+0321051	5125.117	Fe I	4.22	−0.140	42.40	5.49
2MASS J00011195+0321051	5127.360	Fe I	0.92	−3.249	91.45	5.68
2MASS J00011195+0321051	5131.468	Fe I	2.22	−2.515	40.18	5.52
2MASS J00011195+0321051	5133.689	Fe I	4.18	0.140	66.11	5.60
2MASS J00011195+0321051	5137.382	Fe I	4.18	−0.400	42.91	5.71
2MASS J00011195+0321051	5141.739	Fe I	2.42	−2.238	37.32	5.42
2MASS J00011195+0321051	5142.929	Fe I	0.96	−3.080	107.03	5.91
2MASS J00011195+0321051	5150.839	Fe I	0.99	−3.037	94.74	5.63
2MASS J00011195+0321051	5151.911	Fe I	1.01	−3.321	83.71	5.70
2MASS J00011195+0321051	5162.273	Fe I	4.18	0.020	55.02	5.51
2MASS J00011195+0321051	5166.282	Fe I	0.00	−4.123	96.78	5.54
2MASS J00011195+0321051	5171.596	Fe I	1.49	−1.721	122.78	5.53
2MASS J00011195+0321051	5191.455	Fe I	3.04	−0.551	108.22	5.81
2MASS J00011195+0321051	5192.344	Fe I	3.00	−0.421	94.35	5.36
2MASS J00011195+0321051	5194.942	Fe I	1.56	−2.021	99.48	5.39
2MASS J00011195+0321051	5198.711	Fe I	2.22	−2.091	63.62	5.50

Table 2 continued

Table 2 *(continued)*

Star ID	λ (Å)	Species	χ (eV)	log gf	EW (mÅ)	$A(X)$ (dex)
2MASS J00011195+0321051	5202.336	Fe I	2.18	−1.871	94.74	5.86
2MASS J00011195+0321051	5216.274	Fe I	1.61	−2.082	100.43	5.52
2MASS J00011195+0321051	5217.390	Fe I	3.21	−1.162	48.86	5.46
2MASS J00011195+0321051	5225.526	Fe I	0.11	−4.755	59.24	5.58
2MASS J00011195+0321051	5232.940	Fe I	2.94	−0.057	118.30	5.39
2MASS J00011195+0321051	5242.491	Fe I	3.63	−0.967	35.02	5.50
2MASS J00011195+0321051	5247.050	Fe I	0.09	−4.946	54.19	5.66
2MASS J00011195+0321051	5250.210	Fe I	0.12	−4.938	55.01	5.70
2MASS J00011195+0321051	5250.646	Fe I	2.20	−2.180	71.66	5.71
2MASS J00011195+0321051	5254.956	Fe I	0.11	−4.764	74.66	5.85
2MASS J00011195+0321051	5263.305	Fe I	3.27	−0.879	58.46	5.42
2MASS J00011195+0321051	5266.555	Fe I	3.00	−0.385	99.98	5.43
2MASS J00011195+0321051	5281.790	Fe I	3.04	−0.833	77.87	5.46
2MASS J00011195+0321051	5283.621	Fe I	3.24	−0.524	84.03	5.51
2MASS J00011195+0321051	5302.300	Fe I	3.28	−0.720	62.95	5.35
2MASS J00011195+0321051	5307.361	Fe I	1.61	−2.912	62.38	5.58
2MASS J00011195+0321051	5322.040	Fe I	2.28	−2.802	18.95	5.40
2MASS J00011195+0321051	5324.179	Fe I	3.21	−0.103	102.93	5.43
2MASS J00011195+0321051	5328.531	Fe I	1.56	−1.850	127.84	5.81
2MASS J00011195+0321051	5332.900	Fe I	1.55	−2.776	72.29	5.56
2MASS J00011195+0321051	5339.930	Fe I	3.27	−0.720	77.20	5.61
2MASS J00011195+0321051	5364.871	Fe I	4.45	0.228	47.12	5.46
2MASS J00011195+0321051	5365.400	Fe I	3.56	−1.020	29.02	5.34
2MASS J00011195+0321051	5367.467	Fe I	4.42	0.443	54.20	5.34
2MASS J00011195+0321051	5369.962	Fe I	4.37	0.536	56.84	5.23
2MASS J00011195+0321051	5371.489	Fe I	0.96	−1.644	158.67	5.46
2MASS J00011195+0321051	5379.573	Fe I	3.69	−1.514	10.90	5.45
2MASS J00011195+0321051	5383.369	Fe I	4.31	0.645	68.74	5.27
2MASS J00011195+0321051	5389.479	Fe I	4.42	−0.410	22.33	5.55
2MASS J00011195+0321051	5393.168	Fe I	3.24	−0.910	66.04	5.54
2MASS J00011195+0321051	5397.128	Fe I	0.92	−1.982	133.80	5.27
2MASS J00011195+0321051	5405.775	Fe I	0.99	−1.852	145.22	5.45
2MASS J00011195+0321051	5410.910	Fe I	4.47	0.398	46.61	5.30
2MASS J00011195+0321051	5415.199	Fe I	4.39	0.643	59.47	5.20
2MASS J00011195+0321051	5424.068	Fe I	4.32	0.520	72.89	5.49
2MASS J00011195+0321051	5429.696	Fe I	0.96	−1.881	161.40	5.73
2MASS J00011195+0321051	5434.524	Fe I	1.01	−2.126	126.50	5.37
2MASS J00011195+0321051	5446.917	Fe I	0.99	−1.910	149.72	5.58
2MASS J00011195+0321051	5497.516	Fe I	1.01	−2.825	112.60	5.76
2MASS J00011195+0321051	5501.465	Fe I	0.96	−3.046	95.44	5.55
2MASS J00011195+0321051	5506.779	Fe I	0.99	−2.789	104.46	5.52
2MASS J00011195+0321051	5569.618	Fe I	3.42	−0.540	73.92	5.52
2MASS J00011195+0321051	5572.842	Fe I	3.40	−0.275	85.52	5.46
2MASS J00011195+0321051	5576.088	Fe I	3.43	−1.000	52.35	5.59
2MASS J00011195+0321051	5586.756	Fe I	3.37	−0.144	96.33	5.50
2MASS J00011195+0321051	5615.644	Fe I	3.33	0.050	108.73	5.50

Table 2 continued

Table 2 *(continued)*

Star ID	λ (Å)	Species	χ (eV)	log gf	EW (mÅ)	$A(X)$ (dex)
2MASS J00011195+0321051	5624.542	Fe I	3.42	−0.755	58.41	5.45
2MASS J00011195+0321051	5658.816	Fe I	3.40	−0.793	65.78	5.59
2MASS J00011195+0321051	5662.516	Fe I	4.18	−0.573	26.25	5.53
2MASS J00011195+0321051	5701.544	Fe I	2.56	−2.143	38.83	5.48
2MASS J00011195+0321051	5753.122	Fe I	4.26	−0.688	15.76	5.45
2MASS J00011195+0321051	5816.373	Fe I	4.55	−0.601	11.43	5.52
2MASS J00011195+0321051	6065.481	Fe I	2.61	−1.410	76.09	5.45
2MASS J00011195+0321051	6136.615	Fe I	2.45	−1.410	95.04	5.62
2MASS J00011195+0321051	6137.691	Fe I	2.59	−1.346	81.69	5.47
2MASS J00011195+0321051	6151.618	Fe I	2.18	−3.371	18.30	5.79
2MASS J00011195+0321051	6191.558	Fe I	2.43	−1.416	96.58	5.64
2MASS J00011195+0321051	6200.312	Fe I	2.61	−2.437	28.44	5.60
2MASS J00011195+0321051	6213.429	Fe I	2.22	−2.481	44.21	5.48
2MASS J00011195+0321051	6230.723	Fe I	2.56	−1.276	97.09	5.65
2MASS J00011195+0321051	6246.318	Fe I	3.60	−0.877	44.70	5.50
2MASS J00011195+0321051	6252.555	Fe I	2.40	−1.687	77.91	5.49
2MASS J00011195+0321051	6254.257	Fe I	2.28	−2.443	54.68	5.69
2MASS J00011195+0321051	6265.134	Fe I	2.18	−2.540	50.08	5.60
2MASS J00011195+0321051	6297.792	Fe I	2.22	−2.640	39.03	5.55
2MASS J00011195+0321051	6301.499	Fe I	3.65	−0.718	52.17	5.54
2MASS J00011195+0321051	6322.684	Fe I	2.59	−2.469	25.73	5.54
2MASS J00011195+0321051	6335.330	Fe I	2.20	−2.180	64.54	5.50
2MASS J00011195+0321051	6336.835	Fe I	3.69	−1.050	37.59	5.64
2MASS J00011195+0321051	6344.148	Fe I	2.43	−2.877	18.65	5.59
2MASS J00011195+0321051	6355.029	Fe I	2.84	−2.291	20.85	5.53
2MASS J00011195+0321051	6393.601	Fe I	2.43	−1.576	89.95	5.64
2MASS J00011195+0321051	6411.649	Fe I	3.65	−0.595	57.18	5.48
2MASS J00011195+0321051	6421.350	Fe I	2.28	−2.014	72.13	5.55
2MASS J00011195+0321051	6430.846	Fe I	2.18	−1.946	81.37	5.54
2MASS J00011195+0321051	6494.980	Fe I	2.40	−1.239	112.67	5.70
2MASS J00011195+0321051	6498.940	Fe I	0.96	−4.699	21.38	5.75
2MASS J00011195+0321051	6592.912	Fe I	2.73	−1.473	69.29	5.49
2MASS J00011195+0321051	6593.868	Fe I	2.44	−2.366	41.71	5.57
2MASS J00011195+0321051	6609.109	Fe I	2.56	−2.661	24.45	5.65
2MASS J00011195+0321051	6663.440	Fe I	2.42	−2.479	40.33	5.63
2MASS J00011195+0321051	6677.986	Fe I	2.69	−1.418	82.78	5.63
2MASS J00011195+0321051	6750.152	Fe I	2.42	−2.584	34.64	5.62
2MASS J00011195+0321051	6978.850	Fe I	2.48	−2.452	38.96	5.63
2MASS J00011195+0321051	4178.860	Fe II	2.58	−2.510	75.86	5.48
2MASS J00011195+0321051	4233.170	Fe II	2.58	−1.970	99.01	5.46
2MASS J00011195+0321051	4416.817	Fe II	2.78	−2.600	66.39	5.54
2MASS J00011195+0321051	4489.185	Fe II	2.83	−2.970	47.91	5.60
2MASS J00011195+0321051	4491.410	Fe II	2.86	−2.710	50.84	5.43
2MASS J00011195+0321051	4508.283	Fe II	2.86	−2.580	65.29	5.58
2MASS J00011195+0321051	4515.340	Fe II	2.84	−2.600	62.92	5.52
2MASS J00011195+0321051	4520.224	Fe II	2.81	−2.600	59.09	5.42

Table 2 continued

Table 2 *(continued)*

Star ID	λ (Å)	Species	χ (eV)	log gf	EW (mÅ)	$A(X)$ (dex)
2MASS J00011195+0321051	4541.523	Fe II	2.86	−3.050	40.05	5.55
2MASS J00011195+0321051	4555.890	Fe II	2.83	−2.400	80.33	5.68
2MASS J00011195+0321051	4576.340	Fe II	2.84	−2.950	37.79	5.38
2MASS J00011195+0321051	4583.840	Fe II	2.81	−1.930	94.06	5.47
2MASS J00011195+0321051	4620.520	Fe II	2.83	−3.210	26.37	5.39
2MASS J00011195+0321051	4731.439	Fe II	2.89	−3.360	34.82	5.79
2MASS J00011195+0321051	4923.930	Fe II	2.89	−1.320	117.22	5.39
2MASS J00011195+0321051	4993.350	Fe II	2.81	−3.670	13.02	5.42
2MASS J00011195+0321051	5018.450	Fe II	2.89	−1.220	123.97	5.39
2MASS J00011195+0321051	5197.580	Fe II	3.23	−2.220	55.67	5.39
2MASS J00011195+0321051	5234.630	Fe II	3.22	−2.180	56.72	5.37
2MASS J00011195+0321051	5276.000	Fe II	3.20	−2.010	85.76	5.70
2MASS J00011195+0321051	5284.080	Fe II	2.89	−3.190	29.11	5.47
2MASS J00011195+0321051	5325.550	Fe II	3.22	−3.160	18.25	5.54
2MASS J00011195+0321051	5534.834	Fe II	3.25	−2.930	31.91	5.67
2MASS J00011195+0321051	6247.545	Fe II	3.89	−2.510	21.75	5.72
2MASS J00011195+0321051	6432.680	Fe II	2.89	−3.710	18.20	5.67
2MASS J00011195+0321051	6456.383	Fe II	3.90	−2.080	26.68	5.41
2MASS J00011195+0321051	4020.898	Co I	0.43	−2.070	54.79	3.24
2MASS J00011195+0321051	4110.532	Co I	1.05	−1.080	56.31	2.99
2MASS J00011195+0321051	4121.318	Co I	0.92	−0.320	95.04	2.98
2MASS J00011195+0321051	3858.301	Ni I	0.42	−0.951	116.17	3.56
2MASS J00011195+0321051	4605.000	Ni I	3.48	−0.290	22.79	4.13
2MASS J00011195+0321051	4648.659	Ni I	3.42	−0.160	29.42	4.08
2MASS J00011195+0321051	4714.421	Ni I	3.38	0.230	50.44	4.04
2MASS J00011195+0321051	4904.410	Ni I	3.54	−0.170	28.23	4.18
2MASS J00011195+0321051	4980.161	Ni I	3.61	−0.110	26.00	4.15
2MASS J00011195+0321051	5017.591	Ni I	3.54	−0.080	25.13	4.01
2MASS J00011195+0321051	5035.374	Ni I	3.63	0.290	35.01	3.95
2MASS J00011195+0321051	5080.523	Ni I	3.65	0.130	37.02	4.17
2MASS J00011195+0321051	5081.110	Ni I	3.85	0.300	23.18	3.94
2MASS J00011195+0321051	5084.080	Ni I	3.68	0.030	25.09	4.06
2MASS J00011195+0321051	5578.734	Ni I	1.68	−2.640	16.47	4.16
2MASS J00011195+0321051	6108.121	Ni I	1.68	−2.450	21.31	4.08
2MASS J00011195+0321051	6643.640	Ni I	1.68	−2.300	37.74	4.24
2MASS J00011195+0321051	4722.150	Zn I	4.03	−0.390	33.67	2.74
2MASS J00011195+0321051	4810.528	Zn I	4.08	−0.137	38.03	2.63

Table 3. Stellar Atmospheric Parameters of the Target Stars

Star ID	LTE				LTE^{corr}					NLTE							
	T_{eff} (K)	log g (cgs)	ξ_t (km s^{-1})	[Fe/H]	T_{eff} (K)	log g (cgs)	ξ_t (km s^{-1})	[Fe/H]	$\sigma_{[Fe/H]}$ (dex)	T_{eff} (K)	log g (cgs)	ξ_t (km s^{-1})	[Fe/H]	$\sigma_{[Fe/H]}$ (dex)	N$_{Fe\,I}$	N$_{Fe\,II}$	log g^{Gaia} (cgs)
2MASS J00011195+0321051	4710	1.25	1.80	−2.04	4909	1.75	1.85	−1.99	0.12	4820	2.20	1.80	−1.76	0.12	237	26	2.10
2MASS J00101758−1735387	5000	1.40	2.10	−2.64	5229	2.75	1.50	−2.41	0.12	5200	3.00	1.70	−2.19	0.12	262	37	2.91
2MASS J00162809−0505519	4865	1.50	1.75	−3.23	5049	1.90	1.70	−3.07	0.10	4920	2.45	1.75	−2.82	0.10	179	18	2.50
2MASS J00195350−0145445	4590	0.60	2.45	−2.67	4801	1.18	2.29	−2.45	0.13	4720	1.95	2.10	−2.22	0.13	216	24	1.91
2MASS J00282278−3934598	4440	0.40	2.75	−2.88	4666	1.10	2.55	−2.61	0.13	4550	1.45	2.40	−2.36	0.13	194	20	1.38
2MASS J00372794−2045307	4615	0.95	2.25	−2.80	4824	1.50	2.05	−2.64	0.08	4750	2.00	2.10	−2.40	0.08	220	24	1.89
2MASS J00452379−2112161	4570	0.60	2.15	−2.97	4783	1.25	2.05	−2.63	0.14	4650	1.85	2.10	−2.40	0.14	247	26	1.79
2MASS J00463619−3739335	4525	0.60	2.80	−4.26	4743	1.20	2.00	−4.12	0.23	4650	1.50	2.00	−4.02	0.23	67	6	1.44
2MASS J00512646−1053170	6300	3.60	1.55	−2.50	6340	3.65	1.55	−2.38	0.13	6300	4.20	1.70	−2.18	0.13	205	21	3.81
2MASS J00524174−0902235	5000	1.40	1.85	−1.80	5170	1.80	1.80	−1.46	0.18	5040	2.20	1.80	−1.22	0.18	204	25	1.01
2MASS J01165010−6307441	4935	1.70	1.80	−2.10	5112	2.15	1.80	−1.64	0.09	5050	2.40	2.45	−1.40	0.09	188	23	2.29
2MASS J01374434−4301490	4490	0.55	2.65	−3.18	4711	1.15	2.40	−2.78	0.11	4620	1.60	2.45	−2.55	0.11	198	25	1.49
2MASS J01473804−1130474	4750	0.95	2.15	−2.40	4945	1.50	2.15	−2.28	0.15	4850	2.00	2.20	−2.02	0.15	206	24	1.87
2MASS J01501343+0725010	4680	0.95	2.05	−3.19	4882	1.40	1.90	−3.05	0.10	4780	1.90	2.00	−2.81	0.10	157	18	1.83
2MASS J01553180−4919420	4815	1.55	1.70	−3.20	5004	2.10	1.60	−3.01	0.06	4930	2.70	1.70	−2.78	0.06	154	14	2.55
2MASS J01555066−6400155	4565	0.80	2.45	−2.90	4779	1.45	2.25	−2.71	0.06	4680	1.85	2.30	−2.48	0.06	155	18	1.58
2MASS J02005020−4657352	4520	0.50	2.05	−4.44	4738	1.20	1.87	−4.00	0.08	4650	1.65	1.90	−3.75	0.08	121	8	1.45[a]
2MASS J02111462−8107085	5250	2.75	1.25	−2.57	5395	3.10	1.25	−2.34	0.14	5300	3.50	1.30	−2.10	0.14	234	24	3.30
2MASS J02395318−7019014	5700	4.20	1.10	−0.50	5800	4.40	1.40	−0.30	0.19	5720	4.50	1.50	−0.10	0.19	143	21	4.14
2MASS J03073894−0502491	4200	0.28	2.80	−2.45	4450	1.40	3.10	−2.22	0.23	4360	1.75	2.90	−1.98	0.23	156	16	1.39
2MASS J03154102−7626329	4430	0.40	2.65	−2.80	4657	1.20	2.35	−2.71	0.12	4550	1.55	2.30	−2.45	0.12	150	18	1.41
2MASS J03270229+0132322	5000	2.10	1.75	−2.55	5170	2.50	1.75	−2.39	0.13	5100	2.95	1.80	−2.17	0.13	208	18	2.70
2MASS J03423645−1335529	6470	4.25	1.55	−3.24	6493	4.30	1.55	−3.22	0.27	6400	4.25	1.50	−3.00	0.27	37	5	3.90
2MASS J04245677−6500173	4375	0.30	2.85	−2.75	4608	1.15	2.80	−2.37	0.14	4500	1.45	2.80	−2.14	0.14	154	24	0.98
2MASS J04304875−4613535	5055	2.45	1.45	−2.53	5215	2.85	1.40	−2.32	0.11	5140	3.00	1.50	−2.10	0.11	120	13	2.80
2MASS J05030025−7601462	4505	0.55	2.15	−2.37	4725	1.30	2.30	−2.17	0.12	4650	1.60	2.40	−1.95	0.12	151	23	1.49[a]
2MASS J05202930−5825297	4390	0.14	3.10	−3.50	4621	0.93	2.55	−3.21	0.12	4550	1.45	2.50	−2.90	0.12	192	20	1.31
2MASS J05241392−0336543	4270	0.20	3.05	−2.70	4513	1.55	3.25	−2.50	0.20	4430	2.25	3.00	−2.20	0.20	152	12	2.85
2MASS J05384334−5147228	4720	1.14	1.10	−3.05	4918	1.50	1.95	−2.92	0.14	4800	1.85	2.00	−2.70	0.14	247	26	1.98
2MASS J05432623−8051334	4690	0.68	2.22	−2.86	4891	1.14	2.18	−2.61	0.09	4700	1.55	1.70	−2.38	0.09	204	24	1.70[a]
2MASS J05573684−5127209	4900	1.30	2.10	−3.20	5080	1.95	2.12	−2.94	0.20	5000	2.20	2.20	−2.77	0.20	98	7	1.64
2MASS J06392518−7414056	4910	1.75	1.65	−2.74	5089	2.20	1.65	−2.51	0.10	5000	2.65	1.70	−2.27	0.10	220	21	2.59[a]
2MASS J07123398−4814049	4390	0.10	2.70	−2.40	4621	0.90	2.60	−1.98	0.16	4520	1.45	2.60	−1.75	0.16	231	20	1.22
2MASS J07150266−0154092	4650	2.10	2.35	−2.75	4855	2.95	1.93	−2.60	0.15	4790	3.20	2.00	−2.32	0.15	73	8	2.41
2MASS J07151852−5252051	4630	0.45	2.35	−3.12	4837	1.05	2.20	−2.90	0.12	4730	1.85	2.20	−2.65	0.12	225	24	1.63

Table 3 continued

Table 3 *(continued)*

Star ID	LTE				LTE^{corr}					NLTE					$N_{Fe\,I}$	$N_{Fe\,II}$	$\log g^{Gaia}$
	T_{eff} (K)	$\log g$ (cgs)	ξ_t (km s^{-1})	[Fe/H]	T_{eff} (K)	$\log g$ (cgs)	ξ_t (km s^{-1})	[Fe/H]	$\sigma_{[Fe/H]}$ (dex)	T_{eff} (K)	$\log g$ (cgs)	ξ_t (km s^{-1})	[Fe/H]	$\sigma_{[Fe/H]}$ (dex)			(cgs)
2MASS J07250021−7022038	4630	0.85	2.15	−2.87	4837	1.40	2.00	−2.65	0.11	4770	2.00	2.20	−2.40	0.11	156	15	2.02
2MASS J07443970−4425135	4680	1.00	1.88	−2.98	4882	1.50	1.85	−2.85	0.09	4800	1.95	2.00	−2.60	0.09	221	19	2.30
2MASS J08025449−5224304	4240	0.05	3.20	−2.82	4486	0.80	3.05	−2.68	0.16	4300	1.25	2.90	−2.41	0.16	178	25	1.28
2MASS J08295142−7242542	4800	1.00	1.78	−2.40	4990	1.40	1.65	−2.27	0.12	4880	2.05	1.60	−2.04	0.12	103	8	2.27
2MASS J09103481+0518228	4380	0.20	2.65	−3.77	4612	1.00	2.35	−3.36	0.10	4500	1.70	2.30	−3.23	0.10	161	21	1.82[a]
2MASS J09291557+0838002	4320	0.10	2.95	−2.53	4558	0.35	2.38	−2.34	0.10	4430	1.35	2.30	−2.10	0.10	89	9	1.82
2MASS J09531322+0744515	4480	0.90	2.00	−4.00	4702	1.65	2.10	−4.04	0.17	4600	1.95	2.00	−3.75	0.17	219	16	1.69[a]
2MASS J10063414−7030212	4650	1.50	1.75	−2.70	4963	1.95	1.75	−2.20	0.10	4730	2.40	1.80	−1.90	0.10	172	25	2.34
2MASS J10073075+0348357	4350	0.18	3.50	−1.91	4495	0.80	3.40	−1.71	0.24	4410	1.55	3.00	−1.55	0.24	133	10	1.63
2MASS J10524610−0336012	4580	0.70	2.25	−2.89	4790	1.55	2.30	−2.66	0.16	4650	1.85	3.10	−2.42	0.16	130	16	2.01
2MASS J10550658+1931580	4645	1.15	2.25	−2.57	4851	1.65	2.20	−2.32	0.17	4780	2.00	2.30	−2.26	0.17	110	9	1.24
2MASS J11165400−7250160	4180	0.00	2.80	−2.90	4369	0.90	3.00	−2.88	0.15	4280	1.25	2.80	−2.65	0.15	118	18	0.92
2MASS J11191233−1609467	5355	2.25	2.45	−2.55	5490	2.60	2.50	−2.34	0.10	5400	2.85	2.50	−2.10	0.10	130	20	2.29
2MASS J11303693+0224037	4480	0.50	2.70	−2.59	4702	1.10	2.45	−1.86	0.10	4620	1.70	2.50	−1.62	0.10	127	20	1.61
2MASS J11471027+0341265	4610	0.80	2.15	−2.67	4819	1.40	2.00	−2.47	0.05	4700	1.95	2.00	−2.21	0.05	144	21	1.85
2MASS J11510227−6940416	4400	0.35	2.75	−2.79	4630	1.20	2.70	−2.53	0.10	4550	1.65	2.50	−2.30	0.10	175	22	1.32
2MASS J11565537+0320329	4515	0.70	2.25	−2.49	4734	1.40	2.10	−2.31	0.08	4620	1.75	2.20	−2.08	0.08	161	22	1.69[a]
2MASS J12170829+0415146	4400	0.18	2.85	−2.39	4630	1.05	2.80	−2.22	0.19	4540	1.65	2.90	−2.00	0.19	180	17	1.56[a]
2MASS J12203297+0257138	4485	0.60	2.65	−2.88	4707	1.25	2.35	−2.63	0.09	4650	1.95	2.40	−2.40	0.09	172	18	1.83[a]
2MASS J12233047−4216365	4585	1.50	2.60	−2.48	4797	1.00	2.25	−2.33	0.04	4680	1.50	2.30	−2.08	0.04	188	18	1.41
2MASS J12255123−2351074	4800	1.45	1.75	−3.33	4990	2.05	1.70	−3.04	0.11	4800	2.15	2.20	−2.80	0.11	77	9	2.26
2MASS J12331670+1622563	4425	0.40	3.10	−3.30	4653	1.20	2.85	−2.84	0.10	4520	1.60	2.80	−2.71	0.10	111	22	1.15
2MASS J12351734+0945333	4400	0.40	2.65	−2.62	4630	1.20	2.50	−2.39	0.07	4550	1.60	2.50	−2.15	0.07	142	17	1.40[a]
2MASS J12591462−7049592	4220	0.05	3.57	−2.54	4468	1.00	3.90	−2.45	0.20	4320	1.60	2.90	−2.20	0.20	145	18	1.03[a]
2MASS J13052137−1137220	4490	0.45	2.32	−2.29	4711	1.14	2.18	−2.07	0.14	4600	1.80	2.20	−1.82	0.14	217	18	1.67
2MASS J13261792−0945176	4605	0.95	1.95	−3.01	4815	1.55	1.95	−2.88	0.07	4720	1.90	2.10	−2.60	0.07	205	24	1.85
2MASS J13273676−1710384	4720	0.55	2.10	−2.76	4918	1.05	2.00	−2.62	0.07	4830	1.80	2.20	−2.40	0.07	166	23	1.90
2MASS J13275198+0342396	4600	0.85	2.25	−2.56	4810	1.45	2.10	−2.53	0.11	4720	2.05	2.30	−2.30	0.11	225	26	1.71
2MASS J13373017−7717500	4590	0.90	2.00	−2.40	4801	1.35	1.73	−2.28	0.08	4710	2.00	1.80	−2.06	0.08	181	13	2.19
2MASS J13494713−7423395	4575	0.65	2.35	−3.02	4788	1.35	2.10	−2.85	0.06	4650	1.90	2.20	−2.60	0.06	136	15	1.82
2MASS J13511539−7340363	4860	1.90	1.95	−2.54	5044	2.50	1.85	−2.49	0.08	4900	2.90	2.10	−2.25	0.08	200	63	2.86
2MASS J13524835+1254216	4605	0.50	2.50	−2.15	4815	1.10	2.35	−1.96	0.11	4750	1.60	2.30	−1.70	0.11	197	27	1.53
2MASS J13554406−3750455	4800	1.30	1.80	−2.51	4990	1.75	1.80	−2.37	0.09	4920	2.40	1.90	−2.13	0.09	175	17	2.47
2MASS J13592232−6821493	4900	1.95	1.65	−2.82	5080	2.40	1.65	−2.67	0.08	4950	2.70	1.80	−2.41	0.08	207	27	2.50[a]
2MASS J14100568−0701443	4475	0.55	2.30	−2.14	4698	1.25	2.25	−1.98	0.13	4540	1.70	2.30	−1.75	0.13	178	25	1.58
2MASS J14112614−1137453	4120	0.00	3.65	−2.26	4378	0.30	3.65	−2.10	0.13	4300	1.10	3.00	−1.80	0.13	107	13	1.12
2MASS J14234371−4025526	4625	0.60	2.45	−2.96	4833	1.20	2.35	−2.74	0.13	4750	1.65	2.40	−2.50	0.13	162	23	1.22

Table 3 continued

Table 3 *(continued)*

Star ID	LTE				LTE^{corr}					NLTE							
	T_{eff} (K)	log g (cgs)	ξ_t (km s^{-1})	[Fe/H]	T_{eff} (K)	log g (cgs)	ξ_t (km s^{-1})	[Fe/H]	$\sigma_{[Fe/H]}$ (dex)	T_{eff} (K)	log g (cgs)	ξ_t (km s^{-1})	[Fe/H]	$\sigma_{[Fe/H]}$ (dex)	N$_{Fe\,I}$	N$_{Fe\,II}$	log g^{Gaia} (cgs)
2MASS J14335592−1240357	4370	0.15	3.60	−2.80	4603	0.95	3.20	−2.40	0.19	4500	1.45	3.00	−2.15	0.19	179	19	1.24
2MASS J14355850−0719265	4385	0.35	2.20	−3.45	4617	1.25	2.15	−2.99	0.12	4450	1.95	2.20	−2.69	0.12	115	22	1.82
2MASS J14443014−1320092	4570	0.50	2.50	−2.01	4783	1.05	2.25	−1.90	0.11	4650	2.00	2.30	−1.68	0.11	162	16	1.98
2MASS J14533268−3614555	5700	3.45	1.30	−2.95	5800	3.60	1.33	−2.83	0.07	5750	4.10	1.40	−2.60	0.07	120	5	4.17
2MASS J14534137+0040467	4400	0.35	2.50	−3.34	4630	1.15	2.30	−3.09	0.10	4550	1.55	2.30	−2.82	0.10	142	18	1.35[a]
2MASS J14543792+0830379	4690	1.05	1.85	−2.43	4891	1.55	1.85	−2.31	0.08	4770	2.10	1.90	−2.08	0.08	198	25	2.00
2MASS J14564556−1615432	5265	1.45	2.05	−2.47	5409	1.70	2.10	−2.31	0.14	5320	2.20	2.20	−1.70	0.14	137	23	2.13
2MASS J14590234−0916105	4460	0.60	2.40	−2.60	4684	1.30	2.20	−2.38	0.06	4580	1.65	2.20	−2.12	0.06	156	19	1.49[a]
2MASS J15013452−2443310	4580	0.75	2.15	−2.98	4792	1.25	1.95	−2.88	0.07	4600	1.65	2.00	−2.65	0.07	135	13	1.60[a]
2MASS J15042611−2231523	4800	1.68	1.75	−3.04	4990	2.15	1.70	−2.91	0.18	4880	2.70	1.55	−2.68	0.18	219	23	3.72
2MASS J15133549−1244339	4650	1.10	1.90	−2.50	4855	1.60	1.80	−2.04	0.07	4790	2.20	1.90	−1.80	0.07	191	20	2.16
2MASS J15204531−1742486	4685	1.15	1.85	−2.97	4887	1.70	1.75	−2.81	0.08	4980	2.30	1.80	−2.55	0.08	175	19	2.38
2MASS J15240713−0319509	4640	1.05	2.15	−2.96	4846	1.55	2.10	−2.81	0.10	4750	1.90	2.20	−2.57	0.10	171	18	1.80
2MASS J15272126−1445153	4630	0.40	2.50	−2.94	4837	1.00	2.35	−2.79	0.11	4720	1.70	2.40	−2.55	0.11	138	18	1.56[a]
2MASS J16115667−8034422	4790	1.70	2.17	−2.70	4981	2.50	2.17	−2.61	0.24	4780	2.85	2.20	−2.40	0.24	143	11	2.40
2MASS J16163600−5700568	4970	2.05	1.35	−2.0	5143	2.45	1.35	−1.65	0.08	5050	3.00	1.40	−1.40	0.08	236	19	2.98
2MASS J16592172−6827199	4390	0.40	2.55	−3.00	4621	1.35	2.50	−2.80	0.17	4520	1.85	2.70	−2.57	0.17	179	23	0.96[a]
2MASS J17043634−6219457	4680	0.35	2.50	−2.07	4882	0.85	2.27	−1.99	0.18	4790	2.45	2.20	−1.82	0.18	171	19	2.66
2MASS J17060555+0412354	4425	0.40	3.30	−2.97	4653	1.11	2.95	−2.71	0.13	4540	1.50	2.80	−2.47	0.13	157	19	0.97[a]
2MASS J17070759−7817561	4580	0.60	2.11	−3.00	4792	1.28	2.03	−2.81	0.18	4700	1.55	2.15	−2.55	0.18	195	17	1.46
2MASS J17131974−7113010	4610	0.50	2.33	−2.84	4819	1.05	2.23	−2.63	0.14	4720	1.90	2.23	−2.40	0.14	179	18	2.72
2MASS J17163340−7009028	4460	0.48	2.30	−2.50	4684	1.20	2.36	−2.39	0.12	4550	1.80	2.30	−2.10	0.12	169	17	1.75
2MASS J17360167−5145296	4680	1.25	2.00	−2.70	4882	1.75	1.95	−2.60	0.17	4750	2.10	1.95	−2.35	0.17	219	21	1.51
2MASS J17541561−5148268	4600	0.67	2.22	−2.78	4810	1.45	2.28	−2.14	0.15	4740	2.10	2.30	−1.90	0.15	206	25	2.37
2MASS J18272432−5655165	4480	0.60	2.35	−2.50	4702	1.40	2.48	−1.91	0.17	4600	2.00	2.40	−1.65	0.17	195	24	1.16[a]
2MASS J18284356−8441346	4420	2.00	2.30	−2.25	4648	2.95	1.80	−2.03	0.24	4620	3.25	2.00	−1.80	0.24	143	21	1.98
2MASS J18294359−4924253	4390	0.55	2.00	−1.80	4621	1.60	2.05	−1.22	0.17	4520	2.10	2.10	−1.00	0.17	186	19	0.73[a]
2MASS J18332056−3802590	4540	0.80	2.20	−1.92	4756	1.60	2.15	−1.79	0.17	4700	1.90	2.00	−1.55	0.17	211	27	1.72
2MASS J18333188−4840403	4695	1.30	1.80	−2.00	4896	1.80	1.80	−1.87	0.09	4810	2.40	1.90	−1.61	0.09	173	19	2.24
2MASS J18361214−7333443	4540	0.70	2.35	−2.73	4756	1.40	2.15	−2.61	0.10	4680	1.80	2.20	−2.35	0.10	155	21	1.61
2MASS J18405985−4841353	4580	0.90	2.05	−2.66	4792	1.40	1.80	−2.58	0.08	4680	1.75	2.00	−2.32	0.08	200	16	1.19[a]
2MASS J18560360−6403465	4690	1.25	1.90	−3.14	4891	1.80	1.90	−2.94	0.09	4790	2.20	2.00	−2.70	0.09	200	21	2.09
2MASS J19092677−5140208	4510	0.61	2.07	−2.72	4729	1.55	2.11	−2.50	0.09	4650	1.95	2.20	−2.25	0.09	199	17	1.84
2MASS J19105886−4059412	4495	0.45	2.45	−2.45	4716	1.10	2.35	−2.23	0.11	4620	1.85	2.30	−2.00	0.11	156	23	1.91
2MASS J19175585−5440147	4680	1.00	1.90	−2.50	4882	1.50	1.85	−2.36	0.12	4750	1.95	2.40	−2.10	0.12	268	27	1.86
2MASS J19192768−5959140	4310	0.25	2.50	−2.77	4549	1.08	2.76	−2.62	0.17	4580	1.50	2.70	−2.40	0.17	197	18	0.87
2MASS J19282163−2457545	4600	0.65	2.12	−2.74	4810	1.30	2.05	−2.56	0.19	4740	1.70	2.05	−2.30	0.19	218	23	1.40

Table 3 continued

Table 3 *(continued)*

Star ID	LTE				LTE^{corr}					NLTE							
	T_{eff} (K)	log g (cgs)	ξ_t (km s^{-1})	[Fe/H]	T_{eff} (K)	log g (cgs)	ξ_t (km s^{-1})	[Fe/H]	$\sigma_{[Fe/H]}$ (dex)	T_{eff} (K)	log g (cgs)	ξ_t (km s^{-1})	[Fe/H]	$\sigma_{[Fe/H]}$ (dex)	N$_{Fe\,I}$	N$_{Fe\,II}$	log g^{Gaia} (cgs)
2MASS J19291910−5528181	4360	0.55	2.83	−2.50	4594	1.25	2.83	−2.52	0.24	4450	1.65	2.80	−2.30	0.24	117	21	1.08[a]
2MASS J19310426−3707397	4500	0.80	2.25	−2.50	4720	1.55	2.20	−2.21	0.16	4650	2.00	2.10	−1.95	0.16	221	24	1.47
2MASS J19320444−7309178	4220	0.00	5.50	−2.19	4468	0.55	3.45	−2.02	0.10	4380	1.10	3.00	−1.77	0.10	129	16	0.61
2MASS J19504989−3321107	4470	0.28	2.25	−2.84	4693	0.82	1.97	−2.61	0.13	4550	1.55	2.00	−2.36	0.13	172	19	1.52
2MASS J19532495−3647303	4450	0.45	2.30	−3.64	4675	1.15	2.35	−3.30	0.11	4560	1.70	2.30	−3.05	0.11	236	20	3.33
2MASS J19552158−4613569	4540	0.70	2.22	−2.90	4756	1.45	2.16	−2.70	0.13	4650	1.70	2.20	−2.45	0.13	201	17	1.50
2MASS J19563822−4054235	5250	1.10	2.20	−2.50	5395	1.40	2.22	−2.45	0.14	5240	2.00	2.20	−2.20	0.14	186	18	2.07
2MASS J19570893−3317320	4420	0.15	2.44	−2.75	4648	0.90	2.50	−2.57	0.13	4540	1.55	2.50	−2.31	0.13	211	23	1.40
2MASS J20035532−5028100	4540	0.65	2.20	−3.00	4756	1.35	2.12	−2.78	0.14	4630	1.60	2.20	−2.50	0.14	235	23	1.35
2MASS J20192202−6130149	4430	0.25	2.35	−2.67	4657	1.00	2.40	−2.53	0.14	4580	1.80	2.40	−2.30	0.14	241	24	1.14
2MASS J20202917−2707347	4665	1.05	2.15	−3.04	4869	2.10	1.60	−2.84	0.08	4760	2.30	1.70	−2.60	0.08	170	17	1.96
2MASS J20234398−0815472	4750	1.20	1.77	−2.91	4945	1.63	1.73	−2.76	0.09	4850	2.10	1.90	−2.54	0.09	226	22	1.13[a]
2MASS J20242122−2656435	4365	0.25	2.70	−0.70	4599	1.10	2.55	−0.60	0.14	4480	1.45	2.40	−0.40	0.14	186	24	1.12
2MASS J20374042−5520500	4590	0.75	2.30	−3.19	4801	1.45	2.10	−2.98	0.12	4720	2.00	2.25	−2.75	0.12	231	25	1.58
2MASS J20445065−3714000	4380	0.25	2.44	−2.80	4612	1.10	2.55	−2.61	0.20	4540	1.85	2.50	−2.41	0.20	170	18	1.10[a]
2MASS J20501790−0549230	5050	2.10	1.52	−2.70	5215	2.40	1.56	−2.69	0.16	5100	2.90	1.60	−2.40	0.16	199	19	2.89
2MASS J20585505−1759007	4460	0.15	4.05	−3.16	4684	0.80	2.90	−2.89	0.14	4780	1.50	2.80	−2.65	0.14	159	14	1.48
2MASS J21220020−0820333	4500	0.55	2.05	−3.60	4720	1.45	2.13	−3.42	0.17	4650	1.85	2.20	−3.15	0.17	179	25	1.47
2MASS J21234588−0839448	4220	0.00	3.95	−2.25	4468	0.50	3.55	−1.78	0.16	4370	1.25	3.40	−1.50	0.16	172	14	1.26
2MASS J21352343−5722598	4550	0.45	2.28	−3.20	4765	1.05	2.20	−2.91	0.17	4680	1.55	2.20	−2.68	0.17	249	25	1.39
2MASS J21553580−0905118	4525	0.55	2.50	−2.87	4743	1.20	2.30	−2.63	0.09	4680	1.80	2.40	−2.40	0.09	213	27	1.77
2MASS J22182082−3827554	4910	2.05	1.52	−2.79	5089	2.40	1.55	−2.57	0.11	5000	2.70	1.60	−2.32	0.11	202	21	2.47
2MASS J22215794−3602090	4750	1.30	1.72	−2.71	4945	1.75	1.75	−2.40	0.16	4880	2.20	1.95	−2.15	0.16	240	21	2.15
2MASS J22220344−8024592	4460	0.10	2.65	−2.69	4684	0.80	2.60	−2.50	0.12	4580	1.35	2.50	−2.25	0.12	237	25	1.20
2MASS J22253443−2027171	4750	0.65	2.20	−2.99	4945	1.15	2.12	−2.76	0.17	4890	1.75	2.10	−2.50	0.17	239	24	1.70
2MASS J22300238−6332191	4730	0.80	2.35	−2.55	4927	1.20	2.25	−2.48	0.14	4810	1.60	2.20	−2.22	0.14	228	26	1.29[a]
2MASS J22302641−1949527	4430	0.35	2.22	−2.49	4657	1.10	2.30	−2.28	0.15	4520	1.60	2.30	−2.05	0.15	220	24	1.41
2MASS J22344202−0826492	4650	1.00	2.00	−2.94	4855	1.50	1.85	−2.48	0.12	4760	2.20	1.90	−2.22	0.12	215	25	2.15
2MASS J22345447−6605172	4670	0.80	2.50	−2.70	4873	1.30	2.30	−2.49	0.11	4750	1.88	2.20	−2.20	0.11	189	23	1.76
2MASS J22394827−0803536	4300	0.30	2.65	−2.93	4540	1.40	2.55	−2.79	0.17	4480	1.80	2.50	−2.55	0.17	139	23	1.69
2MASS J23100319−7702165	4540	0.50	2.30	−2.10	4756	1.25	2.25	−1.81	0.20	4650	1.75	2.20	−1.55	0.20	197	20	1.56
2MASS J23411581−6406440	4615	0.55	2.50	−2.73	4824	1.10	2.45	−2.78	0.07	4750	1.50	2.40	−2.52	0.07	203	23	1.36[a]

[a] Uncertain log g^{Gaia} due to *Gaia* DR2 parallax-based distance larger than 6 kpc (Bailer-Jones et al. 2018).

Table 4. Stellar Sub-classifications and Associated Abundances

Star ID	[C/Fe]	$[C/Fe]_{corr.}$	[Sr/Fe]	[Ba/Fe]	[Eu/Fe]	[Ba/Eu]	[Sr/Ba]	Sub-Class
2MASS J00011195+0321051	0.00	0.22	0.20	0.20	0.22	−0.02	0.00	non-RPE
2MASS J00101758−1735387	0.00	0.01	0.09	0.43	1.35	−0.92	−0.34	r-II
2MASS J00162809−0505519	0.60	0.66	0.01	−1.21	<0.10	> −1.31	1.22	limited-r?
2MASS J00195350−0145445	−0.45	0.23	−0.32	−0.24	0.28	−0.52	−0.08	non-RPE
2MASS J00282278−3934598	−0.50	0.23	−0.06	−0.40	−0.20	−0.20	0.34	non-RPE
2MASS J00372794−2045307	0.20	0.63	−0.03	−0.39	−0.28	−0.11	0.36	non-RPE
2MASS J00452379−2112161[a]	−0.15	0.50	−0.10	−0.25	0.40	−0.65	0.15	r-I
2MASS J00463619−3739335	< −3.31	< −2.72	−0.64	−0.59	<0.80	> −1.39	−0.05	non-RPE
2MASS J00512646−1053170	< −1.75	< −1.75	0.49	0.50	1.21	−0.71	−0.01	r-II
2MASS J00524174−0902235	−1.37	−1.04	−1.41	−0.72	0.94	−1.66	−0.69	r-I
2MASS J01165010−6307441	0.15	0.86	−0.23	0.00	0.37	−0.37	−0.23	r-I
2MASS J01374434−4301490	−0.20	0.51	−0.49	−0.30	0.00	−0.30	−0.19	non-RPE
2MASS J01473804−1130474	0.85	1.16	0.17	0.70	0.30	0.40	−0.53	CEMP-i
2MASS J01501343+0725010	0.10	0.60	−0.68	< −1.13	<0.10	> −1.23	0.45	non-RPE
2MASS J01553180−4919420	0.40	0.41	0.06	0.15	0.72	−0.57	−0.09	r-I
2MASS J01555066−6400155	−0.20	0.26	−0.14	0.10	0.80	−0.70	−0.24	r-I
2MASS J02005020−4657352	0.51	1.15	−2.18	< −0.19	<0.31	> −0.50	−1.99	CEMP-r-I?
2MASS J02111462−8107085	0.30	0.31	−0.54	< −1.14	< −0.10	> −1.04	0.60	limited-r?
2MASS J02395318−7019014	0.30	0.30	0.10	0.35	0.15	0.20	−0.25	i-process
2MASS J03073894−0502491	−0.57	0.01	1.25	0.14	1.27	−1.13	1.11	r-II
2MASS J03154102−7626329	−0.10	0.55	−0.22	−0.01	0.50	−0.51	−0.21	r-I
2MASS J03270229+0132322	0.35	0.36	−0.05	0.50	1.07	−0.57	−0.55	r-II
2MASS J03423645−1335529	−1.50	−1.50	−1.02	<0.80	<0.80	> −0.01	−1.82	r-I?
2MASS J04245677−6500173	−0.52	0.20	−0.30	0.19	0.30	−0.11	−0.49	r-I
2MASS J04304875−4613535	0.20	0.21	0.05	< −0.16	<0.10	> −0.26	0.21	non-RPE
2MASS J05030025−7601462	−0.20	0.43	0.00	−0.21	0.40	−0.61	0.21	r-I
2MASS J05202930−5825297	−0.30	0.44	−2.08	−1.25	< −0.10	> −1.15	−0.83	non-RPE
2MASS J05241392−0336543	−0.40	0.09	−0.27	0.47	1.50	−1.03	−0.74	r-II
2MASS J05384334−5147228	0.59	0.97	−0.10	−0.66	−0.20	−0.46	0.56	CEMP-limited-r
2MASS J05432623−8051334	−0.99	−0.24	−0.73	−0.59	<0.12	> −0.71	−0.14	non-RPE
2MASS J05573684−5127209	1.70	1.78	−0.89	2.50	2.20	0.30	−3.39	CEMP-i
2MASS J06392518−7414056	0.35	0.36	0.07	−0.28	0.40	−0.68	0.35	r-I
2MASS J07123398−4814049	−0.40	0.26	−2.00	−1.90	< −0.40	> −1.50	−0.10	non-RPE
2MASS J07150266−0154092	0.07	0.08	< −2.42	0.52	0.88	−0.36	−2.94	r-I
2MASS J07151852−5252051	−0.30	0.44	−0.36	−0.87	<0.15	> −1.02	0.51	limited-r?
2MASS J07250021−7022038	0.30	0.77	−0.14	−0.30	0.33	−0.63	0.16	CEMP-r-I
2MASS J07443970−4425135	0.50	0.89	−0.48	−0.40	0.10	−0.50	−0.08	CEMP-no
2MASS J08025449−5224304	−0.55	0.21	0.75	−0.21	0.10	−0.31	0.96	limited-r
2MASS J08295142−7242542	−0.81	−0.22	0.12	0.01	<0.44	> −0.43	0.11	r-I?
2MASS J09103481+0518228	−0.30	0.43	−0.50	−0.38	0.12	−0.50	−0.12	non-RPE
2MASS J09291557+0838002	−0.30	0.44	1.03	−1.00	< −0.30	> −0.70	2.03	limited-r?
2MASS J09531322+0744515	−0.40	−0.21	0.01	0.30	0.50	−0.20	−0.29	r-I
2MASS J10063414−7030212	0.19	0.33	−0.21	0.03	0.39	−0.36	−0.24	r-I
2MASS J10073075+0348357	−0.50	0.11	−1.54	−2.10	< −0.50	> −1.60	0.56	limited-r?
2MASS J10524610−0336012	−0.20	0.26	−0.55	−0.51	−0.05	−0.46	−0.04	non-RPE

Table 4 continued

Table 4 *(continued)*

Star ID	[C/Fe]	$[C/Fe]_{corr.}$	[Sr/Fe]	[Ba/Fe]	[Eu/Fe]	[Ba/Eu]	[Sr/Ba]	Sub-Class
2MASS J10550658+1931580	0.30	0.68	−0.22	−0.50	0.50	−1.00	0.28	*r*-I
2MASS J11165400−7250160	−0.90	−0.14	0.17	−0.30	0.30	−0.60	0.47	*r*-I
2MASS J11191233−1609467	1.51	1.53	0.89	1.51	0.91	0.60	−0.62	CEMP-*s*
2MASS J11303693+0224037	−0.20	0.36	−0.40	−0.40	0.35	−0.75	0.00	*r*-I
2MASS J11471027+0341265	0.10	0.61	−0.84	−0.05	0.40	−0.45	−0.79	*r*-I
2MASS J11510227−6940416	−0.52	0.17	−0.01	−0.17	0.48	−0.65	0.16	*r*-I
2MASS J11565537+0320329	−0.21	0.35	−0.40	−0.10	0.20	−0.30	−0.30	non-RPE
2MASS J12170829+0415146	−0.40	0.31	−0.44	0.15	1.10	−0.95	−0.59	*r*-II
2MASS J12203297+0257138	−0.55	0.14	0.00	0.00	0.45	−0.45	0.00	*r*-I
2MASS J12233047−4216365	−0.40	0.34	−0.28	−0.32	0.30	−0.62	0.04	*r*-I
2MASS J12255123−2351074	0.30	0.32	−0.09	−0.34	0.52	−0.86	0.25	*r*-I
2MASS J12331670+1622563	−0.10	0.55	−0.48	−0.30	0.20	−0.50	−0.18	non-RPE
2MASS J12351734+0945333	−0.40	0.28	−0.50	0.05	0.30	−0.25	−0.55	*r*-I
2MASS J12591462−7049592	−0.60	0.16	0.25	0.25	0.50	−0.25	0.00	*r*-I
2MASS J13052137−1137220	−0.30	0.35	−0.43	0.20	1.09	−0.89	−0.63	*r*-II
2MASS J13261792−0945176	0.10	0.52	−0.07	−0.25	0.40	−0.65	0.18	*r*-I
2MASS J13273676−1710384	−0.30	0.44	0.00	−0.30	<0.20	> −0.50	0.30	non-RPE
2MASS J13275198+0342396	−0.10	0.44	−0.32	−0.40	0.20	−0.60	0.08	non-RPE
2MASS J13373017−7717500	0.20	0.69	0.00	−0.30	<0.20	> −0.50	0.30	non-RPE
2MASS J13494713−7423395	0.10	0.61	0.10	0.05	0.70	−0.65	0.05	*r*-I
2MASS J13511539−7340363	0.00	0.01	−0.20	0.17	0.50	−0.33	−0.37	*r*-I
2MASS J13524835+1254216	−0.20	0.39	−0.20	−0.30	0.30	−0.60	0.10	*r*-I
2MASS J13554406−3750455	−0.05	0.17	−0.44	−0.65	< −0.30	> −0.35	0.21	non-RPE
2MASS J13592232−6821493	0.05	0.06	0.00	0.00	0.20	−0.20	0.00	non-RPE
2MASS J14100568−0701443	−0.30	0.29	0.10	0.10	0.68	−0.58	0.00	*r*-I
2MASS J14112614−1137453	0.40	0.86	−2.35	−1.20	< −0.50	> −0.70	−1.15	CEMP-no
2MASS J14234371−4025526	−0.40	0.28	−0.47	0.10	0.30	−0.20	−0.57	*r*-I
2MASS J14335592−1240357	−0.40	0.34	−0.97	−1.70	<0.15	> −1.85	0.73	limited-*r*?
2MASS J14355850−0719265	−0.40	0.27	0.00	−0.10	0.20	−0.30	0.10	non-RPE
2MASS J14443014−1320092	−0.20	0.38	−0.05	−0.45	<0.09	> −0.54	0.40	non-RPE
2MASS J14533268−3614555	−0.20	−0.20	−0.16	< −0.40	<0.60	> −1.00	0.24	*r*-I?
2MASS J14534137+0040467	−0.41	0.32	0.44	1.05	1.80	−0.75	−0.61	*r*-II
2MASS J14543792+0830379	0.30	0.73	−0.10	0.25	1.10	−0.75	−0.35	*r*-II/CEMP
2MASS J14564556−1615432	−0.10	0.23	0.14	−0.30	<0.30	> −0.60	0.44	*r*-I?
2MASS J14590234−0916105	−0.30	0.32	−0.22	−0.10	0.45	−0.55	−0.12	*r*-I
2MASS J15013452−2443310	0.30	0.85	−2.94	< −0.80	<0.00	> −0.80	−2.14	CEMP-no
2MASS J15042611−2231523	−0.04	−0.03	−0.08	0.16	0.54	−0.38	−0.24	*r*-I
2MASS J15133549−1244339	0.45	0.75	−2.87	−0.10	0.55	−0.65	−2.77	CEMP-*r*-I
2MASS J15204531−1742486	0.30	0.54	−2.85	−0.30	0.35	−0.65	−2.55	*r*-I
2MASS J15240713−0319509	0.10	0.52	0.00	−0.20	<0.05	> −0.25	0.20	non-RPE
2MASS J15272126−1445153	−0.39	0.35	−0.09	−0.09	0.26	−0.35	0.00	non-RPE
2MASS J16115667−8034422	0.70	0.72	0.70	1.35	0.90	0.45	−0.65	CEMP-*i*
2MASS J16163600−5700568	0.30	0.31	0.01	−0.90	< −0.20	> −0.70	0.91	limited-*r*
2MASS J16592172−6827199	−0.60	−0.05	−0.30	−0.20	0.40	−0.60	−0.10	*r*-I?
2MASS J17043634−6219457	−0.10	0.49	−0.16	−0.25	0.55	−0.80	0.09	*r*-I
2MASS J17060555+0412354	−0.10	0.61	−0.57	0.05	0.50	−0.45	−0.62	*r*-I
2MASS J17070759−7817561	−0.07	0.52	0.08	−0.17	0.28	−0.45	0.25	non-RPE

Table 4 continued

Table 4 *(continued)*

Star ID	[C/Fe]	$[C/Fe]_{corr.}$	[Sr/Fe]	[Ba/Fe]	[Eu/Fe]	[Ba/Eu]	[Sr/Ba]	Sub-Class
2MASS J17131974−7113010	−0.20	0.51	−0.10	0.00	0.50	−0.50	−0.10	r-I
2MASS J17163340−7009028	−0.35	0.31	−0.07	0.05	0.89	−0.84	−0.12	r-I
2MASS J17360167−5145296	0.00	0.19	−0.53	−0.15	0.50	−0.65	−0.38	r-I
2MASS J17541561−5148268	−0.60	−0.12	−0.20	−0.05	0.50	−0.55	−0.15	r-I
2MASS J18272432−5655165	−0.70	−0.15	−0.14	0.00	0.40	>-0.40	−0.14	r-I?
2MASS J18284356−8441346	−0.39	−0.38	0.71	1.31	1.21	0.10	−0.60	i
2MASS J18294359−4924253	−0.61	−0.21	−0.11	0.29	0.89	−0.60	−0.40	r-I
2MASS J18332056−3802590	−0.38	0.01	−0.10	−0.20	0.30	−0.50	0.10	r-I
2MASS J18333188−4840403	0.30	0.49	0.06	−0.20	<0.10	>-0.30	0.26	non-RPE
2MASS J18361214−7333443	0.10	0.60	−0.29	−0.40	<-0.30	>-0.10	0.11	non-RPE
2MASS J18405985−4841353	0.60	1.02	0.26	−0.45	<-0.10	>-0.35	0.71	CEMP-limited-r?
2MASS J18560360−6403465	0.25	0.41	0.02	−0.20	0.20	−0.40	0.22	non-RPE
2MASS J19092677−5140208	−0.40	0.10	−0.04	0.25	0.60	−0.35	−0.29	r-I
2MASS J19105886−4059412	−0.29	0.39	−0.41	−0.40	<-0.40	>0.00	−0.01	non-RPE
2MASS J19175585−5440147	0.40	0.81	−0.24	−0.41	0.12	−0.53	0.17	CEMP-no
2MASS J19192768−5959140	−0.60	0.13	−0.05	0.25	0.60	−0.35	−0.30	r-I
2MASS J19282163−2457545	0.00	0.57	−0.35	−0.35	0.20	−0.55	0.00	non-RPE
2MASS J19291910−5528181	−0.59	0.11	−0.56	0.01	0.56	−0.55	−0.57	r-I
2MASS J19310426−3707397	−0.45	0.05	−0.70	−0.40	0.40	−0.80	−0.30	r-I
2MASS J19320444−7309178	−0.20	0.42	−0.15	−1.00	<-0.80	>-0.20	0.85	limited-r?
2MASS J19504989−3321107	0.00	0.70	−0.35	−0.65	0.00	−0.65	0.30	CEMP-no
2MASS J19532495−3647303	−0.30	0.42	−0.11	−0.30	0.20	−0.50	0.19	non-RPE
2MASS J19552158−4613569	−0.25	0.21	−0.25	−0.25	0.37	−0.62	0.00	r-I
2MASS J19563822−4054235	0.00	0.53	0.15	−0.20	0.30	−0.50	0.35	r-I
2MASS J19570893−3317320	−0.12	0.59	−0.32	−0.48	−0.30	−0.18	0.16	non-RPE
2MASS J20035532−5028100	−0.55	0.02	−0.34	−1.40	<-0.35	>-1.05	1.06	limited-r?
2MASS J20192202−6130149	0.20	0.82	0.02	−1.00	<-0.05	>-0.95	1.02	CEMP-limited-r?
2MASS J20202917−2707347	0.25	0.26	−0.20	−0.30	0.10	−0.40	0.10	non-RPE
2MASS J20234398−0815472	0.35	0.67	−1.17	−0.95	<-0.40	>-0.55	−0.22	non-RPE
2MASS J20242122−2656435	−0.50	−0.17	−0.20	−0.70	<0.10	>-0.80	0.50	limited-r?
2MASS J20374042−5520500	0.00	0.51	−0.10	−0.17	0.40	−0.57	0.07	r-I
2MASS J20445065−3714000	0.25	0.87	0.40	−0.18	<-0.15	>-0.03	0.58	limited-r?
2MASS J20501790−0549230	0.50	0.51	−0.05	−0.99	<0.20	>-1.19	0.94	limited-r?
2MASS J20585505−1759007	−0.10	0.66	0.59	−0.90	<-0.35	>-0.55	1.49	limited-r?
2MASS J21220020−0820333	−0.30	0.09	−0.19	0.20	0.40	−0.20	−0.39	r-I
2MASS J21234588−0839448	−0.35	0.24	−2.03	−1.25	<-0.40	>-0.85	−0.78	non-RPE
2MASS J21352343−5722598	−0.10	0.64	−0.39	−0.75	<-0.28	>-0.47	0.36	non-RPE
2MASS J21553580−0905118	−0.50	0.19	−0.19	−0.40	0.02	−0.42	0.21	non-RPE
2MASS J22182082−3827554	0.30	0.31	0.08	0.50	1.10	−0.60	−0.42	r-II
2MASS J22215794−3602090	0.20	0.44	−0.25	−0.25	<-0.20	>-0.05	0.00	non-RPE
2MASS J22220344−8024592	0.20	0.83	−0.80	−0.30	0.37	−0.67	−0.50	CEMP-r-I
2MASS J22253443−2027171	−0.30	0.42	0.00	−0.40	0.20	−0.60	0.40	non-RPE
2MASS J22300238−6332191	−0.25	0.42	−0.09	−0.15	0.25	−0.40	0.06	non-RPE
2MASS J22302641−1949527	−0.20	0.49	−0.28	−0.10	0.40	−0.50	−0.18	r-I
2MASS J22344202−0826492	0.15	0.60	−0.27	−0.60	<0.00	>-0.60	0.33	non-RPE
2MASS J22345447−6605172	−0.30	0.30	−0.03	−0.20	0.40	−0.60	0.17	r-I
2MASS J22394827−0803536	−0.90	−0.35	0.04	−0.10	0.60	−0.70	0.14	r-I

Table 4 continued

Table 4 *(continued)*

Star ID	[C/Fe]	$[C/Fe]_{corr.}$	[Sr/Fe]	[Ba/Fe]	[Eu/Fe]	[Ba/Eu]	[Sr/Ba]	Sub-Class
2MASS J23100319−7702165	−0.10	0.39	−0.23	−0.10	0.65	−0.75	−0.13	*r*-I
2MASS J23411581−6406440	−0.45	0.27	−0.16	−0.10	0.35	−0.45	−0.06	*r*-I

[a] Rediscovery of the ultra metal-poor (UMP) star CD−38 + 245

Table 5. Light-Element and α-Element abundances

Star ID	[O/H]	[Na/H]	[Mg/H]	[Al/H]	[Si/H]	[K/H]	[Ca/H]	[Ti I/H]	[Ti II/H]
2MASS J00011195+0321051	-0.79 ± 0.10	-1.99 ± 0.03	-1.60 ± 0.14	-2.33 ± 0.15	-1.83 ± 0.10	-1.33 ± 0.10	-1.65 ± 0.14	-1.88 ± 0.14	-1.76 ± 0.17
2MASS J00101758−1735387	···	-3.01 ± 0.08	-2.75 ± 0.08	-3.73 ± 0.15	-2.14 ± 0.10	-2.73 ± 0.10	-2.19 ± 0.08	-2.67 ± 0.17	-2.57 ± 0.22
2MASS J00162809−0505519	···	-2.72 ± 0.10	-2.52 ± 0.07	-3.57 ± 0.15	-2.61 ± 0.10	-2.67 ± 0.10	-2.66 ± 0.11	-2.81 ± 0.14	-2.81 ± 0.14
2MASS J00195350−0145445	-1.59 ± 0.04	-2.30 ± 0.20	-2.02 ± 0.08	-2.65 ± 0.15	-1.85 ± 0.09	-1.66 ± 0.13	-2.09 ± 0.14	-2.30 ± 0.08	-2.13 ± 0.18
2MASS J00282278−3934598	-1.56 ± 0.10	-2.49 ± 0.02	-2.18 ± 0.05	-3.25 ± 0.15	-1.93 ± 0.10	-2.15 ± 0.10	-2.28 ± 0.08	-2.37 ± 0.13	-2.17 ± 0.15
2MASS J00372794−2045307	···	-2.51 ± 0.01	-2.13 ± 0.07	-3.18 ± 0.15	-2.02 ± 0.05	-2.19 ± 0.00	-2.12 ± 0.08	-2.50 ± 0.11	-2.42 ± 0.14
2MASS J00452379−2112161	-2.12 ± 0.10	-1.92 ± 0.18	-2.28 ± 0.06	-2.32 ± 0.15	-1.94 ± 0.17	-1.92 ± 0.10	-2.22 ± 0.10	-2.38 ± 0.09	-2.32 ± 0.12
2MASS J00463619−3739335	···	-4.10 ± 0.10	-3.52 ± 0.13	-4.67 ± 0.15	-3.59 ± 0.10	···	-3.66 ± 0.10	-3.04 ± 0.20	-3.66 ± 0.25
2MASS J00512646−1053170	···	-2.30 ± 0.07	-2.10 ± 0.10	-3.27 ± 0.15	-2.03 ± 0.10	-1.78 ± 0.10	-1.96 ± 0.06	-1.88 ± 0.12	-1.99 ± 0.14
2MASS J00524174−0902235	···	-1.02 ± 0.10	-1.21 ± 0.10	···	-0.83 ± 0.10	···	-0.96 ± 0.10	-1.31 ± 0.00	0.00 ± 0.00
2MASS J01165010−6307441	···	-1.83 ± 0.08	-1.28 ± 0.10	-2.26 ± 0.15	-1.34 ± 0.13	-0.87 ± 0.12	-1.24 ± 0.13	-1.39 ± 0.17	-1.28 ± 0.17
2MASS J01374434−4301490	-2.06 ± 0.10	-2.72 ± 0.14	-2.28 ± 0.10	-3.22 ± 0.15	-2.35 ± 0.10	-2.28 ± 0.10	-2.40 ± 0.12	-2.51 ± 0.11	-2.44 ± 0.12
2MASS J01473804−1130474	-1.62 ± 0.10	-1.87 ± 0.14	-1.89 ± 0.06	-2.82 ± 0.15	-1.62 ± 0.12	-1.61 ± 0.10	-1.92 ± 0.18	-2.11 ± 0.12	-1.99 ± 0.16
2MASS J01501343+0725010	-0.96 ± 0.10	-2.57 ± 0.10	-2.51 ± 0.10	-3.42 ± 0.15	-2.49 ± 0.10	-2.59 ± 0.07	-2.62 ± 0.10	-2.67 ± 0.14	-2.72 ± 0.12
2MASS J01553180−4919420	···	-2.79 ± 0.04	-2.53 ± 0.10	-3.44 ± 0.15	-2.53 ± 0.10	-2.52 ± 0.02	-2.57 ± 0.09	-2.65 ± 0.23	-2.68 ± 0.13
2MASS J01555066−6400155	···	-2.56 ± 0.05	-2.24 ± 0.12	-3.50 ± 0.15	-1.90 ± 0.10	-2.22 ± 0.10	-2.36 ± 0.08	-2.46 ± 0.12	-2.36 ± 0.13
2MASS J02005020−4657352	···	-4.01 ± 0.09	-3.18 ± 0.14	-4.43 ± 0.15	-2.72 ± 0.10	-2.80 ± 0.10	-3.29 ± 0.10	-3.59 ± 0.11	-3.74 ± 0.09
2MASS J02111462−8107085	-0.18 ± 0.10	-2.19 ± 0.01	-1.88 ± 0.08	-3.34 ± 0.15	-1.83 ± 0.10	-1.71 ± 0.10	-2.02 ± 0.07	-2.10 ± 0.12	-2.01 ± 0.16
2MASS J02395318−7019014	···	-0.08 ± 0.01	-0.25 ± 0.12	···	-0.19 ± 0.23	-0.27 ± 0.10	-0.13 ± 0.14	-0.43 ± 0.11	-0.04 ± 0.21
2MASS J03073894−0502491	···	-2.22 ± 0.10	-1.89 ± 0.10	-2.17 ± 0.15	-1.26 ± 0.10	···	-1.92 ± 0.10	-1.81 ± 0.00	0.00 ± 0.00
2MASS J03154102−7626329	-1.18 ± 0.10	-2.60 ± 0.11	-2.20 ± 0.15	-3.17 ± 0.15	-2.27 ± 0.10	-2.17 ± 0.10	-2.35 ± 0.13	-2.51 ± 0.11	-2.27 ± 0.15
2MASS J03270229+0132322	···	-1.85 ± 0.07	-2.10 ± 0.07	-3.07 ± 0.15	-1.78 ± 0.11	-1.89 ± 0.03	-2.11 ± 0.08	-2.35 ± 0.10	-2.39 ± 0.18
2MASS J03423645−1335529	···	-3.65 ± 0.05	-2.93 ± 0.12	-3.72 ± 0.15	-3.01 ± 0.10	-1.90 ± 0.10	-2.90 ± 0.10	-2.86 ± 0.00	-2.86 ± 0.00
2MASS J04245677−6500173	-1.30 ± 0.13	-2.28 ± 0.05	-1.91 ± 0.14	-2.67 ± 0.15	-1.67 ± 0.15	-1.66 ± 0.07	-2.13 ± 0.07	-2.13 ± 0.13	-1.91 ± 0.12
2MASS J04304875−4613535	···	-2.21 ± 0.08	-1.94 ± 0.11	-3.10 ± 0.15	-1.43 ± 0.12	-1.84 ± 0.10	-1.99 ± 0.14	-1.93 ± 0.20	-1.90 ± 0.18
2MASS J05030025−7601462	-1.28 ± 0.10	-2.00 ± 0.11	-1.79 ± 0.10	-2.40 ± 0.15	-1.57 ± 0.09	-1.50 ± 0.10	-1.87 ± 0.11	-1.94 ± 0.11	-1.80 ± 0.14
2MASS J05202930−5825297	···	-3.41 ± 0.10	-2.72 ± 0.11	-3.61 ± 0.15	-2.17 ± 0.11	-2.42 ± 0.02	-2.68 ± 0.07	-3.06 ± 0.08	-2.98 ± 0.14
2MASS J05241392−0336543	-1.63 ± 0.12	-1.04 ± 0.09	-2.34 ± 0.16	-2.96 ± 0.15	-2.06 ± 0.10	-1.98 ± 0.06	-2.27 ± 0.17	-2.33 ± 0.14	-2.04 ± 0.16
2MASS J05384334−5147228	···	-2.62 ± 0.00	-2.44 ± 0.15	-3.42 ± 0.15	-2.16 ± 0.00	-2.17 ± 0.10	-2.53 ± 0.08	-2.61 ± 0.10	-2.59 ± 0.16
2MASS J05432623−8051334	-1.79 ± 0.10	-2.64 ± 0.00	-2.62 ± 0.07	-3.63 ± 0.15	-2.48 ± 0.07	-2.20 ± 0.10	-2.68 ± 0.11	-2.80 ± 0.14	-2.83 ± 0.10
2MASS J05573684−5127209	···	-1.76 ± 0.03	-1.45 ± 0.22	-1.98 ± 0.15	-1.55 ± 0.10	-1.21 ± 0.11	-1.48 ± 0.20	-1.58 ± 0.28	-1.57 ± 0.24
2MASS J06392518−7414056	···	-2.14 ± 0.04	-2.06 ± 0.06	-3.34 ± 0.15	-2.13 ± 0.10	-1.96 ± 0.13	-2.17 ± 0.08	-2.29 ± 0.15	-2.24 ± 0.16
2MASS J07123398−4814049	-2.11 ± 0.10	-2.99 ± 0.10	-2.40 ± 0.11	-3.34 ± 0.15	-2.12 ± 0.10	-2.40 ± 0.05	-2.67 ± 0.11	-2.59 ± 0.09	-2.54 ± 0.14

Table 5 continued

Table 5 *(continued)*

Star ID	[O/H]	[Na/H]	[Mg/H]	[Al/H]	[Si/H]	[K/H]	[Ca/H]	[Ti I/H]	[Ti II/H]
2MASS J07150266−0154092	0.12 ± 0.10	−0.09 ± 0.10	−0.66 ± 0.18	···	−0.15 ± 0.15	−0.02 ± 0.10	−0.46 ± 0.19	−0.48 ± 0.00	−0.24 ± 0.20
2MASS J07151852−5252051	−2.01 ± 0.10	−2.34 ± 0.04	−2.32 ± 0.07	−3.41 ± 0.15	−2.10 ± 0.07	−2.19 ± 0.10	−2.36 ± 0.08	−2.50 ± 0.07	−2.46 ± 0.11
2MASS J07250021−7022038	−1.10 ± 0.10	−2.62 ± 0.05	−2.35 ± 0.07	−3.35 ± 0.15	−1.87 ± 0.10	−2.39 ± 0.10	−2.44 ± 0.08	−2.43 ± 0.16	−2.45 ± 0.16
2MASS J07443970−4425135	···	−2.33 ± 0.01	−2.26 ± 0.08	−3.27 ± 0.15	−2.18 ± 0.06	−2.14 ± 0.01	−2.33 ± 0.12	−2.46 ± 0.09	−2.45 ± 0.15
2MASS J08025449−5224304	−1.40 ± 0.05	−1.94 ± 0.00	−1.94 ± 0.09	−2.33 ± 0.15	−2.15 ± 0.10	−1.63 ± 0.10	−2.06 ± 0.11	−2.10 ± 0.14	−1.97 ± 0.16
2MASS J08295142−7242542	···	−3.11 ± 0.10	−2.71 ± 0.09	−4.07 ± 0.15	−2.58 ± 0.02	−2.87 ± 0.01	−2.84 ± 0.05	−3.01 ± 0.10	−3.17 ± 0.10
2MASS J09103481+0518228	−0.97 ± 0.10	−2.15 ± 0.13	−1.81 ± 0.13	−2.66 ± 0.15	−1.73 ± 0.14	−1.68 ± 0.11	−1.97 ± 0.08	−2.00 ± 0.16	−1.72 ± 0.16
2MASS J09291557+0838002	0.71 ± 0.10	−3.19 ± 0.10	−2.59 ± 0.09	−3.55 ± 0.15	−2.56 ± 0.10	−2.36 ± 0.16	−2.37 ± 0.06	−2.04 ± 0.15	−2.36 ± 0.13
2MASS J09531322+0744515	−1.35 ± 0.10	−1.87 ± 0.23	−1.89 ± 0.12	−3.09 ± 0.15	−1.77 ± 0.08	−1.53 ± 0.01	−1.90 ± 0.20	−1.98 ± 0.13	−1.87 ± 0.19
2MASS J10063414−7030212	···	−1.57 ± 0.10	−1.31 ± 0.07	−2.14 ± 0.15	−1.14 ± 0.02	−0.85 ± 0.02	−1.19 ± 0.14	−1.35 ± 0.18	−1.15 ± 0.17
2MASS J10073075+0348357	−1.30 ± 0.10	−2.85 ± 0.06	−2.35 ± 0.17	−3.03 ± 0.15	−2.16 ± 0.16	−2.30 ± 0.10	−2.60 ± 0.13	−2.35 ± 0.22	−2.44 ± 0.16
2MASS J10524610−0336012	−1.62 ± 0.10	−2.19 ± 0.07	−2.05 ± 0.06	−2.91 ± 0.15	−1.75 ± 0.10	−1.74 ± 0.02	−2.05 ± 0.14	−2.11 ± 0.20	−2.00 ± 0.18
2MASS J10550658+1931580	···	−2.52 ± 0.10	−2.31 ± 0.05	−3.39 ± 0.15	−2.31 ± 0.10	−2.35 ± 0.07	−2.37 ± 0.11	−2.44 ± 0.19	−2.38 ± 0.11
2MASS J11165400−7250160	−1.29 ± 0.10	−2.19 ± 0.10	−1.93 ± 0.05	−3.09 ± 0.15	−1.60 ± 0.12	−1.86 ± 0.10	−2.06 ± 0.07	−2.07 ± 0.14	−1.83 ± 0.17
2MASS J11191233−1609467	−0.02 ± 0.10	−1.24 ± 0.10	−1.55 ± 0.14	−2.69 ± 0.15	−1.31 ± 0.16	−1.23 ± 0.05	−1.42 ± 0.14	−1.40 ± 0.18	−1.34 ± 0.19
2MASS J11303693+0224037	−1.98 ± 0.10	−1.86 ± 0.02	−1.98 ± 0.10	−2.13 ± 0.15	−1.76 ± 0.10	···	−2.10 ± 0.12	−2.21 ± 0.15	−2.15 ± 0.11
2MASS J11471027+0341265	−1.38 ± 0.10	−2.24 ± 0.06	−2.13 ± 0.07	−3.19 ± 0.15	−2.04 ± 0.10	···	−2.25 ± 0.16	−2.34 ± 0.12	−2.25 ± 0.10
2MASS J11510227−6940416	−1.35 ± 0.02	−2.07 ± 0.05	−1.78 ± 0.17	−2.51 ± 0.15	−2.05 ± 0.10	−1.62 ± 0.10	−1.96 ± 0.20	−2.05 ± 0.13	−1.99 ± 0.18
2MASS J11565537+0320329	−1.35 ± 0.10	−2.15 ± 0.01	−1.84 ± 0.11	−2.92 ± 0.15	−1.68 ± 0.11	−1.74 ± 0.10	−1.93 ± 0.16	−2.02 ± 0.11	−1.78 ± 0.14
2MASS J12170829+0415146	−1.29 ± 0.10	−2.25 ± 0.10	−2.18 ± 0.15	−2.92 ± 0.15	···	−2.08 ± 0.10	−2.37 ± 0.07	−2.41 ± 0.12	−2.38 ± 0.16
2MASS J12203297+0257138	−0.81 ± 0.10	−2.04 ± 0.01	−1.71 ± 0.07	−2.85 ± 0.15	−1.80 ± 0.05	−1.71 ± 0.03	−1.97 ± 0.07	−1.99 ± 0.08	−1.72 ± 0.15
2MASS J12233047−4216365	···	−2.77 ± 0.07	−2.37 ± 0.16	−2.94 ± 0.15	−2.31 ± 0.10	−2.50 ± 0.08	−2.59 ± 0.09	−2.79 ± 0.12	−2.75 ± 0.17
2MASS J12255123−2351074	···	−2.27 ± 0.06	−2.34 ± 0.07	−3.40 ± 0.15	−2.03 ± 0.10	−2.13 ± 0.10	−2.41 ± 0.07	−2.69 ± 0.00	−2.42 ± 0.09
2MASS J12331670+1622563	···	−1.91 ± 0.07	−1.91 ± 0.16	−2.54 ± 0.15	−2.02 ± 0.03	···	−2.17 ± 0.09	−2.07 ± 0.12	−1.99 ± 0.16
2MASS J12351734+0945333	−1.30 ± 0.10	−1.84 ± 0.17	−1.89 ± 0.20	−2.60 ± 0.15	−2.00 ± 0.10	−2.00 ± 0.10	−2.22 ± 0.16	−2.14 ± 0.15	−1.85 ± 0.20
2MASS J12591462−7049592	−1.38 ± 0.10	−1.26 ± 0.07	−2.04 ± 0.16	···	−1.94 ± 0.05	−1.03 ± 0.10	−1.75 ± 0.15	−1.69 ± 0.23	−1.75 ± 0.24
2MASS J13052137−1137220	−2.13 ± 0.10	−1.74 ± 0.10	−2.41 ± 0.09	−3.20 ± 0.15	−2.06 ± 0.05	−2.05 ± 0.10	−2.49 ± 0.14	−2.60 ± 0.16	−2.60 ± 0.16
2MASS J13261792−0945176	···	−2.26 ± 0.01	−2.10 ± 0.15	−3.12 ± 0.15	−2.04 ± 0.05	−1.98 ± 0.05	−2.22 ± 0.11	−2.32 ± 0.14	−2.20 ± 0.15
2MASS J13273676−1710384	···	−1.78 ± 0.10	−1.96 ± 0.11	−2.42 ± 0.15	−2.06 ± 0.10	−1.86 ± 0.04	−2.03 ± 0.12	−2.26 ± 0.12	−2.11 ± 0.20
2MASS J13275198+0342396	−1.41 ± 0.10	−2.20 ± 0.01	−1.99 ± 0.08	−2.83 ± 0.15	−1.99 ± 0.10	−1.71 ± 0.10	−2.08 ± 0.08	−2.17 ± 0.13	−2.05 ± 0.17
2MASS J13373017−7717500	···	−1.97 ± 0.10	−2.39 ± 0.08	−3.49 ± 0.15	−1.89 ± 0.10	−2.25 ± 0.02	−2.43 ± 0.04	−2.61 ± 0.08	−2.49 ± 0.13
2MASS J13494713−7423395	···	−2.85 ± 0.15	−2.02 ± 0.18	−2.07 ± 0.15	−1.85 ± 0.10	···	−2.07 ± 0.12	−2.17 ± 0.13	−2.08 ± 0.23
2MASS J13511539−7340363	−1.29 ± 0.10	−1.93 ± 0.10	−1.57 ± 0.15	−3.40 ± 0.15	−1.52 ± 0.03	−1.32 ± 0.04	−1.54 ± 0.13	−1.67 ± 0.19	−1.54 ± 0.20
2MASS J13524835+1254216	···	−1.95 ± 0.15	−1.94 ± 0.05	−2.67 ± 0.15	−1.85 ± 0.10	−1.83 ± 0.02	−2.00 ± 0.10	−2.10 ± 0.09	−1.99 ± 0.11
2MASS J13554406−3750455	−2.06 ± 0.10	−2.11 ± 0.05	−2.27 ± 0.10	−3.40 ± 0.15	−1.90 ± 0.10	−2.39 ± 0.10	−2.31 ± 0.11	−2.53 ± 0.15	−2.59 ± 0.17

Table 5 continued

Table 5 *(continued)*

Star ID	[O/H]	[Na/H]	[Mg/H]	[Al/H]	[Si/H]	[K/H]	[Ca/H]	[Ti I/H]	[Ti II/H]
2MASS J13592232−6821493	···	−1.93 ± 0.12	−1.71 ± 0.12	−2.99 ± 0.15	−1.83 ± 0.10	−1.53 ± 0.10	−1.61 ± 0.11	−1.86 ± 0.14	−1.69 ± 0.18
2MASS J14100568−0701443	−1.20 ± 0.10	−2.06 ± 0.06	−1.66 ± 0.16	−2.58 ± 0.15	−1.55 ± 0.09	−1.67 ± 0.10	−1.84 ± 0.12	−1.96 ± 0.14	−1.72 ± 0.19
2MASS J14112614−1137453	−1.33 ± 0.12	−3.21 ± 0.01	−2.43 ± 0.15	−3.37 ± 0.15	−2.15 ± 0.10	−2.60 ± 0.11	−2.81 ± 0.09	−2.69 ± 0.10	−2.62 ± 0.15
2MASS J14234371−4025526	−1.03 ± 0.10	−2.09 ± 0.10	−1.91 ± 0.09	−2.69 ± 0.15	−1.78 ± 0.10	−1.88 ± 0.10	−2.06 ± 0.11	−2.16 ± 0.13	−2.05 ± 0.14
2MASS J14335592−1240357	···	−3.11 ± 0.10	−2.68 ± 0.16	−3.68 ± 0.15	−2.32 ± 0.10	−2.60 ± 0.10	−2.84 ± 0.12	−2.83 ± 0.20	−2.77 ± 0.20
2MASS J14355850−0719265	−0.95 ± 0.07	−1.93 ± 0.04	−1.47 ± 0.11	···	−1.54 ± 0.08	−1.08 ± 0.01	−1.62 ± 0.10	−1.58 ± 0.15	−1.30 ± 0.18
2MASS J14443014−1320092	−1.52 ± 0.10	−2.51 ± 0.05	−2.35 ± 0.06	−3.21 ± 0.15	−2.25 ± 0.10	−2.42 ± 0.04	−2.47 ± 0.12	−2.59 ± 0.12	−2.49 ± 0.12
2MASS J14533268−3614555	···	−2.89 ± 0.18	−2.62 ± 0.09	−3.87 ± 0.15	−2.50 ± 0.10	−2.03 ± 0.10	−2.66 ± 0.08	−2.79 ± 0.09	−2.76 ± 0.13
2MASS J14534137+0040467	−1.23 ± 0.05	−2.15 ± 0.15	−1.90 ± 0.15	−2.86 ± 0.15	−1.89 ± 0.10	−1.78 ± 0.03	−2.03 ± 0.15	−2.10 ± 0.14	−1.82 ± 0.15
2MASS J14543792+0830379	···	−2.22 ± 0.10	−2.01 ± 0.06	−2.92 ± 0.15	−1.95 ± 0.08	−1.87 ± 0.10	−1.99 ± 0.12	−2.22 ± 0.14	−2.04 ± 0.14
2MASS J14564556−1615432	−0.46 ± 0.10	−1.64 ± 0.01	−1.92 ± 0.12	−2.97 ± 0.15	−1.86 ± 0.11	−1.84 ± 0.10	−1.96 ± 0.11	−1.97 ± 0.20	−2.04 ± 0.14
2MASS J14590234−0916105	−1.15 ± 0.10	−2.50 ± 0.01	−2.40 ± 0.08	−3.21 ± 0.15	−2.25 ± 0.02	−2.41 ± 0.03	−2.46 ± 0.13	−2.62 ± 0.12	−2.43 ± 0.14
2MASS J15013452−2443310	···	−2.56 ± 0.03	−2.40 ± 0.07	−2.90 ± 0.15	−2.17 ± 0.10	−2.22 ± 0.11	−2.46 ± 0.09	−2.49 ± 0.19	−2.55 ± 0.17
2MASS J15042611−2231523	−0.54 ± 0.10	−1.79 ± 0.03	−1.61 ± 0.20	−2.83 ± 0.15	−1.64 ± 0.10	···	−1.63 ± 0.12	−1.74 ± 0.15	−1.70 ± 0.21
2MASS J15133549−1244339	−1.86 ± 0.10	−2.63 ± 0.10	−2.38 ± 0.08	−3.30 ± 0.15	−2.32 ± 0.10	−2.21 ± 0.10	−2.38 ± 0.14	−2.54 ± 0.12	−2.42 ± 0.12
2MASS J15204531−1742486	···	−2.41 ± 0.09	−2.31 ± 0.11	−3.07 ± 0.15	−2.18 ± 0.10	−2.22 ± 0.10	−2.36 ± 0.14	−2.48 ± 0.14	−2.41 ± 0.15
2MASS J15240713−0319509	−1.04 ± 0.10	−2.64 ± 0.02	−2.32 ± 0.10	−3.43 ± 0.15	−2.00 ± 0.02	−2.45 ± 0.10	−2.42 ± 0.10	−2.44 ± 0.11	−2.38 ± 0.14
2MASS J15272126−1445153	−1.32 ± 0.10	−2.16 ± 0.09	−1.93 ± 0.08	−2.60 ± 0.15	−2.19 ± 0.10	−2.02 ± 0.10	−2.03 ± 0.08	−2.17 ± 0.16	−2.18 ± 0.13
2MASS J16115667−8034422	−0.70 ± 0.10	−1.75 ± 0.06	−1.54 ± 0.18	−2.55 ± 0.15	−1.48 ± 0.10	−0.88 ± 0.10	−1.29 ± 0.19	−1.42 ± 0.17	−1.15 ± 0.21
2MASS J16163600−5700568	−0.97 ± 0.10	−2.38 ± 0.14	−2.36 ± 0.04	−3.63 ± 0.15	−2.12 ± 0.06	−2.17 ± 0.10	−2.40 ± 0.08	−2.52 ± 0.08	−2.95 ± 0.10
2MASS J16592172−6827199	−0.99 ± 0.20	−2.15 ± 0.03	−1.71 ± 0.21	−2.48 ± 0.15	−2.90 ± 0.14	−1.31 ± 0.10	−1.75 ± 0.07	−1.86 ± 0.16	−1.74 ± 0.19
2MASS J17043634−6219457	···	−2.10 ± 0.02	−2.19 ± 0.12	−3.32 ± 0.15	−2.06 ± 0.13	−2.05 ± 0.10	−2.29 ± 0.13	−2.46 ± 0.09	−2.45 ± 0.12
2MASS J17060555+0412354	−2.05 ± 0.10	−2.30 ± 0.01	−2.34 ± 0.15	−2.62 ± 0.15	−1.88 ± 0.10	−2.36 ± 0.10	−2.47 ± 0.17	−2.54 ± 0.12	−2.41 ± 0.17
2MASS J17070759−7817561	···	−2.09 ± 0.09	−2.10 ± 0.04	−3.17 ± 0.15	−1.82 ± 0.10	−2.13 ± 0.05	−2.31 ± 0.09	−2.44 ± 0.12	−2.32 ± 0.14
2MASS J17131974−7113010	···	−1.91 ± 0.01	−1.90 ± 0.10	−2.77 ± 0.15	−1.72 ± 0.10	−1.84 ± 0.10	−1.95 ± 0.14	−2.15 ± 0.11	−2.15 ± 0.11
2MASS J17163340−7009028	···	−2.36 ± 0.10	−2.09 ± 0.14	−2.56 ± 0.15	−2.29 ± 0.10	−1.99 ± 0.10	−2.23 ± 0.12	−2.34 ± 0.10	−2.27 ± 0.14
2MASS J17360167−5145296	−0.72 ± 0.10	−1.91 ± 0.02	−1.64 ± 0.17	−2.97 ± 0.15	−1.73 ± 0.13	−1.59 ± 0.10	−1.73 ± 0.18	−1.89 ± 0.13	−1.76 ± 0.17
2MASS J17541561−5148268	−1.17 ± 0.03	−1.77 ± 0.08	−1.62 ± 0.09	−2.36 ± 0.15	−1.51 ± 0.19	−1.05 ± 0.10	−1.57 ± 0.10	−1.73 ± 0.14	−1.53 ± 0.26
2MASS J18272432−5655165	−1.00 ± 0.02	−1.92 ± 0.09	−1.63 ± 0.12	−3.78 ± 0.15	−1.66 ± 0.26	−1.24 ± 0.10	−1.68 ± 0.17	−1.77 ± 0.13	−1.68 ± 0.20
2MASS J18284356−8441346	−0.20 ± 0.05	−0.83 ± 0.01	−0.66 ± 0.24	···	−0.09 ± 0.27	−0.57 ± 0.12	−0.78 ± 0.23	−0.80 ± 0.20	−0.53 ± 0.24
2MASS J18294359−4924253	−0.84 ± 0.05	−2.02 ± 0.09	−1.57 ± 0.16	−2.38 ± 0.15	−1.22 ± 0.14	−0.98 ± 0.10	−1.47 ± 0.17	−1.55 ± 0.20	−1.43 ± 0.18
2MASS J18332056−3802590	−1.16 ± 0.10	−1.14 ± 0.02	−1.65 ± 0.14	−9.99 ± 0.15	−1.88 ± 0.10	−0.98 ± 0.10	−1.53 ± 0.19	−1.70 ± 0.12	−1.53 ± 0.19
2MASS J18333188−4840403	···	−2.22 ± 0.03	−2.09 ± 0.11	−2.95 ± 0.15	−1.62 ± 0.10	−1.94 ± 0.08	−2.12 ± 0.11	−2.29 ± 0.12	−2.17 ± 0.12
2MASS J18361214−7333443	···	−2.36 ± 0.01	−2.03 ± 0.13	−3.10 ± 0.15	−2.12 ± 0.01	−2.14 ± 0.10	−2.24 ± 0.08	−2.32 ± 0.12	−2.16 ± 0.14
2MASS J18405985−4841353	···	−2.46 ± 0.10	−2.42 ± 0.09	−3.33 ± 0.15	−2.23 ± 0.10	−2.37 ± 0.04	−2.50 ± 0.06	−2.68 ± 0.11	−2.62 ± 0.13

Table 5 continued

Table 5 *(continued)*

Star ID	[O/H]	[Na/H]	[Mg/H]	[Al/H]	[Si/H]	[K/H]	[Ca/H]	[Ti I/H]	[Ti II/H]
2MASS J18560360−6403465	-0.95 ± 0.10	-2.12 ± 0.06	-1.97 ± 0.12	-2.83 ± 0.15	-1.87 ± 0.11	-1.92 ± 0.10	-2.09 ± 0.09	-2.23 ± 0.11	-2.07 ± 0.10
2MASS J19092677−5140208	-1.08 ± 0.09	-2.03 ± 0.01	-1.86 ± 0.12	-2.83 ± 0.15	-2.02 ± 0.15	-1.59 ± 0.10	-1.96 ± 0.13	-2.05 ± 0.11	-1.77 ± 0.16
2MASS J19105886−4059412	-1.98 ± 0.10	-2.36 ± 0.09	-1.94 ± 0.08	-2.88 ± 0.15	-1.63 ± 0.10	-1.96 ± 0.10	-2.06 ± 0.08	-2.10 ± 0.14	-2.01 ± 0.11
2MASS J19175585−5440147	···	-2.41 ± 0.08	-2.17 ± 0.08	-3.24 ± 0.15	-2.11 ± 0.16	-2.11 ± 0.10	-2.28 ± 0.10	-2.44 ± 0.10	-2.42 ± 0.18
2MASS J19192768−5959140	-1.18 ± 0.10	-2.27 ± 0.08	-2.15 ± 0.12	-3.00 ± 0.15	-1.93 ± 0.08	-2.33 ± 0.10	-2.27 ± 0.18	-2.35 ± 0.13	-2.16 ± 0.13
2MASS J19282163−2457545	-2.05 ± 0.11	-2.25 ± 0.07	-2.19 ± 0.09	-3.39 ± 0.15	-1.94 ± 0.07	-2.06 ± 0.10	-2.26 ± 0.13	-2.49 ± 0.11	-2.39 ± 0.13
2MASS J19291910−5528181	-1.16 ± 0.08	-2.29 ± 0.14	-1.96 ± 0.12	-2.40 ± 0.15	-1.93 ± 0.10	···	-2.00 ± 0.09	-2.02 ± 0.16	-1.88 ± 0.17
2MASS J19310426−3707397	-0.84 ± 0.09	-1.72 ± 0.07	-1.50 ± 0.13	-2.44 ± 0.15	-1.66 ± 0.13	···	-1.91 ± 0.14	-2.04 ± 0.14	-1.90 ± 0.16
2MASS J19320444−7309178	-1.75 ± 0.05	-2.18 ± 0.10	-1.44 ± 0.25	-2.71 ± 0.15	-2.21 ± 0.10	-2.07 ± 0.10	-2.45 ± 0.05	-2.03 ± 0.05	-2.39 ± 0.20
2MASS J19504989−3321107	···	-3.00 ± 0.04	-2.71 ± 0.09	-3.76 ± 0.15	-2.58 ± 0.10	-2.76 ± 0.10	-2.97 ± 0.08	-2.98 ± 0.12	-3.03 ± 0.13
2MASS J19532495−3647303	-1.92 ± 0.08	-2.43 ± 0.03	-2.25 ± 0.13	-3.24 ± 0.15	-2.06 ± 0.10	-2.09 ± 0.10	-2.39 ± 0.09	-2.46 ± 0.08	-2.32 ± 0.12
2MASS J19552158−4613569	-2.18 ± 0.10	-2.18 ± 0.10	-2.06 ± 0.13	-2.83 ± 0.15	-1.90 ± 0.10	-1.69 ± 0.05	-2.12 ± 0.06	-2.21 ± 0.11	-2.13 ± 0.18
2MASS J19563822−4054235	···	-1.68 ± 0.10	-2.03 ± 0.13	-2.94 ± 0.15	-2.03 ± 0.19	-1.81 ± 0.01	-2.09 ± 0.09	-2.21 ± 0.10	-2.29 ± 0.19
2MASS J19570893−3317320	-2.11 ± 0.10	-2.36 ± 0.10	-2.36 ± 0.11	-3.32 ± 0.15	-2.13 ± 0.16	-2.20 ± 0.10	-2.50 ± 0.09	-2.57 ± 0.10	-2.52 ± 0.13
2MASS J20035532−5028100	-1.57 ± 0.10	-2.27 ± 0.10	-2.13 ± 0.11	-2.96 ± 0.15	-2.15 ± 0.10	-2.17 ± 0.01	-2.23 ± 0.13	-2.46 ± 0.10	-2.35 ± 0.12
2MASS J20192202−6130149	-1.71 ± 0.10	-2.19 ± 0.10	-2.22 ± 0.12	-3.04 ± 0.15	-2.12 ± 0.04	-2.25 ± 0.01	-2.50 ± 0.15	-2.63 ± 0.10	-2.55 ± 0.15
2MASS J20202917−2707347	···	-2.37 ± 0.10	-2.23 ± 0.06	-3.11 ± 0.15	-2.30 ± 0.10	-2.33 ± 0.10	-2.31 ± 0.14	-2.43 ± 0.10	-2.34 ± 0.16
2MASS J20234398−0815472	···	-2.65 ± 0.11	-2.55 ± 0.08	-3.78 ± 0.15	-2.50 ± 0.10	-2.41 ± 0.10	-2.68 ± 0.08	-2.80 ± 0.07	-2.87 ± 0.12
2MASS J20242122−2656435	-1.60 ± 0.02	-2.49 ± 0.16	-2.15 ± 0.13	-3.10 ± 0.15	-2.17 ± 0.08	-2.15 ± 0.10	-2.39 ± 0.07	-2.41 ± 0.13	-2.19 ± 0.12
2MASS J20374042−5520500	-1.67 ± 0.10	-1.79 ± 0.10	-2.14 ± 0.14	-3.65 ± 0.15	-1.97 ± 0.10	-1.95 ± 0.10	-2.29 ± 0.10	-2.38 ± 0.10	-2.32 ± 0.15
2MASS J20445065−3714000	-1.46 ± 0.13	-2.28 ± 0.05	-2.25 ± 0.05	-2.94 ± 0.15	-2.09 ± 0.04	-2.38 ± 0.10	-2.47 ± 0.10	-2.57 ± 0.11	-2.40 ± 0.18
2MASS J20501790−0549230	···	-2.68 ± 0.07	-2.51 ± 0.12	-3.64 ± 0.15	-2.33 ± 0.02	-2.36 ± 0.10	-2.48 ± 0.14	-2.55 ± 0.11	-2.63 ± 0.14
2MASS J20585505−1759007	···	-3.40 ± 0.04	-2.95 ± 0.11	-3.87 ± 0.15	-2.67 ± 0.04	-2.82 ± 0.10	-3.07 ± 0.11	-3.13 ± 0.09	-3.16 ± 0.16
2MASS J21220020−0820333	-0.71 ± 0.10	-1.90 ± 0.06	-1.54 ± 0.14	-1.87 ± 0.15	-1.20 ± 0.11	-1.14 ± 0.01	-1.49 ± 0.17	-1.61 ± 0.18	-1.50 ± 0.20
2MASS J21234588−0839448	···	-3.46 ± 0.01	-2.68 ± 0.20	-3.75 ± 0.15	-2.23 ± 0.13	-2.41 ± 0.10	-2.83 ± 0.15	-2.85 ± 0.10	-2.76 ± 0.19
2MASS J21352343−5722598	···	-2.45 ± 0.04	-2.34 ± 0.10	-3.50 ± 0.15	-2.08 ± 0.16	-2.14 ± 0.02	-2.40 ± 0.10	-2.42 ± 0.11	-2.42 ± 0.11
2MASS J21553580−0905118	-1.59 ± 0.10	-2.21 ± 0.03	-2.03 ± 0.10	-3.19 ± 0.15	-2.12 ± 0.09	-1.77 ± 0.13	-2.12 ± 0.08	-2.25 ± 0.10	-2.03 ± 0.11
2MASS J22182082−3827554	···	-1.77 ± 0.13	-2.14 ± 0.09	-2.70 ± 0.15	-1.73 ± 0.04	-1.80 ± 0.10	-2.05 ± 0.13	-2.16 ± 0.10	-2.08 ± 0.14
2MASS J22215794−3602090	-0.97 ± 0.10	-2.17 ± 0.05	-2.11 ± 0.09	-3.30 ± 0.15	-1.90 ± 0.10	-1.85 ± 0.07	-2.13 ± 0.08	-2.29 ± 0.10	-2.23 ± 0.14
2MASS J22220344−8024592	-1.28 ± 0.10	-2.18 ± 0.18	-2.22 ± 0.12	-3.25 ± 0.15	-2.12 ± 0.10	-2.22 ± 0.10	-2.47 ± 0.09	-2.61 ± 0.15	-2.53 ± 0.13
2MASS J22253443−2027171	-0.93 ± 0.10	-1.45 ± 0.01	-1.97 ± 0.07	-2.61 ± 0.15	-1.73 ± 0.13	-1.69 ± 0.10	-2.07 ± 0.08	-2.21 ± 0.09	-2.15 ± 0.13
2MASS J22300238−6332191	-1.57 ± 0.10	-1.84 ± 0.10	-1.77 ± 0.06	-2.76 ± 0.15	-1.47 ± 0.03	-1.62 ± 0.10	-1.85 ± 0.13	-2.03 ± 0.15	-1.94 ± 0.15
2MASS J22302641−1949527	-1.53 ± 0.09	-2.20 ± 0.03	-2.04 ± 0.10	-2.99 ± 0.15	-2.06 ± 0.04	-1.87 ± 0.10	-2.15 ± 0.11	-2.28 ± 0.11	-2.10 ± 0.16
2MASS J22344202−0826492	···	-2.52 ± 0.02	-2.33 ± 0.09	-3.14 ± 0.15	-2.25 ± 0.10	-2.27 ± 0.10	-2.38 ± 0.13	-2.51 ± 0.11	-2.50 ± 0.15
2MASS J22345447−6605172	-1.05 ± 0.10	-2.37 ± 0.04	-2.24 ± 0.08	-3.39 ± 0.15	-2.21 ± 0.10	-2.07 ± 0.06	-2.31 ± 0.13	-2.42 ± 0.11	-2.36 ± 0.11

Table 5 continued

Table 5 *(continued)*

Star ID	[O/H]	[Na/H]	[Mg/H]	[Al/H]	[Si/H]	[K/H]	[Ca/H]	[Ti I/H]	[Ti II/H]
2MASS J22394827−0803536	-0.92 ± 0.10	-1.95 ± 0.09	-1.53 ± 0.09	···	-1.48 ± 0.06	-1.27 ± 0.10	-1.50 ± 0.32	-1.53 ± 0.17	-1.36 ± 0.32
2MASS J23100319−7702165	-0.96 ± 0.10	-2.47 ± 0.03	-2.16 ± 0.11	-3.15 ± 0.15	-2.00 ± 0.11	-2.04 ± 0.11	-2.25 ± 0.11	-2.37 ± 0.09	-2.30 ± 0.14
2MASS J23411581−6406440	-1.72 ± 0.10	-2.14 ± 0.04	-2.10 ± 0.06	-3.28 ± 0.15	-1.91 ± 0.06	-1.83 ± 0.04	-2.16 ± 0.12	-2.31 ± 0.12	-2.27 ± 0.11

Table 6. Fe-Peak Element Abundances

Star ID	[Sc/H]	[V/H]	[Cr/H]	[Mn/H]	[Co/H]	[Ni/H]	[Zn/H]
2MASS J00011195+0321051	-1.97 ± 0.12	-1.72 ± 0.17	-1.88 ± 0.04	-2.35 ± 0.12	-1.92 ± 0.12	-2.17 ± 0.16	-1.87 ± 0.05
2MASS J00101758−1735387	-3.20 ± 0.18	-2.56 ± 0.17	-2.25 ± 0.07	-3.08 ± 0.07	-2.66 ± 0.20	-3.02 ± 0.00	-3.09 ± 0.00
2MASS J00162809−0505519	-3.04 ± 0.12	-2.48 ± 0.19	-3.17 ± 0.00	-3.43 ± 0.11	-2.74 ± 0.11	-2.82 ± 0.14	-2.72 ± 0.00
2MASS J00195350−0145445	-2.35 ± 0.10	-2.24 ± 0.09	-2.40 ± 0.07	-2.84 ± 0.08	-2.42 ± 0.18	-2.45 ± 0.16	-2.28 ± 0.04
2MASS J00282278−3934598	-2.47 ± 0.12	-2.07 ± 0.14	-2.37 ± 0.01	-2.99 ± 0.11	-2.50 ± 0.20	-2.46 ± 0.12	-2.27 ± 0.06
2MASS J00372794−2045307	-2.66 ± 0.08	-2.37 ± 0.08	-2.53 ± 0.02	-2.66 ± 0.10	-2.44 ± 0.13	-2.53 ± 0.13	-2.22 ± 0.07
2MASS J00452379−2112161	-2.51 ± 0.09	-2.38 ± 0.10	-2.49 ± 0.02	-2.98 ± 0.12	-2.42 ± 0.15	-2.55 ± 0.13	-2.43 ± 0.05
2MASS J00463619−3739335	-3.92 ± 0.16	···	-3.08 ± 0.00	-4.77 ± 0.29	-3.44 ± 0.17	-3.65 ± 0.23	-3.38 ± 0.02
2MASS J00512646−1053170	-2.20 ± 0.04	-2.02 ± 0.07	-2.28 ± 0.10	-2.86 ± 0.08	-2.15 ± 0.09	-2.36 ± 0.14	-2.37 ± 0.00
2MASS J00524174−0902235	-1.33 ± 0.00	0.00 ± 0.00	-1.60 ± 0.00	···	-1.54 ± 0.00	-1.51 ± 0.00	-1.55 ± 0.00
2MASS J01165010−6307441	-1.55 ± 0.11	-1.50 ± 0.06	-1.64 ± 0.04	-1.96 ± 0.09	-1.36 ± 0.13	-1.66 ± 0.12	-1.60 ± 0.03
2MASS J01374434−4301490	-2.73 ± 0.06	-2.27 ± 0.17	-2.66 ± 0.06	-3.10 ± 0.05	-2.53 ± 0.15	-2.72 ± 0.15	-2.52 ± 0.10
2MASS J01473804−1130474	-2.21 ± 0.21	-1.83 ± 0.12	-2.11 ± 0.12	-2.72 ± 0.08	-1.93 ± 0.19	-2.28 ± 0.11	-2.17 ± 0.04
2MASS J01501343+0725010	-2.96 ± 0.11	-2.74 ± 0.16	-2.80 ± 0.06	-3.30 ± 0.03	-2.73 ± 0.12	-2.85 ± 0.16	-2.73 ± 0.18
2MASS J01553180−4919420	-2.84 ± 0.22	-2.65 ± 0.23	-2.68 ± 0.13	-3.00 ± 0.12	-2.67 ± 0.28	-2.68 ± 0.16	-2.70 ± 0.15
2MASS J01555066−6400155	-2.57 ± 0.16	-2.27 ± 0.10	-2.53 ± 0.00	-2.99 ± 0.07	-2.48 ± 0.21	-2.59 ± 0.12	-2.45 ± 0.03
2MASS J02005020−4657352	-3.66 ± 0.03	···	···	-5.03 ± 0.06	-3.70 ± 0.18	-4.04 ± 0.07	···
2MASS J02111462−8107085	-2.13 ± 0.02	-2.00 ± 0.06	-2.21 ± 0.06	-2.58 ± 0.14	-2.19 ± 0.10	-2.33 ± 0.16	-2.36 ± 0.00
2MASS J02395318−7019014	-0.01 ± 0.09	···	-0.19 ± 0.03	-0.12 ± 0.04	-0.03 ± 0.17	-0.25 ± 0.13	-0.31 ± 0.06
2MASS J03073894−0502491	-1.82 ± 0.00	···	-2.29 ± 0.00	···	-1.76 ± 0.00	-2.27 ± 0.00	-2.27 ± 0.00
2MASS J03154102−7626329	-2.50 ± 0.07	-2.21 ± 0.07	-2.30 ± 0.00	-3.02 ± 0.00	-2.40 ± 0.08	-2.65 ± 0.08	-2.54 ± 0.00
2MASS J03270229+0132322	-2.63 ± 0.05	-2.43 ± 0.09	-2.55 ± 0.09	-2.79 ± 0.08	-2.22 ± 0.16	-2.45 ± 0.22	-2.24 ± 0.02
2MASS J03423645−1335529	-2.63 ± 0.08	-1.93 ± 0.00	···	-3.37 ± 0.00	-2.51 ± 0.00	-3.27 ± 0.27	···
2MASS J04245677−6500173	-2.10 ± 0.11	-1.48 ± 0.00	-2.43 ± 0.15	-2.76 ± 0.03	-1.98 ± 0.27	-2.34 ± 0.16	-2.43 ± 0.00
2MASS J04304875−4613535	-1.92 ± 0.19	-2.03 ± 0.08	-1.88 ± 0.08	-2.58 ± 0.22	-2.11 ± 0.13	-2.19 ± 0.17	-2.28 ± 0.00
2MASS J05030025−7601462	-2.04 ± 0.07	-1.06 ± 0.00	-2.37 ± 0.11	-2.55 ± 0.03	-1.74 ± 0.02	-2.12 ± 0.12	-2.07 ± 0.05
2MASS J05202930−5825297	-3.10 ± 0.09	-2.90 ± 0.16	-3.01 ± 0.03	-3.65 ± 0.07	-3.01 ± 0.16	-3.21 ± 0.11	-2.98 ± 0.04
2MASS J05241392−0336543	-2.15 ± 0.15	-1.91 ± 0.00	-2.14 ± 0.00	-2.83 ± 0.27	-2.26 ± 0.09	-2.49 ± 0.18	-2.55 ± 0.04
2MASS J05384334−5147228	-3.15 ± 0.11	···	-3.13 ± 0.11	-3.42 ± 0.03	-2.75 ± 0.11	-2.87 ± 0.13	-2.71 ± 0.11
2MASS J05432623−8051334	-3.09 ± 0.04	···	-3.28 ± 0.15	-3.15 ± 0.13	-2.91 ± 0.05	-3.05 ± 0.10	-2.80 ± 0.00
2MASS J05573684−5127209	-1.42 ± 0.30	···	···	-2.09 ± 0.15	···	-1.56 ± 0.28	-1.81 ± 0.00
2MASS J06392518−7414056	-2.57 ± 0.12	-2.34 ± 0.10	-2.73 ± 0.16	-2.94 ± 0.16	-2.40 ± 0.11	-2.51 ± 0.13	-2.28 ± 0.15

Table 6 continued

Table 6 *(continued)*

Star ID	[Sc/H]	[V/H]	[Cr/H]	[Mn/H]	[Co/H]	[Ni/H]	[Zn/H]
2MASS J07123398−4814049	−2.78 ± 0.09	−2.61 ± 0.12	−2.80 ± 0.04	−3.54 ± 0.09	−2.58 ± 0.19	−2.88 ± 0.15	−2.68 ± 0.07
2MASS J07150266−0154092	−0.10 ± 0.16	···	−0.47 ± 0.00	−0.20 ± 0.00	···	−0.38 ± 0.31	−0.28 ± 0.00
2MASS J07151852−5252051	−2.65 ± 0.08	−2.57 ± 0.11	−2.64 ± 0.10	−2.90 ± 0.06	−2.48 ± 0.11	−2.60 ± 0.11	−2.44 ± 0.03
2MASS J07250021−7022038	−2.79 ± 0.10	−2.34 ± 0.14	−2.62 ± 0.16	−3.25 ± 0.12	−2.60 ± 0.10	−2.58 ± 0.20	−2.50 ± 0.00
2MASS J07443970−4425135	−2.75 ± 0.08	−2.60 ± 0.13	−2.49 ± 0.14	−2.86 ± 0.11	−2.48 ± 0.15	−2.51 ± 0.08	−2.43 ± 0.05
2MASS J08025449−5224304	−2.08 ± 0.13	−2.33 ± 0.00	−2.19 ± 0.04	−2.59 ± 0.07	−1.99 ± 0.19	−2.25 ± 0.17	−2.15 ± 0.01
2MASS J08295142−7242542	−3.47 ± 0.03	···	−3.79 ± 0.02	−4.16 ± 0.01	−3.06 ± 0.09	−3.29 ± 0.09	···
2MASS J09103481+0518228	−1.88 ± 0.07	−2.05 ± 0.14	−2.00 ± 0.06	−2.76 ± 0.08	−1.61 ± 0.15	−2.16 ± 0.17	−2.01 ± 0.13
2MASS J09291557+0838002	−2.50 ± 0.06	···	−2.51 ± 0.16	−3.11 ± 0.07	−2.37 ± 0.18	−2.57 ± 0.19	−2.37 ± 0.00
2MASS J09531322+0744515	−2.05 ± 0.12	−2.13 ± 0.05	−2.12 ± 0.00	−2.54 ± 0.15	−2.23 ± 0.16	−2.20 ± 0.16	−2.18 ± 0.04
2MASS J10063414−7030212	−1.49 ± 0.16	−1.54 ± 0.09	−1.48 ± 0.08	−1.94 ± 0.05	−1.36 ± 0.07	−1.58 ± 0.11	−1.61 ± 0.06
2MASS J10073075+0348357	−2.60 ± 0.17	−2.50 ± 0.10	−2.19 ± 0.00	−2.92 ± 0.19	−2.21 ± 0.12	−2.35 ± 0.20	−2.50 ± 0.00
2MASS J10524610−0336012	−2.11 ± 0.12	−2.14 ± 0.13	−2.52 ± 0.12	−2.63 ± 0.01	−2.31 ± 0.07	−2.20 ± 0.14	−2.19 ± 0.00
2MASS J10550658+1931580	−2.81 ± 0.11	−2.44 ± 0.10	−2.49 ± 0.00	−3.10 ± 0.13	−2.60 ± 0.14	−2.81 ± 0.11	···
2MASS J11165400−7250160	−2.12 ± 0.14	···	−1.97 ± 0.18	−2.60 ± 0.06	−1.77 ± 0.00	−2.31 ± 0.16	−2.19 ± 0.13
2MASS J11191233−1609467	−1.62 ± 0.06	−1.55 ± 0.00	−1.34 ± 0.28	−2.10 ± 0.28	−1.76 ± 0.01	−1.63 ± 0.16	−1.50 ± 0.07
2MASS J11303693+0224037	−2.33 ± 0.10	−1.93 ± 0.29	−2.29 ± 0.04	−2.76 ± 0.09	−2.18 ± 0.25	−2.37 ± 0.15	−2.26 ± 0.10
2MASS J11471027+0341265	−2.48 ± 0.06	−2.14 ± 0.25	−2.27 ± 0.00	−2.69 ± 0.10	−2.36 ± 0.18	−2.44 ± 0.20	−2.38 ± 0.06
2MASS J11510227−6940416	−2.13 ± 0.10	−2.09 ± 0.05	−2.29 ± 0.05	−2.73 ± 0.09	−2.12 ± 0.14	−2.34 ± 0.18	−2.35 ± 0.02
2MASS J11565537+0320329	−2.06 ± 0.11	−1.84 ± 0.18	−2.01 ± 0.04	−2.51 ± 0.20	−2.00 ± 0.09	−2.14 ± 0.11	−2.11 ± 0.01
2MASS J12170829+0415146	−2.59 ± 0.12	···	−2.80 ± 0.12	−3.12 ± 0.06	−2.57 ± 0.13	−2.58 ± 0.10	−2.47 ± 0.04
2MASS J12203297+0257138	−2.04 ± 0.08	−1.69 ± 0.08	−2.02 ± 0.09	−2.49 ± 0.12	−2.01 ± 0.17	−2.28 ± 0.11	−2.09 ± 0.00
2MASS J12233047−4216365	−3.07 ± 0.05	−2.82 ± 0.09	−2.75 ± 0.00	−3.38 ± 0.04	−2.64 ± 0.12	−2.92 ± 0.13	−2.76 ± 0.13
2MASS J12255123−2351074	−2.81 ± 0.00	−2.52 ± 0.09	−3.14 ± 0.01	−3.30 ± 0.00	−2.55 ± 0.01	−2.69 ± 0.00	−2.48 ± 0.00
2MASS J12331670+1622563	−2.11 ± 0.08	−2.25 ± 0.00	−2.21 ± 0.01	−2.71 ± 0.14	−1.94 ± 0.09	−2.31 ± 0.08	−2.23 ± 0.08
2MASS J12351734+0945333	−2.02 ± 0.10	−1.93 ± 0.11	−1.96 ± 0.07	−2.69 ± 0.06	−1.87 ± 0.10	−2.25 ± 0.15	−2.17 ± 0.06
2MASS J12591462−7049592	−1.75 ± 0.14	···	−1.89 ± 0.11	−2.61 ± 0.15	−2.08 ± 0.00	−2.16 ± 0.25	−2.13 ± 0.02
2MASS J13052137−1137220	−2.82 ± 0.08	−2.62 ± 0.06	−2.86 ± 0.10	−3.45 ± 0.09	−2.67 ± 0.14	−2.89 ± 0.09	−2.93 ± 0.04
2MASS J13261792−0945176	−2.46 ± 0.07	−2.37 ± 0.13	−2.35 ± 0.06	−2.89 ± 0.20	−2.41 ± 0.15	−2.58 ± 0.15	−2.40 ± 0.09
2MASS J13273676−1710384	−2.43 ± 0.11	−2.27 ± 0.05	−2.25 ± 0.04	−2.85 ± 0.10	−2.31 ± 0.10	−2.47 ± 0.17	−2.27 ± 0.07
2MASS J13275198+0342396	−2.22 ± 0.15	−2.19 ± 0.15	−2.47 ± 0.10	−2.61 ± 0.05	−2.32 ± 0.18	−2.23 ± 0.12	−2.30 ± 0.06
2MASS J13373017−7717500	−2.92 ± 0.08	−2.40 ± 0.20	−2.77 ± 0.02	−3.30 ± 0.15	−2.67 ± 0.14	−2.73 ± 0.09	−2.54 ± 0.07
2MASS J13494713−7423395	−2.32 ± 0.13	−2.19 ± 0.10	−2.37 ± 0.00	−2.77 ± 0.10	−2.07 ± 0.17	−2.34 ± 0.18	−2.27 ± 0.02
2MASS J13511539−7340363	−1.77 ± 0.09	−1.70 ± 0.11	−1.75 ± 0.15	−2.22 ± 0.03	−1.93 ± 0.20	−1.85 ± 0.12	−1.69 ± 0.06

Table 6 continued

Table 6 *(continued)*

Star ID	[Sc/H]	[V/H]	[Cr/H]	[Mn/H]	[Co/H]	[Ni/H]	[Zn/H]
2MASS J13524835+1254216	-2.27 ± 0.09	-2.03 ± 0.20	-2.21 ± 0.06	-2.75 ± 0.09	-2.25 ± 0.11	-2.31 ± 0.09	-2.14 ± 0.04
2MASS J13554406−3750455	-2.79 ± 0.16	-2.82 ± 0.16	-2.40 ± 0.00	-3.03 ± 0.11	-2.62 ± 0.17	-2.77 ± 0.08	-2.26 ± 0.00
2MASS J13592232−6821493	-1.84 ± 0.12	-1.75 ± 0.11	-1.80 ± 0.03	-2.42 ± 0.02	-1.95 ± 0.08	-1.99 ± 0.13	-2.01 ± 0.00
2MASS J14100568−0701443	-1.97 ± 0.13	-0.85 ± 0.00	-1.86 ± 0.15	-2.38 ± 0.11	-1.69 ± 0.20	-2.11 ± 0.16	-1.97 ± 0.06
2MASS J14112614−1137453	-2.72 ± 0.14	-2.17 ± 0.17	-3.05 ± 0.16	-3.31 ± 0.13	-2.26 ± 0.27	-2.47 ± 0.13	-2.23 ± 0.00
2MASS J14234371−4025526	-2.33 ± 0.17	-2.00 ± 0.14	-2.24 ± 0.00	-2.74 ± 0.12	-2.25 ± 0.15	-2.28 ± 0.10	-2.23 ± 0.02
2MASS J14335592−1240357	-3.07 ± 0.20	-2.67 ± 0.06	-3.06 ± 0.00	-3.52 ± 0.14	-2.84 ± 0.24	-3.03 ± 0.09	-2.86 ± 0.02
2MASS J14355850−0719265	-1.59 ± 0.07	-1.38 ± 0.00	-1.70 ± 0.13	-1.84 ± 0.13	-1.26 ± 0.20	-1.87 ± 0.17	-1.73 ± 0.05
2MASS J14443014−1320092	-2.67 ± 0.11	-2.51 ± 0.12	-2.57 ± 0.03	-3.01 ± 0.09	-2.47 ± 0.10	-2.53 ± 0.23	-2.45 ± 0.12
2MASS J14533268−3614555	-3.11 ± 0.05	···	-2.87 ± 0.00	-3.84 ± 0.04	-2.83 ± 0.12	-3.13 ± 0.22	···
2MASS J14534137+0040467	-2.09 ± 0.09	-1.57 ± 0.00	-1.71 ± 0.00	-2.76 ± 0.12	-1.46 ± 0.07	-2.29 ± 0.16	-2.31 ± 0.00
2MASS J14543792+0830379	-2.37 ± 0.13	-1.54 ± 0.00	-2.12 ± 0.06	-2.67 ± 0.05	-2.11 ± 0.19	-2.29 ± 0.13	-2.25 ± 0.02
2MASS J14564556−1615432	-2.26 ± 0.09	-2.17 ± 0.12	-2.24 ± 0.02	-2.64 ± 0.11	-2.21 ± 0.11	-2.29 ± 0.17	-2.19 ± 0.02
2MASS J14590234−0916105	-2.67 ± 0.12	-2.36 ± 0.05	-2.64 ± 0.07	-3.25 ± 0.10	-2.63 ± 0.13	-2.76 ± 0.08	-2.59 ± 0.00
2MASS J15013452−2443310	-2.62 ± 0.17	-2.40 ± 0.02	-2.60 ± 0.16	-2.85 ± 0.06	-2.59 ± 0.17	-2.90 ± 0.05	-2.45 ± 0.13
2MASS J15042611−2231523	-1.94 ± 0.11	-1.85 ± 0.03	-1.87 ± 0.09	-2.36 ± 0.12	-1.71 ± 0.21	-2.00 ± 0.13	-1.95 ± 0.08
2MASS J15133549−1244339	-2.72 ± 0.05	-2.51 ± 0.12	-2.60 ± 0.01	-3.13 ± 0.14	-2.62 ± 0.15	-2.65 ± 0.10	-2.54 ± 0.11
2MASS J15204531−1742486	-2.70 ± 0.10	-2.46 ± 0.16	-2.45 ± 0.06	-2.98 ± 0.08	-2.49 ± 0.12	-2.70 ± 0.12	-2.79 ± 0.03
2MASS J15240713−0319509	-2.61 ± 0.10	-2.48 ± 0.06	-2.43 ± 0.06	-3.21 ± 0.17	-2.51 ± 0.17	-2.70 ± 0.11	-2.50 ± 0.08
2MASS J15272126−1445153	-2.42 ± 0.11	-2.15 ± 0.16	-2.40 ± 0.05	-2.81 ± 0.08	-2.29 ± 0.18	-2.53 ± 0.11	-2.19 ± 0.02
2MASS J16115667−8034422	-1.32 ± 0.11	···	-1.37 ± 0.00	-1.91 ± 0.21	···	-1.73 ± 0.14	-1.28 ± 0.08
2MASS J16163600−5700568	-2.81 ± 0.05	-2.71 ± 0.01	-2.65 ± 0.01	-3.91 ± 0.08	-2.61 ± 0.09	-2.75 ± 0.12	-2.55 ± 0.00
2MASS J16592172−6827199	-1.73 ± 0.10	-1.81 ± 0.00	-1.92 ± 0.07	-2.14 ± 0.00	-2.40 ± 0.00	-2.05 ± 0.19	-2.87 ± 0.00
2MASS J17043634−6219457	-2.71 ± 0.10	-2.56 ± 0.23	-2.65 ± 0.07	-3.08 ± 0.14	-2.54 ± 0.17	-2.69 ± 0.09	-2.49 ± 0.05
2MASS J17060555+0412354	-2.67 ± 0.19	-2.53 ± 0.00	-2.59 ± 0.15	-3.28 ± 0.05	-2.56 ± 0.19	-2.79 ± 0.11	-2.55 ± 0.04
2MASS J17070759−7817561	-2.68 ± 0.11	-2.53 ± 0.04	-2.68 ± 0.10	-2.82 ± 0.18	-2.60 ± 0.20	-2.38 ± 0.16	···
2MASS J17131974−7113010	-2.38 ± 0.11	-2.36 ± 0.10	-2.29 ± 0.09	-2.64 ± 0.21	-2.21 ± 0.12	-2.29 ± 0.14	···
2MASS J17163340−7009028	-2.56 ± 0.13	-2.18 ± 0.14	-2.36 ± 0.14	-2.86 ± 0.05	-2.34 ± 0.15	-2.43 ± 0.15	-2.24 ± 0.02
2MASS J17360167−5145296	-1.97 ± 0.10	-1.89 ± 0.05	-2.06 ± 0.03	-2.41 ± 0.20	-2.01 ± 0.20	-2.12 ± 0.16	-2.11 ± 0.00
2MASS J17541561−5148268	-1.74 ± 0.14	-1.66 ± 0.11	-1.78 ± 0.07	-2.17 ± 0.07	-1.87 ± 0.16	-1.95 ± 0.12	-1.83 ± 0.02
2MASS J18272432−5655165	-1.80 ± 0.12	-1.83 ± 0.00	-1.86 ± 0.06	-2.31 ± 0.04	-1.94 ± 0.18	-2.02 ± 0.17	-1.97 ± 0.09
2MASS J18284356−8441346	-0.36 ± 0.17	···	-0.87 ± 0.00	-0.83 ± 0.04	···	-1.02 ± 0.19	-0.92 ± 0.14
2MASS J18294359−4924253	-1.50 ± 0.13	-1.01 ± 0.00	-1.79 ± 0.00	-1.89 ± 0.11	-1.17 ± 0.28	-1.93 ± 0.19	-1.97 ± 0.07
2MASS J18332056−3802590	-1.60 ± 0.13	-1.75 ± 0.00	-1.99 ± 0.18	-2.01 ± 0.12	-1.63 ± 0.23	-1.90 ± 0.17	-1.77 ± 0.03

Table 6 continued

Table 6 *(continued)*

Star ID	[Sc/H]	[V/H]	[Cr/H]	[Mn/H]	[Co/H]	[Ni/H]	[Zn/H]
2MASS J18333188−4840403	-2.45 ± 0.08	-2.39 ± 0.06	-2.52 ± 0.10	-2.99 ± 0.20	-2.43 ± 0.12	-2.56 ± 0.14	-2.35 ± 0.02
2MASS J18361214−7333443	-2.43 ± 0.09	-2.26 ± 0.06	-2.26 ± 0.08	-2.82 ± 0.09	-2.38 ± 0.13	-2.49 ± 0.09	-2.18 ± 0.07
2MASS J18405985−4841353	-2.92 ± 0.08	-2.79 ± 0.03	-2.87 ± 0.13	-2.46 ± 0.16	-2.80 ± 0.08	-2.92 ± 0.10	-2.62 ± 0.04
2MASS J18560360−6403465	-2.36 ± 0.05	-2.24 ± 0.10	-2.43 ± 0.13	-2.77 ± 0.08	-2.24 ± 0.16	-2.42 ± 0.13	-2.19 ± 0.09
2MASS J19092677−5140208	-2.00 ± 0.14	-1.97 ± 0.02	-2.06 ± 0.05	-2.58 ± 0.06	-2.33 ± 0.19	-2.26 ± 0.16	-2.05 ± 0.09
2MASS J19105886−4059412	-2.22 ± 0.14	-1.96 ± 0.14	-2.27 ± 0.06	-2.53 ± 0.09	-2.17 ± 0.15	-2.15 ± 0.14	-2.27 ± 0.01
2MASS J19175585−5440147	-2.66 ± 0.09	-2.51 ± 0.07	-2.55 ± 0.03	-2.93 ± 0.06	-2.40 ± 0.11	-2.55 ± 0.11	-2.54 ± 0.02
2MASS J19192768−5959140	-2.31 ± 0.12	-2.32 ± 0.13	-2.42 ± 0.09	-2.91 ± 0.05	-2.37 ± 0.15	-2.61 ± 0.17	-2.43 ± 0.06
2MASS J19282163−2457545	-2.72 ± 0.12	-2.66 ± 0.11	-2.46 ± 0.06	-2.82 ± 0.21	-2.64 ± 0.08	-2.63 ± 0.19	-2.60 ± 0.01
2MASS J19291910−5528181	-1.92 ± 0.13	-2.05 ± 0.00	-2.14 ± 0.14	-2.57 ± 0.03	-2.35 ± 0.24	-2.26 ± 0.19	-2.24 ± 0.04
2MASS J19310426−3707397	-1.79 ± 0.11	-1.46 ± 0.00	-1.95 ± 0.04	-2.88 ± 0.04	-1.99 ± 0.11	-2.14 ± 0.16	-2.05 ± 0.01
2MASS J19320444−7309178	-2.30 ± 0.09	-2.21 ± 0.16	-2.64 ± 0.08	-3.17 ± 0.12	-2.64 ± 0.16	-2.75 ± 0.13	-2.61 ± 0.00
2MASS J19504989−3321107	-3.40 ± 0.05	-3.29 ± 0.08	-3.22 ± 0.00	-3.94 ± 0.04	-3.07 ± 0.12	-3.19 ± 0.13	-3.11 ± 0.00
2MASS J19532495−3647303	-2.53 ± 0.17	-2.32 ± 0.12	-2.44 ± 0.16	-3.07 ± 0.12	-2.60 ± 0.11	-2.68 ± 0.16	-2.50 ± 0.10
2MASS J19552158−4613569	-2.34 ± 0.10	-2.05 ± 0.20	-2.39 ± 0.05	-2.80 ± 0.13	-2.35 ± 0.05	-2.45 ± 0.14	-2.29 ± 0.09
2MASS J19563822−4054235	-2.52 ± 0.10	-2.41 ± 0.14	-2.45 ± 0.00	-3.12 ± 0.15	-2.41 ± 0.19	-2.63 ± 0.20	-2.23 ± 0.08
2MASS J19570893−3317320	-2.84 ± 0.14	-2.43 ± 0.15	-2.76 ± 0.11	-3.07 ± 0.05	-2.74 ± 0.17	-2.75 ± 0.13	-2.66 ± 0.01
2MASS J20035532−5028100	-2.72 ± 0.08	-2.44 ± 0.10	-2.28 ± 0.07	-2.49 ± 0.13	-2.64 ± 0.15	-2.62 ± 0.19	-2.56 ± 0.14
2MASS J20192202−6130149	-2.74 ± 0.14	-2.57 ± 0.15	-2.75 ± 0.05	-3.23 ± 0.08	-2.74 ± 0.14	-2.84 ± 0.11	-2.66 ± 0.02
2MASS J20202917−2707347	-2.64 ± 0.07	-2.38 ± 0.00	-2.01 ± 0.02	-3.06 ± 0.14	-2.64 ± 0.12	-2.65 ± 0.08	-2.45 ± 0.00
2MASS J20234398−0815472	-3.00 ± 0.10	-2.89 ± 0.10	-2.99 ± 0.04	-3.26 ± 0.08	-2.80 ± 0.10	-2.92 ± 0.15	-3.03 ± 0.00
2MASS J20242122−2656435	-2.42 ± 0.13	-2.22 ± 0.11	-2.52 ± 0.13	-2.88 ± 0.02	-2.52 ± 0.19	-2.55 ± 0.12	-2.36 ± 0.01
2MASS J20374042−5520500	-2.52 ± 0.10	-2.42 ± 0.11	-2.49 ± 0.03	-3.00 ± 0.09	-2.54 ± 0.18	-2.62 ± 0.15	-2.49 ± 0.01
2MASS J20445065−3714000	-2.65 ± 0.20	-2.31 ± 0.08	-2.52 ± 0.12	-3.09 ± 0.11	-2.70 ± 0.14	-2.61 ± 0.12	-2.54 ± 0.13
2MASS J20501790−0549230	-2.80 ± 0.18	-2.43 ± 0.09	-2.68 ± 0.08	-3.13 ± 0.18	-2.64 ± 0.06	-2.78 ± 0.22	-2.56 ± 0.03
2MASS J20585505−1759007	-3.42 ± 0.14	-3.34 ± 0.11	-3.29 ± 0.02	-4.04 ± 0.26	-3.17 ± 0.15	-3.17 ± 0.20	-2.64 ± 0.01
2MASS J21220020−0820333	-1.54 ± 0.06	-1.37 ± 0.00	-1.61 ± 0.24	-2.03 ± 0.03	-1.55 ± 0.23	-1.85 ± 0.17	-1.91 ± 0.08
2MASS J21234588−0839448	-2.85 ± 0.15	-2.66 ± 0.17	-2.89 ± 0.09	-3.25 ± 0.18	-2.94 ± 0.17	-2.88 ± 0.15	-2.95 ± 0.03
2MASS J21352343−5722598	-2.56 ± 0.07	-2.41 ± 0.12	-2.49 ± 0.01	-2.43 ± 0.24	-2.27 ± 0.15	-2.35 ± 0.14	-2.18 ± 0.06
2MASS J21553580−0905118	-2.28 ± 0.05	-2.01 ± 0.20	-2.26 ± 0.00	-2.85 ± 0.09	-2.28 ± 0.16	-2.36 ± 0.11	-2.30 ± 0.06
2MASS J22182082−3827554	-2.35 ± 0.09	-2.15 ± 0.13	-2.21 ± 0.06	-2.61 ± 0.29	-2.26 ± 0.13	-2.37 ± 0.11	-2.21 ± 0.08
2MASS J22215794−3602090	-2.52 ± 0.07	-2.17 ± 0.28	-2.34 ± 0.03	-2.73 ± 0.10	-2.39 ± 0.13	-2.47 ± 0.18	-2.35 ± 0.01
2MASS J22220344−8024592	-2.69 ± 0.17	-2.57 ± 0.12	-2.71 ± 0.09	-3.16 ± 0.10	-2.81 ± 0.10	-2.70 ± 0.08	-2.57 ± 0.11
2MASS J22253443−2027171	-2.43 ± 0.09	-2.24 ± 0.20	-2.37 ± 0.03	-2.85 ± 0.13	-2.42 ± 0.16	-2.48 ± 0.12	-2.30 ± 0.00

Table 6 continued

Table 6 *(continued)*

Star ID	[Sc/H]	[V/H]	[Cr/H]	[Mn/H]	[Co/H]	[Ni/H]	[Zn/H]
2MASS J22300238−6332191	-2.19 ± 0.09	-2.09 ± 0.13	-2.15 ± 0.06	-2.60 ± 0.09	-2.27 ± 0.12	-2.18 ± 0.12	-2.07 ± 0.00
2MASS J22302641−1949527	-2.36 ± 0.14	-2.16 ± 0.20	-2.66 ± 0.25	-2.87 ± 0.09	-2.45 ± 0.02	-2.45 ± 0.16	-2.40 ± 0.00
2MASS J22344202−0826492	-2.78 ± 0.06	-2.52 ± 0.14	-2.70 ± 0.06	-2.97 ± 0.18	-2.53 ± 0.11	-2.63 ± 0.16	-2.55 ± 0.05
2MASS J22345447−6605172	-2.61 ± 0.05	-2.36 ± 0.13	-2.47 ± 0.03	-3.12 ± 0.09	-2.43 ± 0.29	-2.67 ± 0.10	-2.38 ± 0.09
2MASS J22394827−0803536	-1.61 ± 0.10	···	-1.58 ± 0.24	-1.94 ± 0.16	-0.99 ± 0.26	-1.87 ± 0.21	-1.97 ± 0.01
2MASS J23100319−7702165	-2.55 ± 0.09	-2.22 ± 0.13	-2.51 ± 0.11	-2.91 ± 0.05	-2.53 ± 0.14	-2.51 ± 0.14	-2.38 ± 0.02
2MASS J23411581−6406440	-2.50 ± 0.04	-2.22 ± 0.16	-2.51 ± 0.05	-3.00 ± 0.06	-2.40 ± 0.19	-2.55 ± 0.10	-2.33 ± 0.08